

**The Sierra Ballena Shear zone:
kinematics, timing and its significance for the geotectonic
evolution of southeast Uruguay**

Dissertation
zur Erlangung des Doktorgrades
der Mathematisch-Naturwissenschaftlichen Fakultäten
der Georg-August-Universität zu Göttingen

vorgelegt von

Pedro Bernardo Oyhançabal Cironi

aus
Montevideo

Göttingen 2005

D 7

Referentin/Referent: Prof. Dr. Siegfried Siegesmund

Korreferentin/Korreferent: Prof. Dr. Bent T. Hansen

Tag der mündlichen Prüfung: 30.05.05

Acknowledgments

I would like to express my special gratitude to my supervisor and to Dr. Klaus Wemmer for the initiation of this investigation and for the ongoing support and encouragement.

Without the stimulating environment and the laboratory facilities provided during my stay at the Institut für Geologie und Dynamik der Lithosphere of the Georg-August University of Göttingen this thesis would not have been possible.

Many thanks also to my colleagues at the Geology Department of the School of Sciences, Universidad de la República, in Montevideo: Natalie Aubet, Leda Sánchez Bettucci, Jorge Spoturno, and Ernesto Pecoits for many discussions.

Lastly but not least importantly, I would like to thank my family who has always supported me.

A research fellowship by the German Research Foundation also contributed to make this investigation possible.

Abstract

The Sierra Ballena Shear Zone is a high-strain transcurrent structure that divides the Neoproterozoic Dom Feliciano Belt of South America into two different domains. The eastern and western domains of this Shear Zone consist of basement gneisses, low-grade Neoproterozoic supracrustal successions, and granitic intrusions.

In the basement at both sides of the Shear Zone, a first deformation stage is recognized as a high temperature mylonitic foliation associated with migmatization. The microstructures indicate that diffusion creep was an important deformation mechanism, probably enhanced by partial melting. The age of this episode is estimated in the 800-600 Ma range.

The magmatic suites studied show an evolution beginning with highly-fractionated calc-alkaline granites (Solís the Mataojo Granitic Complex ~584 Ma), followed by mildly alkaline granites and shoshonitic volcanics (Maldonado Granite ~575 Ma, and Las Flores basalts), and concluding with peralkaline intrusions and volcanics (Sierra de las Ánimas Complex ~540-520 Ma). The signature of this magmatism indicates a post-collision setting during the activity of the Sierra Ballena Shear Zone, which played a major role in the emplacement of these magmatic associations.

The deformation observed in the Sierra Ballena Shear Zone took place in regional low-grade conditions, as indicated by metasediments of associated strike-slip basins. The second deformation phase was transpressional, pure shear dominated, with conjugate dextral and sinistral shear zones forming at this phase. Granites emplaced during this phase show evidence of important flattening. The age of these intrusions, allow us to estimate an interval of 590 to 540 Ma for this event. The microstructures observed in quartz of granitic mylonites of this stage are characteristic of the dislocation creep regime 2, and fabric pol-figures are asymmetric crossed girdles and asymmetric single girdles with rhomb - <a> as the active slip system, indicating middle greenschist facies conditions during transpressional deformation.

The third stage is a simple shear dominated sinistral strike-slip event. Alkaline porphyries emplaced in the shear zone similar to Cambrian alkaline rocks emplaced in the low-strain domains, together with the lack of Brasiliano granites cutting the shear zone, bracket this stage between 550 and 500 Ma. Quartz mylonites and mylonitic porphyries of the Sierra Ballena Shear Zone display quartz microstructures characteristic of the transition between regime 2 and regime 3, with grain boundary migration as an important recovery mechanism. The fabric pol-figures display Y maximum patterns, with prism - <a> being the main slip system. These characteristics indicate deformation in upper greenschist to lower amphibolite facies (~500 °C). This medium to high temperature of deformation in a regional low-grade crust level is ascribed to temperature rise produced by emplacement of the porphyries.

Correlation of the above-described evolution with the stages illustrated by Konopásek *et al.* (2005) for the Purros Shear Zone of the Kaoko Belt of Namibia indicates that the Sierra Ballena Shear Zone represents the continuation of the former.

Zusammenfassung

Die *Sierra Ballena Scherzone* ist eine horizontale Verschiebungsstruktur, die den Neoproterozoischen Gürtel *Dom Feliciano* in Südamerika in zwei unterschiedliche Domäne teilt. Die östlichen und westlichen Domäne dieser Scherzone bestehen aus prä-orogenem Grundgebirge (pre-Brasiliano), Neoproterozoisch suprakrustalen Abfolgen sowie granitischen Intrusionen.

Im Grundgebirge wird an beiden Seiten der Scherzone als erstes Verformungsstadium eine mylonitische Hochtemperaturfoliation erkannt, die mit Migmatiten in Verbindung steht. Die Mikrostrukturen zeigen an, dass „diffusional creep“ ein wichtiger Deformationsprozess war, vermutlich verstärkt durch teilweise Schmelzen. Das Alter dieser Episode wird auf 800-600 Ma geschätzt.

Die untersuchte magmatische Suite zeigt eine Entwicklung, die mit den hoch-fraktionierten calc-alkalischen Graniten beginnt, gefolgt von schwach alkalischen Graniten und shoshonitischen Eruptivgesteinen. Abschließend treten peralkalinische Intrusionen und Eruptivgesteine auf. Die Signatur dieses Magmatismus deutet auf ein *post-collision tectonic setting* während der Tätigkeit in der Sierra Ballena Scherzone. Die Sierra Ballena Scherzone übernimmt damit eine Hauptrolle für die Platznahme dieser magmatischen Einheiten.

Die Verformung in der Sierra Ballena Scherzone fand in den regionalen grünschieferfaziellen Bedingungen statt, die durch Metasedimente in der angrenzenden Becken angezeigt sind. Die zweite Deformationsphase war transpressional, und reine Scherung beherrscht. Die Deformation führte zur Ausbildung von dextralen und sinistralen Scherzonen. Die Platznahme von Graniten während dieser Phase zeigt Beweise des wichtigen *flattening*. Das Alter der Intrusionen erlaubt, den Zeitraum für diese Phase auf 590 bis 540 Ma einzugrenzen. Die Mikrostrukturen im Quarz, die an einem granitartigen Mylonit dieses Stadiums beobachtet werden können, sind charakteristisch für *dislocation creep* Regime 2. Textur Pol-Figuren sind asymmetrische gekreuzte Gürtel und asymmetrisch einfache Gürtel mit Rhomb- $\langle a \rangle$ als aktivem Gleitsystem. Mikrostrukturen und Pol-Figuren zeigen mittlere grünschieferfazielle Bedingungen während der transpressional Verformung.

Das dritte Stadium war *strike-slip* artig mit sinistraler, dominant einfacher Scherung. Alkalische Porphyre, die in der Scherzone aufgestiegen sind, zeigen ähnliche Merkmale wie die kambrischen alkalischen Porphyre und Intrusionen, die in die Niedrig-Strain Domäne intrudiert sind. Diese Tatsache zusammen mit dem Fehlen von Brasiliano Graniten, die die Scherzone schneiden, beschränken dieses Stadium auf ein Alter zwischen 550 und 500 Ma. Quarzmylonite und mylonitische Porphyre der Sierra Ballena Scherzone zeigen Mikrostrukturen in Quarz, die für den Übergang von *dislocation creep* Regime 2 zu *dislocation creep* Regime 3 charakteristisch sind. Die beobachtete Korngrenzenmigration ist hierbei ein wichtiger Mechanismus der Erholung. Die Textur Pol-Figuren zeigen ein c-Achsen Maximum in Y-Richtung, mit Prism- $\langle a \rangle$ als Hauptgleitsystem. Die Eigenschaften zeigen eine Deformation bei oberen grünschiefer- bis unteren amphibolitfaziellen Bedingungen an (~500 °C). Diese Mittel- bis Hochtemperatur Verformung in einem regionalen grünschieferfaziellen Krusteniveau wird dem Temperaturanstieg zugeschrieben, der durch Platznahme der Porphyre produziert wird.

Die Korrelation der oben beschriebenen Entwicklung mit den Stadien, die von Konopásek *et al.* (2005) für die Purros Scherzone vom Kaoko Gürtel in Namibia beschrieben werden zeigt, dass die Sierra Ballena Scherzone die Fortsetzung der Purros Scherzone darstellt.

CONTENTS

Acknowledgements	<i>i</i>
Abstract	<i>ii</i>
Zusammenfassung	<i>iii</i>
CHAPTER 1 – Introduction	1
CHAPTER 2 – Regional Geology	3
2.1 Overview of the geology of the Uruguayan Basement	3
2.2 Brasiliano Units of Southern Brazil: correlations and geotectonic models	8
CHAPTER 3 – Lithological Units of the study area	11
3.1 Outline of the structure of the area	11
3.2 Domain I: West of the SYSZ (Piedra Alta Terrane)	11
3.3 Domain II: Sarandí del Yí Shear Zone	13
3.4 Domain III: Between the SYSZ and the SBSZ (Nico Pérez Terrane)	14
3.4.1 Basement: Medium to high-grade rocks (Campanero Units)	14
3.4.2 Cover: Supracrustal successions	15
3.4.3 Granitic magmatism	17
3.5 Domain IV: Between the SBSZ and the CSZ (Las Cañas Shear Belt)	18
3.5.1 Mylonitic Porphyries	19
3.5.2 Granitic Mylonites	20
3.5.3 Phyllonites	20
3.5.4 Synkinematic granitoids	21
3.6 Domain V: East of the CSZ	23
3.6.1 Basement	23
3.6.2 Cover	24
3.6.3 Granites	25
CHAPTER 4 – Meso and macrostructures	26
4.1. Macrostructure	26
4.1.1 Strike-slip shear zones	26
4.1.2 Thrusts	29
4.1.3 Folds	30
4.1.4 Structurally-controlled intrusions	30
4.1.5 Vendian to Cambrian basins	33
4.2 Mesostructures	34

CHAPTER 5 – The pre-Brasiliano Basements West of the Sierra Ballena Shear	
Zone: Campanero Unit	43
5.1 Petrography of the main lithologies	43
5.1.1 Orthogneisses and stripped orthogneisses	43
5.1.2 Scapolite gneisses	44
5.1.3 Amphibolites	44
5.1.4 Micaschists	45
5.1.5 Banded iron formation	45
5.1.6 Migmatites	45
5.2 Geochemistry of orthogneisses and stripped orthogneisses of the Campanero Unit	47
CHAPTER 6 – Brasiliano magmatism: petrographic and geochemical characterization of three intrusions and one volcanic association	51
6.1 Solis de Mataojo granitic Complex	51
6.1.1 Geochemistry	53
6.2 Maldonado Granite	59
6.2.1 Geochemistry	60
6.3 Pan de Azúcar Pluton (Sierra de las Ánimas Complex)	64
6.3.1 Geochemistry	66
6.4 Geochemical contrast between the Solis de Mataojo, Maldonado and Pan de Azúcar Plutons	73
6.5 Tectonics setting considerations	76
6.6 Geochemistry of the mylonitic porphyries of Sierra Ballena Shear Zone	79
6.7 Las Flores basic volcanics	80
6.7.1 Geochemistry	81
CHAPTER 7 – Microstructural and textural aspects of medium-low and high T tectonites	83
7.1 Microstructures	83
7.1.1 Low-medium T tectonites	83
7.1.2 High T tectonites	87
7.2 Texture investigation	90
7.3 Conclusions	95
CHAPTER 8 – Geochronology	97
8.1 New geochronological data	99
8.1.1 Solis de Mataojo granitic Complex	99
8.1.2 Cooling ages	101
8.2 Conclusions	102

CHAPTER 9 – Geotectonic evolution and relation to other Pan-African-Brasiliano belts of South America and Africa	106
9.1 Geotectonic evolution	106
9.1.1 Paleoproterozoic basement	106
9.1.2 First deformation stage (Neoproterozoic high temperature deformation-metamorphism)	106
9.1.3 Basement cover relationships	107
9.1.4 Second deformation stage (Vendian low temperatures deformation-metamorphism)	108
9.1.5 Third deformation stage (Late Vendian-Cambrian low temperature deformation-metamorphism)	108
9.2 Correlation with Brazil and South Africa	110
CHAPTER 10 – Conclusions	112
References	115
Appendix 1 Geological map of the study area	122
Appendix 2 Abbreviations	124
Appendix 3	
Location of field observation points	125
Coordinates of geochronology samples	126
Appendix 4 Major, trace and rare earth elements analysis	127

CHAPTER 1 INTRODUCTION

Strike-slip shear zones of crustal-scale are recognized for playing a major role in the evolution of orogens. These shear zones can correspond to continental transform faults, such as the San Andreas Fault in California or the Alpine Fault in New Zealand (Moore and Twiss, 1995, p. 144). They can also provide accommodation for continental collision, like the Tibetan Fault systems, or accommodate the strike-slip component of subduction in the upper plate, as in the cases of the Andes, the North Cascades and Sumatra, among other examples (Saint Blanquat *et al.*, 1998; Konopásek *et al.*, 2005, and references therein).

The term transpression has been adopted to describe oblique convergence in orogens, as well as the strain regime where pure and simple shear strain components are present. Strain is usually partitioned in transpressional orogens (Jones and Tanner, 1995), and high-strain shear zones (where simple shear prevails) occur as boundaries between low-strain blocks (where pure shear predominates).

An important relation has been indicated between shear zones and generation, ascent, and emplacement of granitic melts (Hutton and Reavy, 1992; Lemos *et al.*, 1992, Weinberg, 2004). In addition, strike-slip basins associated with transform or transcurrent faults are frequently formed in transpressional orogens (Nilsen and Sylvester, 1995). Furthermore, shear zones may constitute the boundaries between accreted terranes, and their study can provide insight into the history of accretion involved in the evolution of an orogen.

These links between magmatism, sedimentary basins, and terrane accretion make the study of the kinematic evolution of major shear zones a key topic for reconstructing the history of orogens.

The Dom Feliciano Belt of southern Brazil and Uruguay is crosscut by an orogen parallel major shear zone, nearly 1000 km long, known in Brazil as the Dorsal do Canguçu and in Uruguay as the Sierra Ballena Shear Zone. As of Porada (1979) investigation, a link between the Dom Feliciano Belt of South America and the Kaoko and Gariep Belts of southwestern Africa is admitted, but no agreement exists to date with respect to different large-scale tectonic models, due to the scarcity of geological information.

The Kaoko Belt in Namibia also contains a crustal scale structure, known as the Purros Shear Zone. The possible correlation of the Purros and Sierra Ballena Shear Zones could contribute to a better understanding of the evolution of the Pan-African - Brasiliano orogens.

The objectives of this investigation are to:

- i) Construct a geological map at 1:250,000 scale of the southernmost exposures of the Dom Feliciano Belt, at both sides of the Sierra Ballena Shear Zone, gathering all relevant structural information.
- ii) Carry out a preliminary investigation on the microstructures and textures of the tectonites of the area, with the aim of determining the conditions during deformation and revealing the kinematics.
- iii) Conduct a first petrographical and geochemical characterization of some selected magmatic units, establishing their relation with the tectonic events.
- iv) Obtain some new age determinations to increase the database and enhance our knowledge of the chronology of the events.
- v) Discuss current geotectonic models.

Such a regional investigation is deemed essential to constrain the hypotheses and guide further, more-detailed investigations.

CHAPTER 2 REGIONAL GEOLOGY

2.1. Overview of the geology of the Uruguayan Basement

Uruguay is part of the South American Platform and its geology consists of a Precambrian basement cropping out in the south, and Palaeozoic to Mesozoic sediments and basaltic flows that are part of the Parana Basin in the north (Fig. 2.1). Two Mesozoic rift basins related to the opening of the Atlantic Ocean are present in the south (Santa Lucía Basin) and east (Laguna Merín Basin).

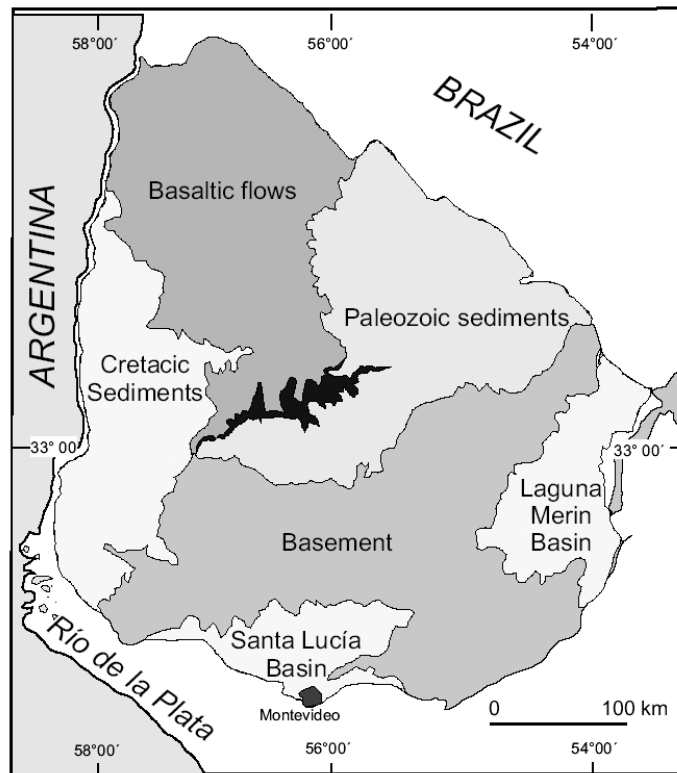


Figure 2.1 - Main geological units of Uruguay (schema based on Preciozzi *et al.*, 1985)

The Precambrian basement extends over nearly 45% of the country, and different approaches have been applied in the last 30 years to define its main units. A first division was proposed by Ferrando and Fernandez (1971), based on two age groups: the first in the southwest, related to the Transamazonian Cycle (2.2 - 1.8 Ga), and the second in the east,

related to the Brasiliano Cycle (900 - 550 Ma). Using a plate tectonic approach, Fragoso-Cesar (1980) defined the Rio de La Plata Craton and the Dom Feliciano Mobile Belt. The latter had formerly been considered a part of the Ribeira Belt.

Recently a tectonostratigraphical terrane approach (Bossi and Ferrando, 2001) takes two major shear zones (Sierra Ballena and Sarandí del Yí) as basis for defining three different terranes, namely the Piedra Alta Terrane in the west, the Nico Pérez Terrane in the centre, and the Dom Feliciano Belt in the east (Fig. 2.2).

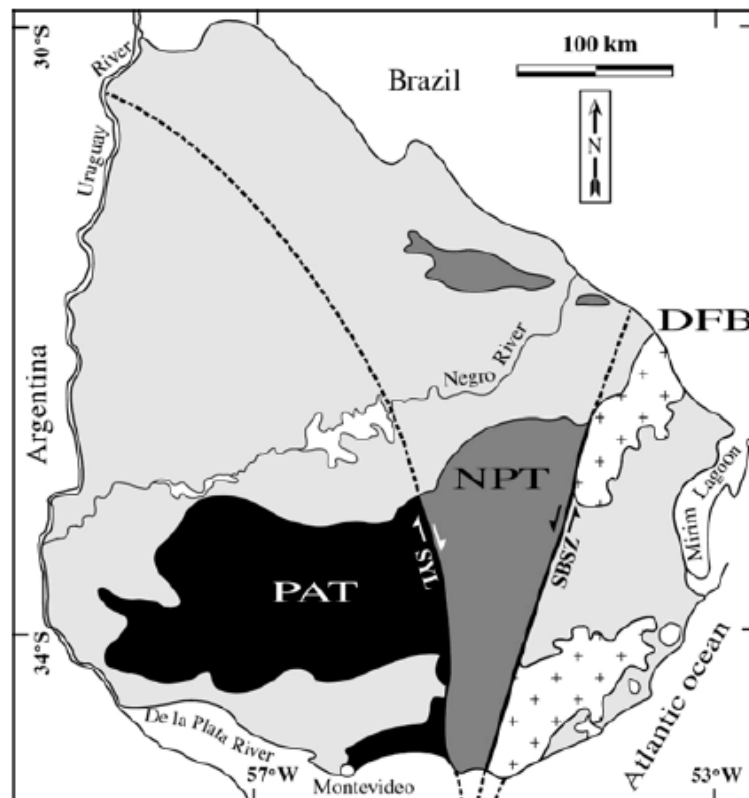


Fig. 2.2 - Tectonostratigraphic division of the Uruguayan Crystalline Basement. SYL: Sarandí del Yí Shear Zone; SBSZ: Sierra Ballena Shear Zone. PAT: Piedra Alta Terrane, NPT: Nico Perez Terrane, DFB: Dom Feliciano Belt (from Bossi and Ferrando, 2001).

The **Piedra Alta Terrane** consists of a central granitic region with frequent gneiss and amphibolite xenoliths, ranging from mappable to metre-sized, and two metamorphic belts: Arroyo Grande and Montevideo (Oyhantçabal *et al.*, 2003). The oldest tectono-thermal event recorded in this terrane is Palaeoproterozoic.

The Montevideo Belt (Fig. 2.3) is composed of a medium-grade metamorphic unit in the south (Montevideo Formation), comprising amphibolites, gneisses, and staurolite-

garnet micaschists, and a low-grade metamorphic unit in the north (Paso Severino Formation), containing metabasalts, meta-andesites, metadacites, and metapelites. The contact between both formations is an E-W oriented high-strain zone, northward thrusting, in which sheared granitic rocks are frequently emplaced (Oyhantçabal *et al.*, 2003). The minimum age of the Piedra Alta Terrane is constrained by a dolerite dike swarm with a baddeleyite U/Pb age of 1790 ± 5 Ma (Halls *et al.*, 2001).

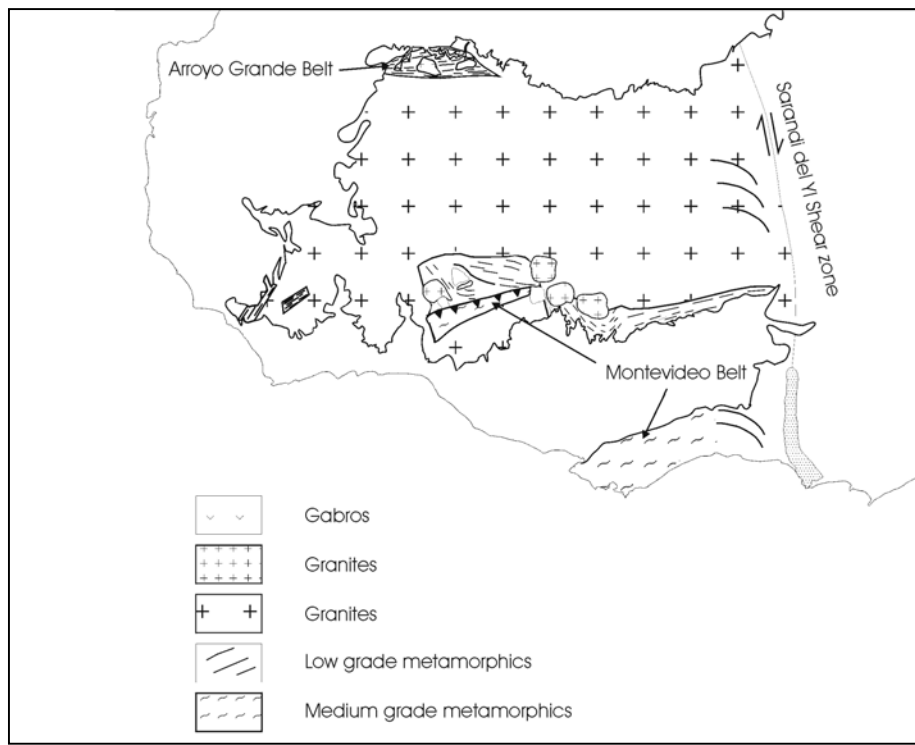


Fig. 2.3 - Schematic geological map of the Piedra Alta Terrane (based on Oyhantçabal *et al.*, 2003).

The **Nico Pérez Terrane** is a complex unit located between the two major shear zones (Sarandí del Yí and Sierra Ballena). Based on a SHRIMP U/Pb reconnaissance geochronology on zircon, Hartmann *et al.* (2001) recognized five different lithotectonic units (Fig. 2.4). The Valentines Complex comprises granulites of tonalitic to granitic composition. The protolith age for this complex was dated at 2.6 Ga and the high-grade metamorphism at 2.2 Ga. The La China Complex is composed of mafic and ultramafic rocks associated to metacherts, with U/Pb SHRIMP ages on zircon of 3.4 Ga in cores of Zircon grains -interpreted as the magmatic age- and 3.1 Ga in rims -interpreted as the age of metamorphism. The Las Tetras Complex is a platform succession comprising

metaconglomerates, quartzites, and muscovite gneisses, interpreted as being deformed and metamorphosed at 2.7 Ga (based on ages of zircon rims). The Lavalleja Group (also known as Fuente del Puma Group) is a low-grade volcano-sedimentary succession composed of metabasalts, phyllites, limestones, and quartzites, whose age is not well constrained (Meso to Neoproterozoic). Lastly, the Arroyo del Soldado Group is a platform succession of sandstones, limestones, siltstones, and conglomerates, with microfossils of Vendian to Cambrian age (Gaucher, 2000).

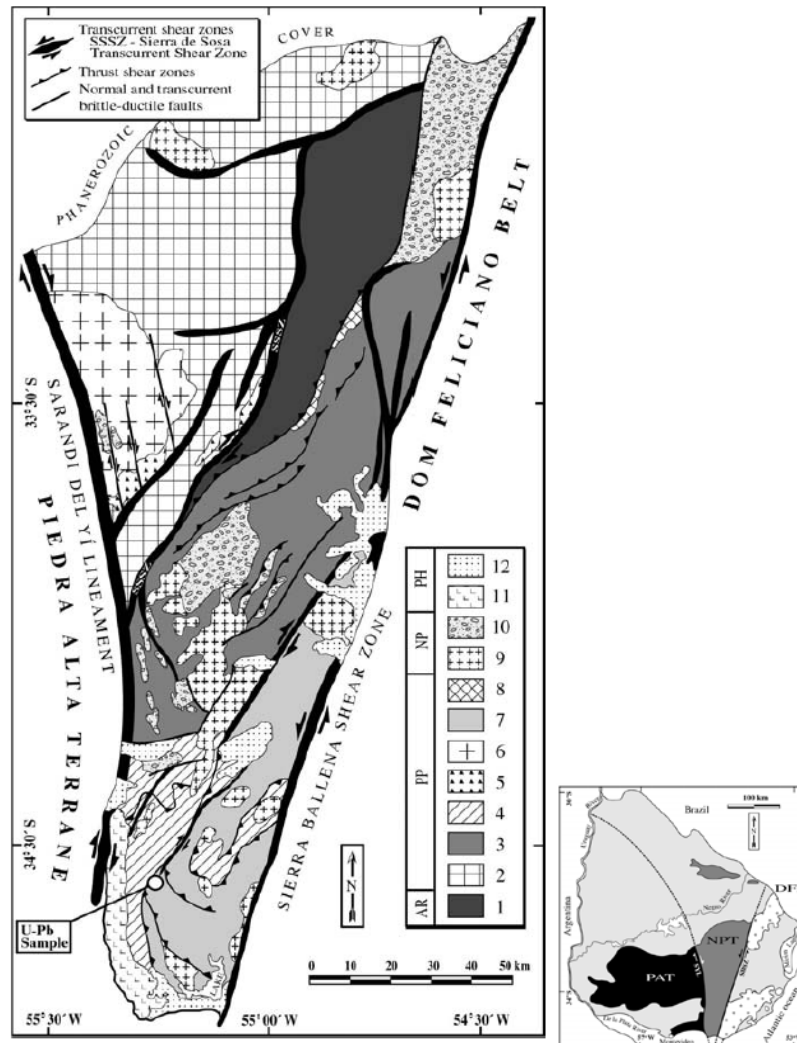


Fig. 2.4 - Geological sketch map of the Nico Pérez Terrane (After Mallmann 2003). 1- La China Complex, 2- Valentines Formation, 3- Las Tetas Complex, 4- Lavalleja Group, 5- Diorites, 6- Illescas Rapakivi Batholith, 7- Carapé Complex, 8- Undivided granites, 9- Brasiliano granites, 10- Arroyo del Soldado Group, 11- Las Animas Complex, 12- Phanerozoic cover.

Additional supracrustal successions are the Zanja del Tigre Formation (Sánchez-Bettucci and Ramos, 1999), composed of metamorphosed limestones, quartzites, pelites,

sandstones, and minor BIFs, interbedded with acidic volcanoclastic rocks, of uncertain age (Meso to Neoproterozoic), and the Las Ventanas Formation, containing microfossils of Vendian age deposited unconformably over the Lavalleja Group (Pecoits, 2003).

Hartmann *et al.* (2001) considered the easternmost portion of the Uruguayan Shield, eastward of the Sierra Ballena Lineament, a third terrane, namely the **Cuchilla Dionisio Terrane** (Fig. 2.5). Although little-studied, this terrane is thought to have generated during the Paleoproterozoic and to have been intensely reworked during the Brasiliano Cycle. Some authors (Preciozzi *et al.*, 1999) also proposed a fourth terrane located in the southeastern margin of the Cuchilla Dionisio Terrane, which they named the Punta del Este Terrane. This terrane is correlated to the African Namaqua Complex and was presumably formed at 1.0-0.9 Ga, being perhaps linked to the Grenvillian of North America (Preciozzi *et al.*, 1999).

The Cuchilla Dionisio Terrane is made up of three fundamental units: (1) a granitic unit (Aiguá Batholith); (2) a high-grade metamorphic unit comprising gneisses and migmatites, paragneisses, and amphibolites (Cerro Olivo Complex); and (3) the Rocha Group, composed of low-grade metasediments (the age is uncertain, but granites intruding the group yielded Rb/Sr WR ages between 537 ± 7 and 559 Ma, suggesting that the minimum age is Neoproterozoic). A minor unit is the Sierra de Aguirre Formation, which includes lavas, pyroclastics, and sediments, with a total thickness of 1,200 m and an age of 571 ± 8 Ma (U/Pb SHRIMP on zircon, Bossi *et al.*, 2001).

The Sierra Ballena Shear Zone (Figs. 2.1, 2.4, 2.5), which was postulated as the boundary between the Cuchilla Dionisio and Nico Pérez Terranes, is 4 km wide, striking NNE, and is composed of protomylonites and ultramylonites with sinistral kinematic indicators. The minimum age of the onset of the sinistral displacement is *ca.* 587 ± 16 Ma, considering the age of some syntranscurrent granites. The late major events was generally thought to be older than 520 ± 5 Ma (Rb/Sr WR, Bossi *et al.*, 1993), given the usual interpretation of the age of the Sierra de las Ánimas Complex as post-orogenic magmatism (Sánchez-Bettucci and Rapalini, 2002).

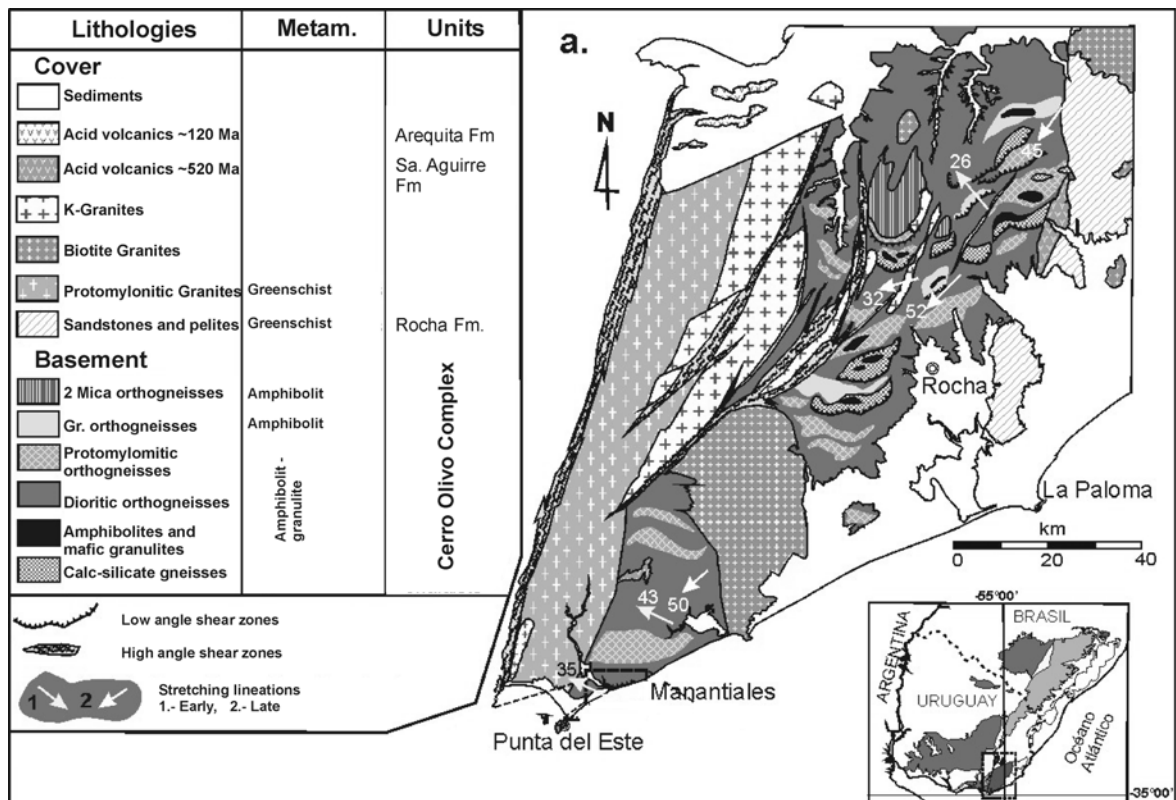


Fig. 2.5 - Geological sketch map of the Cuchilla Dionisio Terrane (after Masquelín, 2004).

2.2. Brasiliano Units of Southern Brazil: correlation and geotectonic models.

The Neoproterozoic to Cambrian geological events of South America correspond to what Almeida *et al.* (1971) defined as the Brasiliano Cycle or Orogenesis, which is correlated to the Pan-African of Southern Africa. The geological units associated with the Brasiliano Orogenesis in South America are exposed along the margin of the continent from Uruguay to northern Brazil. They comprise several belts. The southernmost one is the Dom Feliciano Belt which extends to southern Uruguay. The regional distribution of the main units of the Dom Feliciano Belt can be observed in figure 2.6 (from Basei *et al.*, 2000).

Prior to the tectonostratigraphic terrane approach, and given the Brasiliano supracrustal successions, granitic intrusions and deformation present in both sides of the Sierra Ballena Shear Zone, it was usually held that the Dom Feliciano Belt in Uruguay extended out at both sides of this shear zone. The Sierra Ballena Shear Zone in Uruguay is the extension of the Dorsal de Canguçu Shear Zone in Brazil. The Dorsal de Canguçu in

Brazil has also been interpreted as a suture zone (Issler, 1982; Fragoso-Cesar, 1991), or as an intracontinental transcrustal shear zone (Tommasi *et al.*, 1994; Fernandez and Koester, 1999). In fact, no evidence that this important lineament constitutes a suture zone has been found to date, and the question of whether this is really a terrane boundary is still a matter of debate.

The Dom Feliciano Belt is related to the convergence of the Rio de La Plata Craton and the Kalahari Craton (Porada 1979) and the closure of the Adamastor Ocean. Fragoso-Cesar (1980) proposed a subduction to the west giving rise to a magmatic arc represented in the Granite Belt of Brazil and Uruguay. Some authors (Fernandes *et al.*, 1992; Sánchez-Bettucci and Ramos, 1999) proposed that the Lavalleja Group might be related to a back-arc basin of the magmatic arc.

Based on radiometric ages and isotopic signatures, Basei *et al.* (2000) posited that the magmatic arc and what they called the “Schist Belt” were produced in separate contexts, and that the two were later juxtaposed in a collisional context. They also suggested that the Gariep and Kaoko Belts of Africa represent back-arc basins related to an eastward subduction of the oceanic lithosphere that ultimately resulted in the collision of the Schist Belt and Granite Belt of the Dom Feliciano Belt. Nevertheless, recent investigations in the Kaoko Belt (Paschier *et al.*, 2002) indicate that the nature of the turbidites and the palaeocurrent directions is connected with a passive margin from the northeast, without evidence of back-arc sedimentation associated with volcanics. The data of Paschier *et al.* (2002) seems to fit better the model of Porada (1989). It is clear that more research and data are needed to develop an improved geotectonic model for these Brasilano/Pan African Belts.

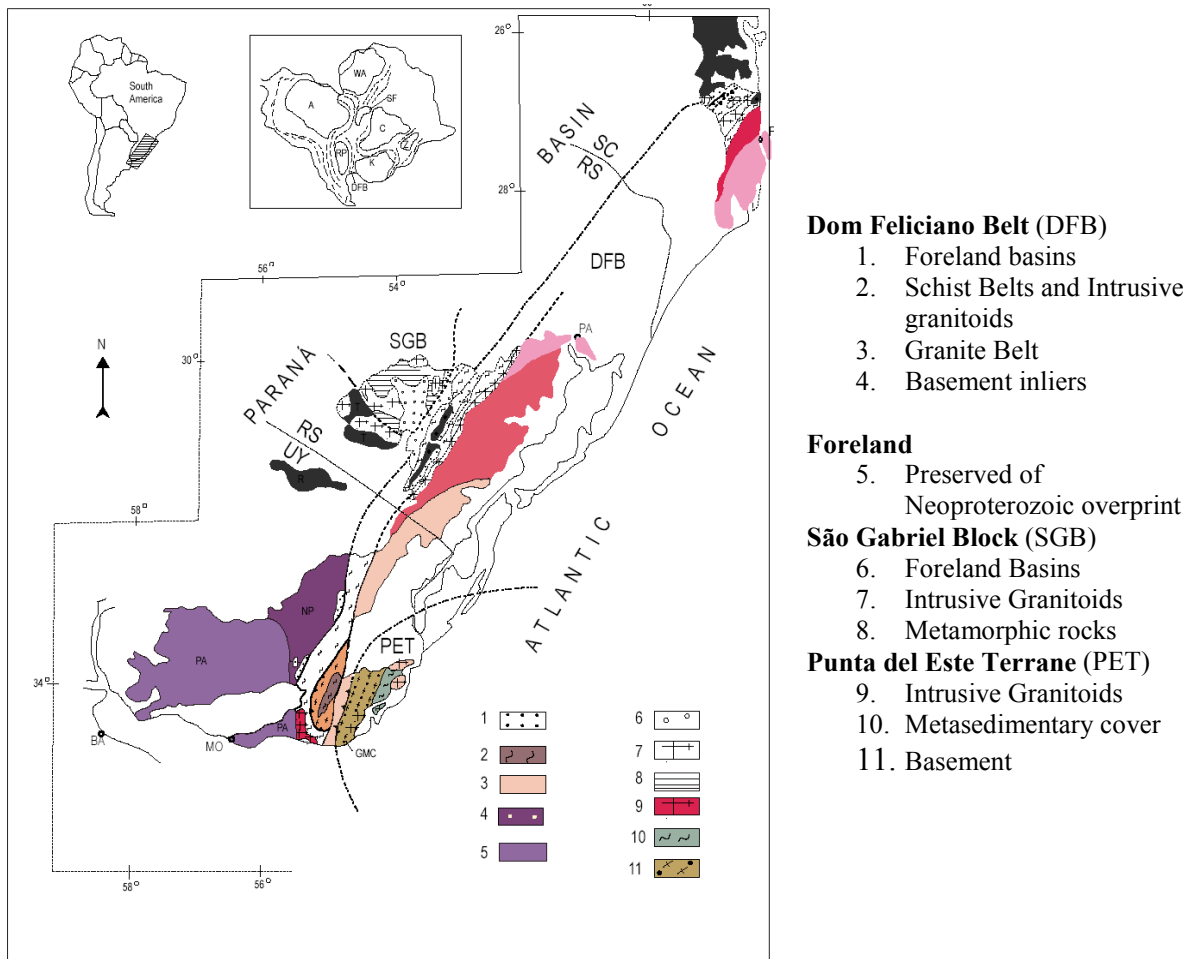


Fig 2.6 - Geological Map of south-eastern Brazil and Uruguay (simplified from Basei *et al.*, 2000). NP: Nico Pérez Terrane, PA: Pietra Alta Terrane, PET: Punta del Este Terrane, SGB: San Gabriel Block, A: Amazonas Craton; C: Congo Craton; DFB: Dom Feliciano Belt; K: Kaoko Craton; SF: San Francisco Craton; RP: Rio de La Plata Craton; WA: West Africa Craton; Z: Zaire Craton; UY: Uruguay; RS: Rio Grande do Sul, Brazil; SC: Santa Catarina, Brazil; MO: Montevidéo; BA: Buenos Aires; PA: Porto Alegre.

CHAPTER 3 LITHOLOGICAL UNITS OF THE STUDY AREA

3.1. Outline of the structure of the area

The geological map of the study area is presented in Map 1 (Appendix 1). Two major shear zones, Sarandí del Yí (SYSZ) and Sierra Ballena (SBSZ), control the structure of the basement. The Cordillera Shear Zone (CSZ), which is a conjugate shear zone associated to the SBSZ, also conditions the distribution of the main lithological units.

The three shear zones mentioned above are the basis for considering five different domains that will be treated independently when describing the different lithological units present in the study area.

The five domains are indicated in schematic form in Table 3.1. The westernmost domain, located west of the SYSZ, corresponds to the Paleoproterozoic Piedra Alta Terrane. The second domain, the Sarandí del Yí Shear Zone, is nearly 10 km thick, and comprises mylonites, a deformed granitic pluton, and a slightly to non-deformed granite intrusion. The third Domain, between the SYSZ and the SBSZ, corresponds to the Nico Pérez Terrane and is composed of a pre-Brasiliano basement, supracrustal successions and Neoproterozoic to Cambrian magmatic rocks. The fourth domain, located between the SBSZ and the CSZ, is represented in the area exclusively by slightly deformed to mylonitic Neoproterozoic granites and mylonites associated with the activity of these two shear zones. The fifth domain, east of the CSZ, comprises pre-Brasiliano basement, a supracrustal succession and Neoproterozoic granites.

3.2. Domain I: West of the SYSZ (Piedra Alta Terrane)

Four main lithological units are present in this domain: mylonites related to a shear zone (called “Cuchilla Cabo de Hornos Shear Zone” here), two granites (Soca and Arroyo Coronilla), and a very low-grade sedimentary succession.

Domain		I	II	III	IV			V			
		West of SYSZ	SYSZ	SYSZ – SBSZ			SBSZ - CSZ	East of CSZ			
Strain partitioning		Low Strain	High Strain	Low Strain			H-S	L-S	H-S	Low Strain	
Terrane		Piedra Alta		Nico Perez			Las Cañas Shear Belt		Punta del Este		
Neoproterozoic – Cambrian	Vendian to Cambrian	<i>Piedras de Afilar F.</i> (sandstones, pelites, limestones) PS	Cerro Caperuza Granite	<i>Sa Animas Cx</i> (alk. volc. and intrusives)	<i>Arroyo del Soldado G.</i> (siltstones, sandstones, limestones) PS	Mylonitic porphyries	Aigua Granite	Florencia Granite	Valdivia Granite.	Mylonitic porphyries	José Ignacio Granite
	Lower Vendian		Solis de Matajojo Cx. Mylonites (sinistral shearing)								
Meso-proterozoic ?		Mylonites (dextral shearing)	<i>Lavalleja G.</i> (basic volc., schists, limestones)								
Paleo-proterozoic		Granites (Soca, Arroyo Coronilla) <i>Cuch. Cabo de Hornos SZ</i> (Mylonites)		<i>Zanja del Tigre G.</i> (limestones, pelites, BIFs) PS	<i>Campanero Unit</i> (orthogneisses, stripped orthogneisses, scapolite-gneisses amphibolites, migmatites and BIFs)					<i>Cerro Olivo Cx.</i> (paragneisses - orthogneisses)	

Table 3.1 - Distribution of the main lithostratigraphic units in the different domains.

PS: platform succession; *italics*: lithostratigraphic names; Cx.: Complex; F.: Formation; G.: Group; alk: alkaline ; calc-alk: calc-alkaline

The **Cuchilla Cabo de Hornos Shear Zone** is composed of mylonites deriving from granitic and para-metamorphic protoliths. The granitic mylonites contain plagioclase and microcline porphyroclasts in a fine-grained matrix composed of quartz, biotite, muscovite and feldspar. The mylonites derived from para-metamorphic protoliths are rich in biotite and graphite, with garnet and sillimanite as common accessories. Retrograde metamorphism is evidenced in neoformation of chlorite and sericite (Spoturno *et al.*, 2005). On a regional scale, the foliation of these mylonitic rocks is deflected by the dextral activity of the SYSZ.

The **Soca Granite** was recently studied by Oyhançabal *et al.* (1998). It is a coarse-grained porphyritic leucogranite with ferrous biotite and ferrous amphibole, high alkalis, Nb, Y and LREE and high K_2O/Na_2O and $FeO^*/[FeO^*+MgO]$ ratios. These characteristics indicate that it can be classified as a rapakivi granite. Bossi *et al.* (2001) determined a U/Pb SHRIMP age on zircon of 2054 ± 11 Ma.

The **Arroyo Coronilla Granite** is medium-grained and leucocratic. It is composed of microcline, orthoclase, biotite, and muscovite (Spoturno *et al.*, 2005). No geochemical or geochronological data is available for this intrusion.

The **Piedras de Afilas Formation** is a succession of sandstones, pelites, and limestones with very low-grade metamorphism. The age is not very well constrained, but taking into account that it is intruded by granite, the minimum age of the succession is thought to be Cambrian (Coronel *et al.*, 1982; Pecoits *et al.*, 2005).

3.3. Domain II: Sarandí del Yí Shear Zone

This shear zone is a large structural lineament, more than 600 km long and up to 15 km wide. Preciozzi *et al.* (1979) recognized this lineament and pointed out that it constitutes the boundary between different provinces in the basement of Uruguay. Bossi and Campal (1992) indicated a dextral sense of shearing for this lineament, while Oyhançabal *et al.* (1993c) demonstrated that the dextral shearing was overprinted by a later sinistral phase. The age of the dextral shearing is not well constrained (Meso to Neoproterozoic).

Three different lithologies are recognized in this domain in the study area: mylonites, a deformed granitic complex (Solís de Mataojo Granitic Complex), and a

slightly to non-deformed granitic pluton (Cerro Caperuza Granite). The mylonites are the country rock of both intrusions.

The **mylonites** of this shear zone range from protomylonites to ultramylonites. The nature of the protolith is normally granitic, but mylonites derived from micaschists and amphibolites have also been recognized.

The **Solis de Matajojo Granitic Complex** is an elongated syntectonic intrusion composed of three main lithological facies: tonalite, granodiorite, and granite. Microstructural features indicate that deformation of this complex began in the magmatic stage and continued at high temperature close to the magmatic solidus. Magmatic fabric, as well as solid-state structures, indicates a sinistral sense of shearing (Oyhantçabal *et al.*, 1993b; Oyhantçabal *et al.*, 2001).

The **Cerro Caperuza Granite** is medium-grained and contains biotite and amphibole (Oyhantçabal *et al.*, 1993c). These authors associate this granite to the magmatism of the Sierra de las Animas Complex. The slightly to non-deformed nature of this intrusion indicates that it was intruded after the main phase of sinistral reactivation of the SYSZ. No detailed petrographic or chemical data is available for this intrusion.

3.4. Domain III: Between the SYSZ and the SBSZ (Nico Pérez Terrane)

3.4.1. Basement: Medium to high-grade rocks (Campanero Unit)

The Campanero Unit was defined as pre-tectonic granitoids with mylonitic to gneissic texture (Sanchez-Bettucci, 1998). The age of this unit is Paleoproterozoic (see detail of available age determinations in chapter 5). During this investigation the different lithologies were identified and mapped: orthogneisses, stripped orthogneisses, scapolite gneisses, amphibolites, micaschists, banded iron formations, and migmatites. A detailed description is presented in chapter 5.

3.4.2. Cover: supracrustal successions

3.4.2.1. Low to medium-grade supracrustal rocks

Lavalleja Group

This unit is a low-grade volcano-sedimentary succession composed mainly of basic volcanics, schists, calc-schists, and limestones.

The basic volcanic rocks are lavas, sometimes with preserved pillow structure, and hyaloclastic rocks. The texture of the lavas is porphyritic with plagioclase phenocrysts in a very fine-grained matrix. The paragenesis is albite, chlorite, epidote, amphibole, and quartz.

The schists and calc-schists preserve the original stratification and the paragenesis is quartz, sericite, carbonate and chlorite.

Midot (1984) indicates a first phase of isoclinal folding overprinted by open to close upright folds of a later event.

Zanja del Tigre Formation

According to Rossini and Legrand (2003) this formation comprises: *i*) a sedimentary sequence composed of limestones, quartzites, pelites, sandstones, and minor BIFs, metamorphosed in lower greenschists facies conditions; and *ii*) a volcano-sedimentary sequence composed of limestones, pelites, and BIFs, interbedded with minor acid volcanic rocks, metamorphosed in upper greenschists to lower amphibolite facies.

Both sequences are in tectonic contact and represent platform deposits of uncertain age (probably Meso- to Neoproterozoic age).

The formation is affected by folding, thrusting, and NNE sinistral transcurrent faults (see Chapter 4).

3.4.2.2. *Very low to low-grade supracrustal rocks*

Maldonado Group

Pecoits *et al.* (2005) defined this group as composed by two formations: Playa Hermosa and Las Ventanas. The group is affected by low-grade metamorphism.

The **Playa Hermosa Formation** is a 1500 m thick succession composed of breccias, conglomerates, diamictites, rhythmites, and pelites (Sánchez-Bettucci *et al.*, 1996; Masquelin and Sánchez Bettucci, 1993). According to Pazos *et al.* (2003) this unit represents the record of the Varangerian glaciation (570-560 Ma) in an unstable tectonic environment. A continuous transition between the Playa Hermosa and Las Ventanas Formations is observed (Pecoits *et al.*, 2005).

The **Las Ventanas Formation** is a volcano-sedimentary succession affected by low-grade metamorphism. The sedimentary rocks are conglomerates, sandstones, and pelites related to sheetflood-dominated alluvial fans and fan deltas. Basic volcanic rocks are interbedded with the sediments (Pecoits, 2003). These basic volcanics will be referred to as “Las Flores basalts,” a lithostratigraphic name already proposed by Oyhantçabal *et al.* (1993a). A Lower Vendian depositional age was proposed for Las Ventanas Formation based on geological and palaeontological evidence (Pecoits, 2003; Blanco and Gaucher, 2004). Pecoits *et al.* (2005) point out that this unit is probably related to a transtensional basin.

Arroyo del Soldado Group

Oyhantçabal *et al.* (2001b) detected the occurrence of the Arroyo del Soldado Group in the study area, formerly recognized only north of the city of Minas.

Only the Yermal, Polanco and Cerro Espuelitas Formations of the Group are present in the area. The Yermal Formation, which represents the onset of the Vendian transgression, is represented by fine sandstones and banded siltstones, and passes concordantly into the carbonates of the Polanco Formation. Cerro Espuelitas includes black shales and BIFs. Bedding and primary sedimentary structures are well preserved. The main structural features are open to closed folds showing a dome and basin interference pattern, and slaty or fracture cleavage.

3.4.3. Granitic magmatism

Several granitic intrusions are present in this domain. A summary of petrographical and chemical features has been recently published by Sánchez-Bettucci *et al.* (2003). These authors recognize a metaluminous to peraluminous suite with medium to high K₂O calc-alkaline affinity (Carapé Granitic Suite), and a metaluminous to peralkaline suite with post-collisional alkaline affinity (Sierra de las Animas Complex).

3.4.3.1. Carapé Granitic Complex

Most of the intrusions are medium to coarse-grained leucocratic biotite granites with near isotropic to slightly foliated texture. The petrographic features of the main intrusions are presented in Table 3.2 and the location of the plutons is identified in Map 1 (Appendix 1).

Pluton	Area km ²	Grain size	Mineralogy		
			Main	Accessories	Secondary
Dos Hermanos	50	Coarse	Qtz, Pl, Or, Hbl, Bt,	Ap, Zrn,	Ep, Ser
La Calera	120	Coarse	Qtz, perthitic Kfs, Mic, Pl, Bt.	Ms	Ep, Ser
Minas	25	Medium	Qtz, Kfs, Pl, Bt	Zrn, Ttn	Ep
Cortez Blanco	25	Medium	Qtz, Pl, Kfs, Bt, Amp	Zrn, Ttn	Ep, Chl
El Renegado	100	Coarse	Qtz, Kfs, Pl, Bt	Ap, Zrn,	
Mateo	50			Zr	
Guayabo	115	Medium to coarse	Qtz, Mic, Pl, Bt, Amp.	Ttn, Ap	Ep, Chl
Sauce	10	Coarse	Qtz, Or, Pl, Bt, Amp	Ap	

Table 3.2.- Petrographic characteristics of some intrusions of the Carapé Complex. Modified from Sánchez-Bettucci *et al.* (2003). Abbreviations from Kretz (1983) see Appendix 2.

Sánchez-Bettucci *et al.* (2003) characterized the Carapé Complex as late to post orogenic, with petrographic and geochemical characteristics of mature magmatic arcs.

3.4.3.2. *Sierra de las Animas Complex*

This complex is a bimodal magmatic assemblage comprising mafic and felsic rocks (Oyhantçabal *et al.* 1993a).

Felsic rocks include alkaline silica oversaturated plutonic, subvolcanic, and volcanic rocks, such as syenites, quartz-syenites, granites, granophyres, quartz-trachytic porphyries, and rhyolites. The syenites and the quartz-trachytic porphyries are composed of orthoclase, aegirine–augite, Na-rich amphiboles, and quartz.

The mafic rocks (Las Flores basalts) are amygdaloidal basalts, dolerite dikes, and hyaloclastic breccias. The petrography is described in detail in chapter 6.

These rocks are overprinted by very low to low-grade metamorphism, which could be correlated to the low-grade metamorphism described in the Las Ventanas Formation by Pecoits (2003). As no differences have been recognized, it is proposed here that the volcanic rocks interbedded with sediments in the Las Ventanas Formation (Pecoits, 2002) correspond to the magmatism of the Sierra de las Animas Complex. Basic dikes intruding the Maldonado Group suggest that the time span for the basic magmatism of the Sierra de las Animas Complex was long. Field evidence of coeval basic and acid dikes was found during this investigation.

The emplacement of this complex appears to be regionally controlled by the Sarandí del Yí Shear Zone and the Sierra de Cabral drag-fold (see Chap. 4), while the strike of the dikes is normally 040°.

Available age determinations (K/Ar WR and Rb/Sr isochrons) indicate a Neoproterozoic to Cambrian age (615±30 Ma and 490±15 Ma) see table 8.4.

3.5. Domain IV: Between the SBSZ and the CSZ (Las Cañas Shear Belt)

This domain is composed exclusively of rocks related to the activity of the SBSZ and the CSZ: synkinematic granitoids, mylonitic porphyries, and mylonites derived from the first.

3.5.1. Mylonitic porphyries

These deformed porphyries are one of the most outstanding features of the Sierra Ballena Shear Zone because they are highly resistant to weathering and form very elongated hills (*Sierra Ballena* and *Sierra de los Caracoles* in the southern part of Uruguay and *Cerro Largo* in the north) contrasting geomorphologically with the surroundings.

These rocks are black-coloured, when not weathered, and show a very fine-grained banded matrix with small feldspar phenocrysts. They occur as folded bodies up to 200 m thick, emplaced in mylonitic rocks of granitic protolith. The emplacement of these porphyries as dikes in a granitic mylonite country rock can be clearly observed in the case of narrow bodies at the outcrop scale. Thick bodies develop colluvium and their relation to country rock is not normally exposed.

The texture is porphyritic with euhedral alkali feldspar phenocrysts (about 0.5 x 0.2 mm). Where the strain is low, the euhedral shape is very well-preserved, while as the strain increases, fractured crystals, undulose extinction, and subgrain development can be observed.

Quartz phenocrysts (about 0.5 mm) are also common in some outcrops. They show undulose extinction and subgrain development and sometimes recrystallization to very elongated quartz aggregates (ribbons).

The matrix is composed mainly of very fine grains of anhedral quartz and feldspar. Thin layers of opaque minerals, segregated during deformation, form a banded flow texture, which wraps the phenocrysts.

The quartz-rich bands of the matrix show an SC structure where elongated, and, in variable degree, dynamic recrystallized quartz grains form an S plane affected by the shear planes.

Mafic minerals are scarce. The most frequent is a Na-amphibole with pale blue to yellow pleochroism occurring in fine needles (about 0.02 mm long) and occasionally associated to aegirin-augite. Very fine biotite flakes are also present in some cases. Euhedral pyrite cubes are frequently recognized.

3.5.2. Granitic mylonites

A strong mylonitic foliated matrix wrapping alkali feldspar and plagioclase porphyroclasts is observed in these rocks.

The porphyroclasts are usually more or less rounded. The geometry of the recrystallized tails indicates σ -type morphology. Alkali feldspar porphyroclasts are usually pink-coloured and range from 5 mm to 5 cm, while plagioclase porphyroclasts are white-coloured and 3-10 mm sized. The porphyroclasts show core and mantle structures, bent twins, and subgrains, and are frequently fractured, with the necks filled with quartz (Fig. 3.1c). The microstructures observed in quartz include ribbons, subgrains and dynamic recrystallization to very fine-grained quartz.

The main ferromagnesian mineral is biotite. Pleochroism is brown to brownish-yellow, while a younger generation of biotite linked to epidote shows pleochroism in greenish tints.

Accessories include allanite and epidote, often in trains of grains. Spene is another frequently-found accessory mineral, usually in euhedral crystals wrapped by the mylonitic foliation.

Pegmatitic and quartz dikes, interpreted as syn-magmatic to the protolith, are frequent in these granitic mylonites and are also strongly folded and deformed (see Fig. 4.5).

3.5.3. Phyllonites

The phyllonites are very fine-grained and display compositional layering. On a microscopic scale, they show small rounded porphyroclasts (0.3 – 0.7 mm) in a very fine-grained matrix rich in white mica. The distribution of the micas around the porphyroclasts is asymmetric, pointing out the shear sense (sinistral).

Muscovite mica fishes are also present. Quartz is segregated into very elongated and partially recrystallized ribbons. Epidote and opaque minerals are also present in trains parallel to the mylonitic foliation.

The mica-rich matrix is fine-layered (0.2-0.5 mm thick layers) and slightly pleochroic in brownish tints, a feature associated with tiny biotite laths. The main orientation of the phyllosilicates is parallel to the layering, but there is also C' foliation

(extensional crenulation cleavage) with obliquely-oriented phyllosilicates (see figure 3.1e). When fine quartz layers are present they also evidence an SC structure. Epidote is especially abundant in these same layers and could be related to a breakdown of plagioclase. Tourmaline, carbonate, and relicts of sphene are frequent accessories.

The protolith of these mylonites is not evident, but the presence of K-feldspar and plagioclase porphyroclasts suggests that the influx of fluids causing syntectonic alteration could be the source of the mica-rich matrix. Studies in other large shear zones (Imber *et al.*, 1997 and references therein) indicate that in mid-crustal conditions phyllonites can derive from granitic protolith through comminution of feldspar and retrograde alteration to phyllosilicates such as muscovite.

3.5.4. Synkinematic granitoids

Maldonado Granite

This granite is an elongated body emplaced between Sierra Ballena and Cordillera Shear Zones. Three facies have been recognized: i) porphyritic biotite granite, ii) granodiorite and iii) leucocratic granite. The intrusion shows signs of high temperature magmatic and subsolidus deformation and displays evidences of important flattening and a vertical stretching lineation. Petrographic details are presented in chapter 6.

Aiguá Granite

This pluton is an elongated body in contact with mylonites of the Sierra Ballena Shear Zone to the west, and with the Florencia Granite to the east.

The texture is normally porphyritic with microcline phenocrysts, in a medium to coarse-grained matrix with variable development of a protomylonitic to mylonitic foliation. Quartz is anhedral and elongated (5 x 3 mm) and shows evidence of high T deformation (probably sub-solidus), such as chessboard structure and dynamic recrystallization. Alkali feldspar is microcline. Grains exhibit patchy extinction and incipient recrystallization along fractures. Biotite laths (~1 mm) are bent and display dark greenish-brown to brownish-yellow pleochroism. Plagioclase (oligoclase) is subhedral and up to 4 mm in length, and shows bent twins. Sphene, allanite, opaque and apatite are the main accessories, while epidote and muscovite (secondary?) are the main secondary minerals.

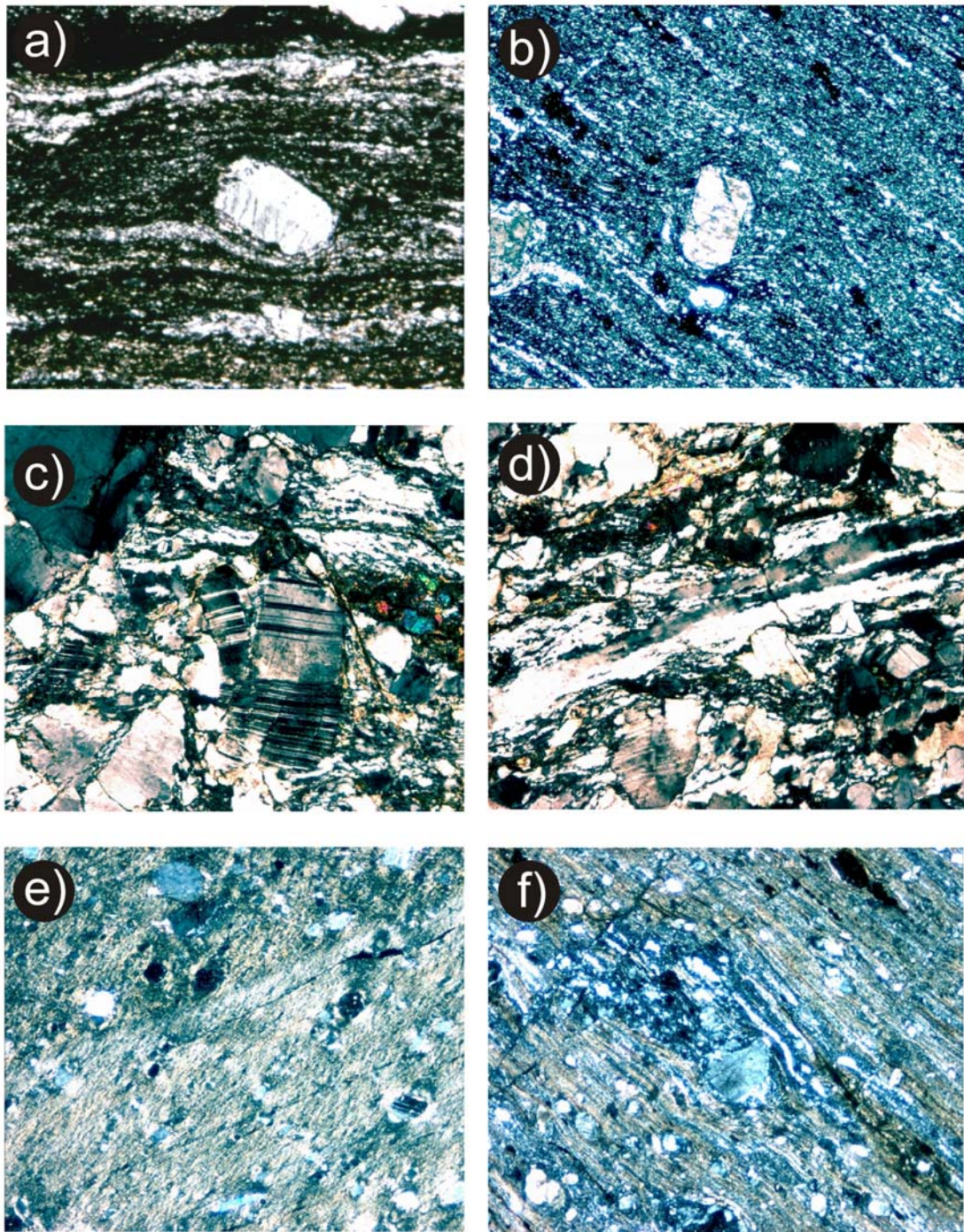


Fig. 3.1 Photomicrographs of mylonitic rocks (width of view 3 mm in all cases)

- a) Mylonitic porphyry. Euhedral phenocryst of K-feldspar in fine grained matrix rich in opaque grains. Plane polarized light.
- b) Mylonitic porphyry. Euhedral phenocryst of K-feldspar in fine grained matrix rich in quartz. δ shaped tails indicate sinistral sense (inverted thin section). Crossed polarized light.
- c) Granitic mylonite. Brittle plagioclase and quartz deformed by regime 2 dislocation creep. Crossed polarized light.
- d) Granitic mylonite. Coalescence of Quartz. Ribbons of quartz and rounded feldspar porphyroclasts. Crossed polarized light.
- e) Phyllonite. Rounded feldspar porphyroclasts. Development of layering and oblique C' shear band cleavage. Crossed polarized light.
- f) Quartzo-feldspathic ultramylonite. Quartz segregated in layers dominated by quartz ribbons. Fractured feldspars wrapped by matrix. Crossed polarized light.

Preciozzi *et al.* (1993) published a Rb/Sr WR age of 582 ± 31 Ma ($R_0 = 0.7232$), while Basei *et al.* (2000) reported U/Pb ages on zircon of 572 ± 2 Ma and 587 ± 16 Ma for two granitoids of the Las Cañas region. Even though the exact location of the samples is not disclosed, given their general location, they probably correspond to the Aiguá and Florencia Granites.

Florencia Granite

It is an elongated pluton located between the Aiguá and Valdivia Granites.

According to Ledesma and Piñeiro (unpublished), it is protomylonitic granite composed of microcline, muscovite and some biotite. Preciozzi *et al.* (1993) reported a Rb/Sr age of 591 ± 95 ($R_0 = 0.7047$) for this pluton.

Arroyo de los Píriz Granite

This pluton is also an elongated body emplaced directly in the eastern SBSZ in the central part of this domain. The granite is nearly isotropic to slightly foliated, usually medium-grained, equigranular to porphyritic with K-feldspar megacrysts. A biotite and muscovite-rich facies has been recognized, and muscovite pegmatites are common.

Petrographic details of this granite are not yet available.

3.6. Domain V: East of the CSZ

3.6.1. Basement

The basement of the domain east of the Cordillera Shear Zone is composed of banded gneisses with garnet and sillimanite and hypersthene gneisses. They correspond to the Cerro Olivo Complex of Masquelin (2004).

The high grade paragneisses are banded rocks with general trend of the foliation ranging between 060° and 140° . Tight and near similar isoclinal folds are a common feature. Small sinistral shear zones associated to deflection of an older foliation usually cut this lithological unit (see Fig. 4.16).

These rocks are light coloured and have a granoblastic texture. Banding is related to differences in grain size and modal composition. The yellowish bands are finer grained (0,1 – 0,2 mm) and have more quartz and garnet, while grey bands are coarser grained (near 0,5 mm) and richer in feldspar.

At the microscopic scale, the texture is granoblastic and triple points between feldspar are common.

Quartz is the main component of these rocks. It is anhedral, near 0,2 mm sized, round shaped and has undulose extinction. Fine rutile needles included in quartz grains were sometimes observed.

Alkali feldspar (0,2 – 0,5 mm) is anhedral with string and drop perthites.

Plagioclase (0,3 mm) is subhedral, oligo-andesine in composition (An₃₀₋₃₅).

Biotite has *Y-Z*: redish brown, *X*: brownish yellow pleochroism and occurs in 0.2 mm disseminated laths.

Pale brownish yellow garnet occurs as anhedral to subhedral grains (0.1 to 1 mm)

Prismatic sillimanite crystals are oriented parallel to layering and more or less transformed to sericite.

Apatite, rutile and zircon are the main accessory minerals.

3.6.2. Cover

Very low to low-grade supracrustal rocks (San Carlos Formation)

According to Pecoits *et al.* (2005), this formation is a 500 m thick succession of conglomerates, sandstones, and pelites. The conglomerates are polymictic with clasts of granite, schist, and quartzite. The palaeocurrents indicate NE transport direction. These authors also report the presence of *Bavlinella faveolata*, a microfossil typical of Neoproterozoic time. A distal alluvial fan environment is indicated for this unit.

The metamorphism of this sequence has not been investigated, but field observations indicate very low to low-grade metamorphism. An axial plane foliation classified as slaty cleavage is present in the pelites (really metapelites). The S₀-S₁ intersection lineation is oriented 30°/210°, parallel to the orientation of stretching lineations in the Sierra Ballena Shear Zone.

Masquelin and Pías (1989) suggested a transtensional basin for the deposition of this unit.

3.6.3. Granites

Garzón Granite

According to Preciozzi *et al.* (1993), this granite is a complex intrusion including porphyritic granite with microcline phenocrysts, and equigranular biotitic granite. Major element data (Preciozzi *et al.*, 1993) indicates a calc-alkaline peraluminous affinity for this intrusion. These authors also reported a Rb/Sr age of 601 ± 20 , $R_0 = 0.7071$.

CHAPTER 4 MESO AND MACROSTRUCTURES

4.1. Macrostructure

The main structural features at macro scale are represented in the schematic map of figure 4.1. As mentioned in Chapter 3, two main shear zones (SYSZ and SBSZ) control the architecture of the Dom Feliciano Belt in the study area.

4.1.1. Strike-slip shear zones

4.1.1.1 *Sarandí del Yi Shear Zone (SYSZ)*

The SYSZ is a main structural lineament of continental magnitude that strikes from north-western to southern Uruguay (Fig. 2.2). The strike of this structural element varies from NW in the north to NS in the south, with an arc shape. It is associated to a gravity discontinuity (Halinann and Mantovani, 1993) that also indicates its importance. It has long been recognized (Bossi, 1983) that the Florida mafic dike swarm (~1.7 Ga) is deflected by this shear zone, making up a “drag fold”. Oyhantçabal *et al.* (1993c) reported that the foliation of the Cuchilla Cabo de Hornos Shear Zone, in the southern part of the Rio de la Plata Craton, is deflected with a similar geometry. This deviation in pre-existing structures suggests a main dextral event for the SYSZ, affecting a broad zone of basement. The width of the affected area (~ 20 km) can be considered a sign of deep crustal setting. Oyhantçabal *et al.* (*op. cit.*) documented that the outcrop scale kinematic indicators in the shear zone (such as porphyroclasts) evidenced a sinistral sense of shearing, and suggested that the main dextral event was followed by sinistral reactivation. This investigation for the first time proposes that the Sierra de Cabral fold is also a structure originated by rotation of a pre-existing foliation and represents the counterpart of the abovementioned structure in the western part of the SYSZ (Figs. 4.1 and 4.2). The Sierra de Cabral fold also has a half-wavelength of nearly 20 km and seems to be related to a ductile crust.

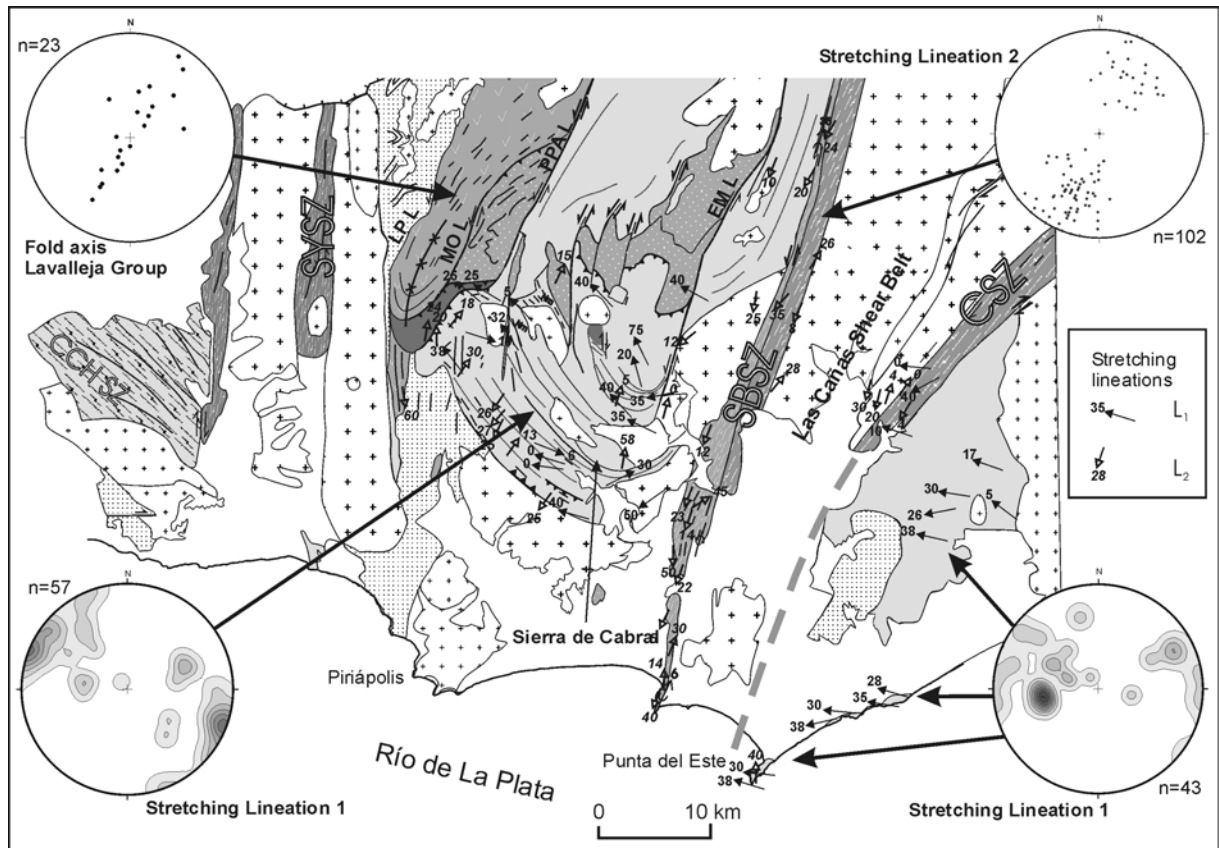


Fig. 4.1 – Structural Map of the study area.

Shear Zones: SBSZ: Sierra Ballena, CSZ: Cordillera, SYSZ: Sarandí del Yi, CCHSZ : Cuchilla Cabo de Hornos.

Lineaments: LP L: La Plata, MO L: Mina Oriental, PPA L: Puntas de Pan de Azucar, EM L: Edén de Mataojo.

Stereograms: Schmidt, lower hemisphere. Contours: 1, 3, 5... times uniform distribution

4.1.1.2. Sierra Ballena and Cordillera Shear Zones

The other main tectonic lineament is the Sierra Ballena Shear Zone (SBSZ). This is a continental-scale structure correlated to the Dorsal de Canguçu of southern Brazil (Fernandez and Koester 1999). The sinistral sense of shearing is documented in the area by deflection of the pre-existing structure of the basement. Deflection of the regional structures can be clearly observed in satellite images of the surrounding areas of towns Eden de Mataojo and Aigua in the western side of the SZ (see schema in Fig. 4.2). There is also a system of left-lateral faults parallel to the SZ that displaces the supracrustal sequences and their tectonic contact with the basement.

Rocks not affected by the SBSZ could be recognized to the west of a lineament located east of the town of Eden de Mataojo, which strikes 017° , and east of another

lineament that strikes 033° (see Fig. 4.1). The name “Eden de Mataojo Lineament” is proposed here for the former, while the latter corresponds to the “Cordillera Shear Zone” of Masquelin (1990).

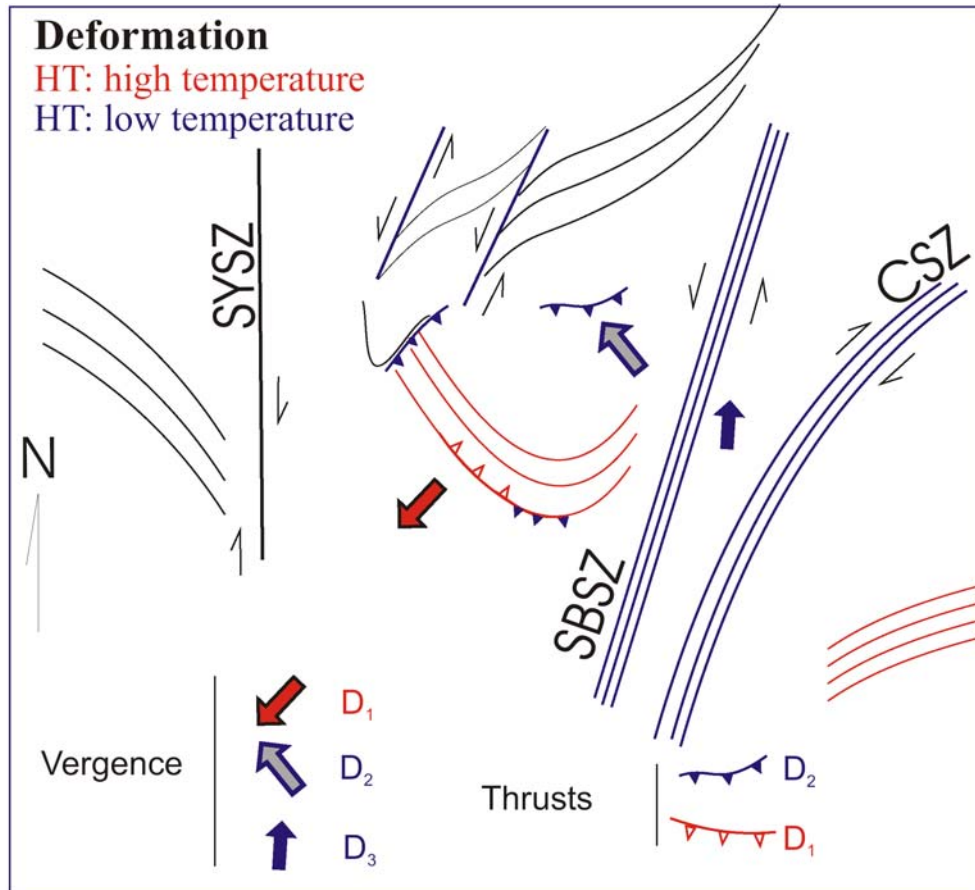


Fig. 4.2 – Structural schema for the study area. D₁, D₂ and D₃: deformation phases. Other abbreviations see Fig. 4.1

The definition of the Sierra Ballena Shear Zone that has been used to date only takes into account the mylonites that have a high-relief contrast with the surroundings, namely those from porphyry and quartz protoliths, having a maximal width of up to 5 km. However, rocks genetically related to or affected by the sinistral shearing activity of the Sierra Ballena Shear Zone -including syntectonic granitoids, granitic mylonites, ultramylonites, mylonitic porphyries, and transposed-reworked basement- have in fact been found in the area between the Eden de Mataojo Lineament and the Cordillera Shear Zone, with a maximal width in the area of more than 30 km.

The dextral Cordillera Shear Zone is considered a conjugate shear of the SBSZ. Ramsay (1980) indicated that ductile shear zones normally occur in conjugate sets, that the

obtuse angle faces the main shortening direction, and that generally one of them occurs later and displaces the older of the two. All these features are observed in the case of the Sierra Ballena and Cordillera Shear Zones. The influence of the Sierra Ballena SZ determines a sigmoidal shape (S-C like geometry) in the Cordillera Shear Zone. A similar geometrical feature is observed west of the SBSZ, even at different scales, for example between the SBSZ and the Puntas del Pan de Azúcar Lineament and between the Puntas del Pan de Azúcar and Mina Oriental Lineaments (see Figs. 4.1 and 4.2). Hippertt (1999), reviewing own and published data, indicated that S-C fabrics at thin-section, hand-specimen and outcrop scale, as well as conjugate fault/mylonite zones at map scale define a scale-invariant geometry over ten orders of magnitude. This kind of relation seems to hold also for the Sierra Ballena area.

In view of these findings, we now define the Las Cañas Shear Belt, limited by the Eden de Mataojo Lineament to the west and the Cordillera Shear Zone to the east, as including a conjugate system of mylonite zones and associated syntranscurrent granitoids. Bitencourt and Nardi (2000) used a similar approach to define with broader criteria the Southern Brazilian Shear Belt. The definition of these authors entails in fact a redefinition of the entire Dom Feliciano Belt.

4.1.2. Thrusts

Thrust structures of different structural levels and different vergence are recognized:

4.1.2.1 Low angle shears with vergence to the south

Some low angle high-T shear zones with vergence to the south were recognized during this work in the eastern side of the SBSZ, affecting gneisses and high-T mylonites. The high-T foliation and the structures with vergence to the south correspond to the first deformation stage recognized (D_1 in Fig. 4.2). Also Masquelin *et al.* (2001) reported low angle shear zones with vergence to the south in high-grade paragneisses (Cerro Olivo Complex) in the region west of the city of Rocha.

4.1.2.2. *Low angle faults with vergence to the northwest*

The more prominent thrust structures in the western domain of the Sierra Ballena Shear Zone are those related to the tectonic contact between the medium to high-grade rocks of the basement, and the low to medium-grade supracrustals of the Neoproterozoic cover (Figs. 4.1 and 4.2). These thrusts show vergence to the northwest (towards the foreland) and are associated to a second deformation stage (D_2 in Fig. 4.2). Flat and ramp structures that also have the same vergence were observed affecting limestones of the Zanja del Tigre Formation (Fig. 4.3) and constitute evidence of medium to upper crust conditions during this deformational stage. Lineations related to this structure are $10^\circ/097^\circ$ and are overprinted by later strike slip faults with lineations oriented $15-45^\circ/205-220^\circ$ (related to a third deformation stage, D_3 in Fig. 4.2). The flat and ramp structure indicates tectonic transport to the northwest, while the strike-slip faults are related to the last kinematic stage (D_3).

Tectonic unconformities in low-angle faults showing transport of Las Ventanas Formation metasediments over low-grade metamorphic rocks of the Lavalleja Group also display direction of tectonic transport to the northwest and constrain a maximum Vendian age for this kinematics.

4.1.3. **Folds (Macro)**

Several kilometre-scale folds have long been recognized. One of the more conspicuous, the synform of road Nr. 81, is represented in Fig. 4.1. The axial plane of these folds is normally $020^\circ - 040^\circ$ sub-vertical, while the fold axis has a low to medium dip angle to the southwest or northeast (see also the mesostructures section).

4.1.4. **Structurally-controlled intrusions**

A main feature of the area is the role played by the macrostructures in the emplacement of plutons and subvolcanic rocks.

The observation of the geological map (Appendix 1) indicates that granitic plutons were preferentially intruded between the Sierra Ballena and Cordillera Shear Zones. Examples are the Aiguá, Maldonado, Florencia and Arroyo de la Quinta Granites. The confluence of both shear zones in a triple point could be a major factor in determining the ascent and emplacement of huge amounts of granite magma, as pointed out by Weinberg (2004) for the Borborema Province in Brazil. A schema of the situation in the study area is shown in Fig. 4.4.

The Solis de Mataojo pluton is related to the southern extreme of the SYSZ. Detailed structural studies by Oyhançabal *et al.* (2001a) indicate that a jog in SYSZ is a probable intrusion mechanism.

In the case of the Renegado Granite and the volcanic-subvolcanic Sierra de Las Animas Complex, and even though there are no detailed structural studies available, the relation to the SYSZ and the Sierra de Cabral Drag Fold is evident in the geological map (Appendix 1).

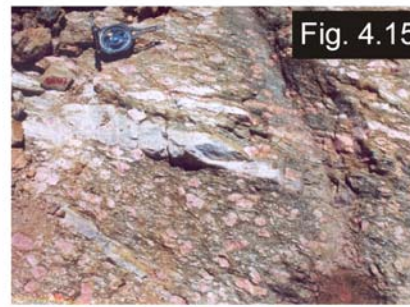
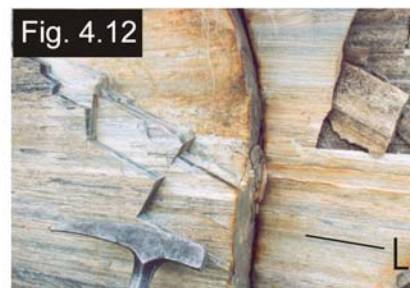
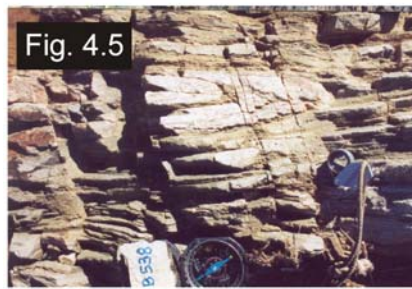


Fig. 4.3 Flat and ramp structure affecting limestones of the Zanja del Tigre Group. Vergence to the northwest (arrow).

Fig 4.5. Tight fold in pegmatite of granitic mylonite

Fig 4.6. Open fold in mylonitic porphyry.

Fig. 4.7. Axial plane fracture cleavage (Sf) in folded mylonitic foliation (Smyl) of mylonitic porphyry.

Fig. 4.12. Stretching lineation (L) in quartz mylonite.

Fig. 4.14. S-C structure in Maldonado granite.

Fig. 4.15. K-feldspar porphyroclasts in porphyritic mylonitic granite.

The 040° preferential strike of the dikes of the Sierra de las Animas Complex is not compatible with the regional stress field for sinistral shearing, and it is a possible indication of an extensional event, also probably recorded in the evolution of the basins of the Maldonado Group and the San Carlos Formation. The hypothesis of an extensional episode is favoured by the alkaline nature of Sierra de las Animas magmatism.

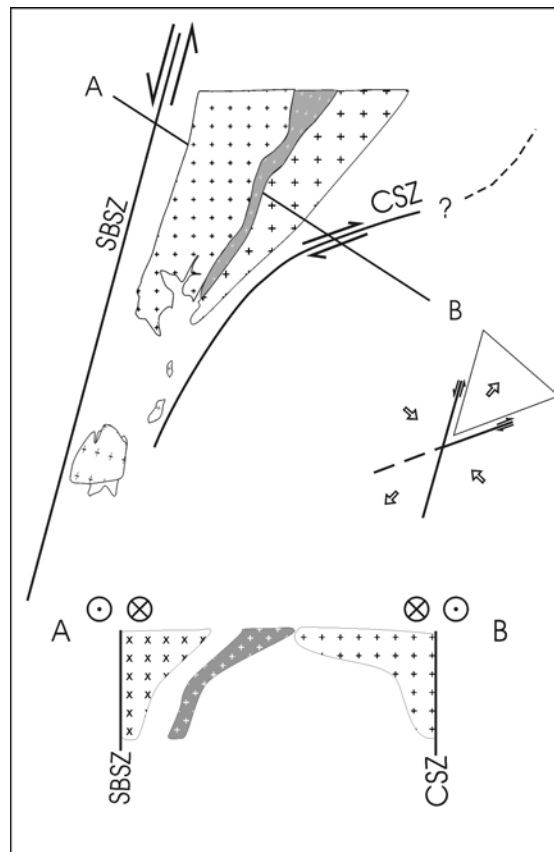


Fig. 4.4 Probable model for the emplacement of Aiguá, Florencia, Valdivia and Maldonado granites in the confluence of SBSZ and CSZ.

4.1.4. Vendian to Cambrian basins

A pull-apart origin for the basin associated with the deposition of these sediments was proposed by Masquelin and Sánchez-Bettuci (1993). Pecoits *et al.* (2005) pointed out that the lower Vendian volcano-sedimentary successions of the Dom Feliciano belt (the Las Ventanas, Playa Hermosa and San Carlos Formations) were deposited in tectonic unstable environments and constraint the age of these successions between 600 and 565

Ma. The estimated age interval for the deposition overlaps the period of shearing of the Sierra Ballena Shear Zone.

Some features observed in the Maldonado Group as detachment faults, small thrust planes, talus breccias, conglomerates, and rapid facies changes, are characteristic of strike-slip basins (Nilsen and Sylvester, 1995). These facts together with the sedimentary evidence of tectonic instability pointed out by Pecoits *et al.* (2005), and the subparallel trend of these units to the Sierra Ballena Shear Zone could be considered consistent indications of a connection of these basins with the shear activity. Nevertheless, as pointed out, basic dikes of the Sierra de las Animas Complex intruding the Maldonado Group have a preferential strike of 040° , which could be evidence that the region evolved into an extensional-collapse-dominated regime with an extension direction that was nearly perpendicular to the Orogen.

4.2. Mesostructures

4.2.1.1. Folds in shear zones

Two main kinds of folds were identified in the Sierra Ballena Shear Zone: a first deformational stage (related to D_2) is registered in the mylonites of granitic protolith as tight folds of similar geometry. These folds affect the mylonitic foliation and pegmatitic dikes (Fig. 4.5) already present in the granitic protolith. The attitude of the fold axis is $30-40^\circ/210-220^\circ$ and the shape of the folds is normally non-cylindrical. No folds of this kind are observed in the mylonitic porphyries.

A second deformational stage (related to D_3) is represented by open to closed folds of parallel geometry observed in the granitic mylonites as well as in the mylonitic porphyries, and sometimes displaying axial plane fracture cleavage (Figs. 4.6 and 4.7).

The preferential attitude of the fold axis is $25^\circ/205^\circ$ to $30^\circ/025^\circ$. The parallelism of both generations of folds is explained by the reorientation effect induced by shearing in the fold axes (Berthé and Brun, 1980).

A spherical projection of a D_3 fold evidencing cylindrical geometry is presented in Fig. 4.8.

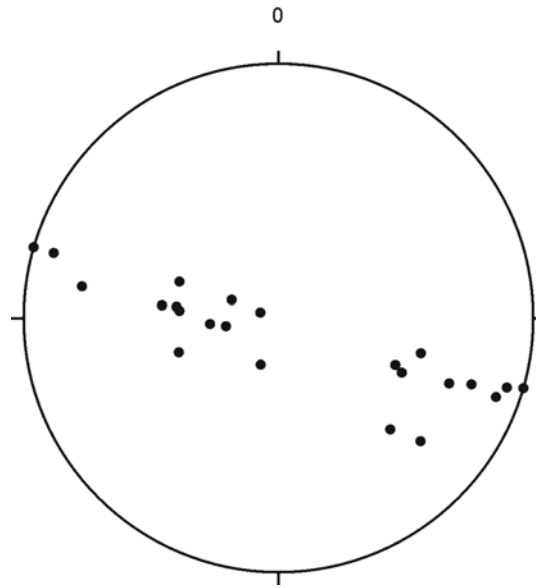


Fig. 4.8.- Poles of mylonitic foliation in a D_3 fold. $N = 22$.

4.2.1.2. *Folds in the Neoproterozoic cover:*

The folding in the superstructure was not the subject of this investigation, but most authors since Midot (1984) agree that at least three different deformation stages can be recognized in the supracrustals of the Lavalleja Group: *i*) early isoclinal folds related to thrusting, peak metamorphism, and development of slaty cleavage; *ii*) folding affecting the slaty cleavage with occasional development of axial plane fracture cleavage; and *iii*) kink folds and faults. These three stages can be correlated with the three deformation stages pointed out in this investigation.

Deformation stage *i*) is present only in the metamorphic rocks of the Lavalleja Group and Zanja del Tigre Formation while in the very low to low-grade rocks of the Maldonado and Arroyo del Soldado Groups -where a good preservation of sedimentary structures is a common feature- only deformation stages *ii*) and *iii*) are observed. This is consistent with micropaleontological data (Gaucher, 2000 and Pecoits, 2003), thus suggesting that these units are younger (Vendian to Cambrian). The fact that the Arroyo del Soldado Group is cut by the Sierra Ballena Shear Zone indicates that it was affected by deformation related to the activity of the SBSZ. The coincidence of the plane containing the stretching lineations of the SBSZ and the plane defined by the fold axis of deformation

stage *ii*) indicates that the second folding stage was contemporaneous with the shearing in SBSZ and is also consistent with available age constraints (see Fig. 4.1).

4.2.1.3. *Tension gashes*

The basement of the domain east of the SBSZ revealed tension gashes oriented about 120° and arranged in shear zones with a 060° strike. The orientation of these gashes is consistent with dextral kinematic indicators observed in the Cordillera Shear Zone and is a symptom of field stress with a NNE-SSW extension direction.

4.2.1.4. *Mylonitic foliations*

High T mylonitic foliation

A high-T mylonitic foliation is present in the rocks of the basement of the eastern and western domains of the SBSZ and is assigned to the first deformation phase (D_1). Although these rocks display a highly deformed fabric at the mesoscopic scale, they do not show significant intracrystalline deformation at the microscopic scale, a fact that could be related to the high temperature of the deformation or to superposed static recrystallization (see chapter 7 for a discussion of this topic). The high-T foliation forms a fold (“drag fold”, see Fig. 4.2) evolving from 260° to 355° strikes, with a maximum at 325°/90°. Fig. 4.9 compares data from this study with data from the eastern side of the SZ (mostly from the basement of the Punta del Este Area). In the eastern side of SBSZ the foliation is strongly reworked by later events.

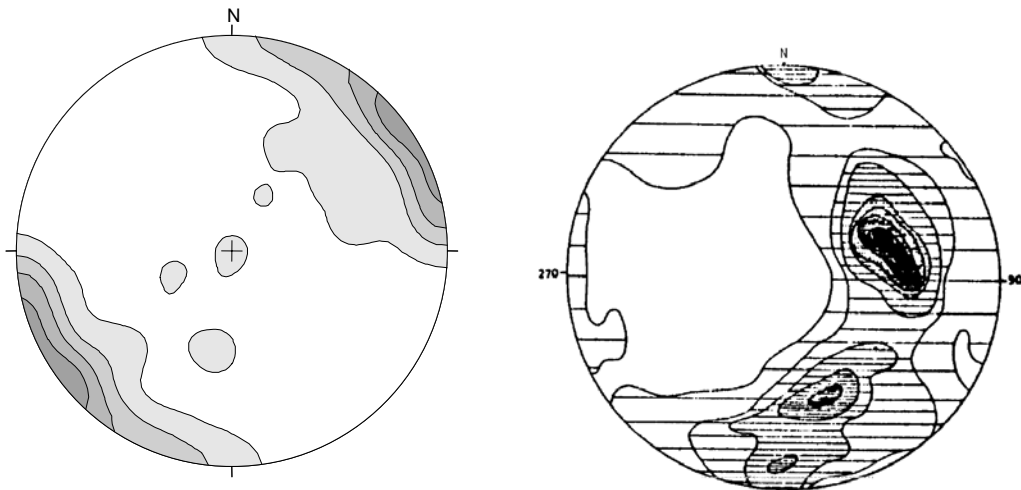


Fig. 4.9.- Density contours of High T mylonitic foliation - left: data gathered in the present study, from the western side of the SBSZ (n = 148); right: data from the eastern side of the SZ, n = 399 (mostly from the Punta del Este Area Basement) from Masquelin (1990).

Medium to low T mylonitic foliations

Medium to low-T mylonitic foliation is characteristic of the Sierra Ballena (strike $\sim 020^\circ$) and Cordillera (strike $\sim 060^\circ$) shear zones, as well as several minor strike slip shear zones with the same kinematics. Two foliations can be recognized in some outcrops of the SBSZ: a younger 020° foliation ($Smyl2_a$) that forms an S-C like structure with the older 065° foliation ($Smyl2_b$). These mylonitic foliations are related to the Sierra Ballena and Cordillera Conjugate Shear Zones, the Cordillera Shear Zone being the earlier-developed of the two (see macrostructure). The influence of both shear systems can be observed in the asymmetric pattern of the density contours of the foliation poles. (see Fig. 4.10).

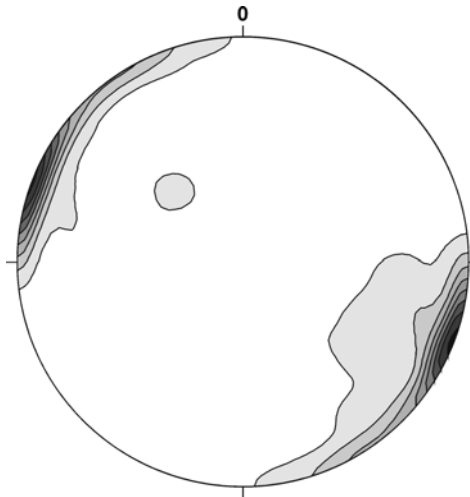


Fig. 4.10.- Density contours of low T mylonitic foliation. $N = 225$. Contours at 1, 3, 5... multiples of uniform distribution.

4.2.1.5. *Stretching lineations*

Two different stretching lineations -related to the high and the medium to low-T deformation respectively- were measured.

Stretching lineations of high-T deformation are evidenced by quartz-feldspar and biotite aggregates. Two maxima can be observed in the contour diagram (Fig. 4.11): i) $0^\circ/290^\circ$; and ii) $40^\circ/260^\circ$, related to eastern and western domains of SBSZ.

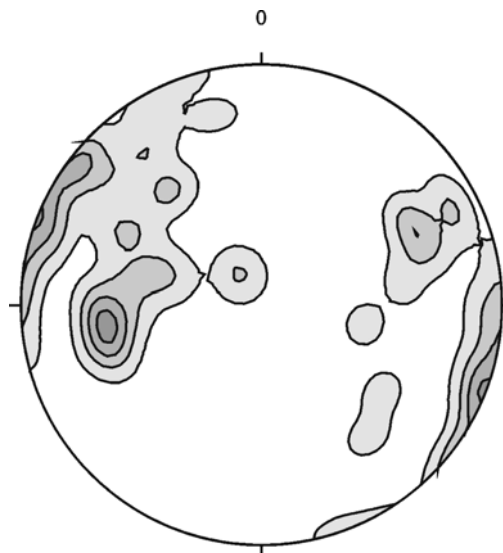


Fig. 4.11. High-T stretching lineations. $N = 100$, contours: 1, 3, 5... multiples of uniform distribution.

The medium-low T stretching lineation has less spread, with a maximum observed at $30^\circ/205^\circ$. A secondary maximum is also observed at $5^\circ/203^\circ$. The typical aspect in outcrop of this lineation is shown in Fig. 4.12.

This low to medium-T stretching lineation is related mainly to deformation phases D_3 , and form an average angle of almost 9° with Sierra Ballena Shear Zone, consistent with the sinistral sense of shearing. If this angle (θ) is used to make a rough estimation of the shear strain (γ , assuming simple shear, and using the relation:

$$\tan 2\theta = 2/\gamma \quad (\text{Ramsay, 1980})$$

a value of 6 is obtained. If simple shear assumption would be acceptable (a fact not confirmed by numerous transpression evidences), considering an average width for the SBSZ of 5 km, this value of γ would imply a displacement of 30 km.

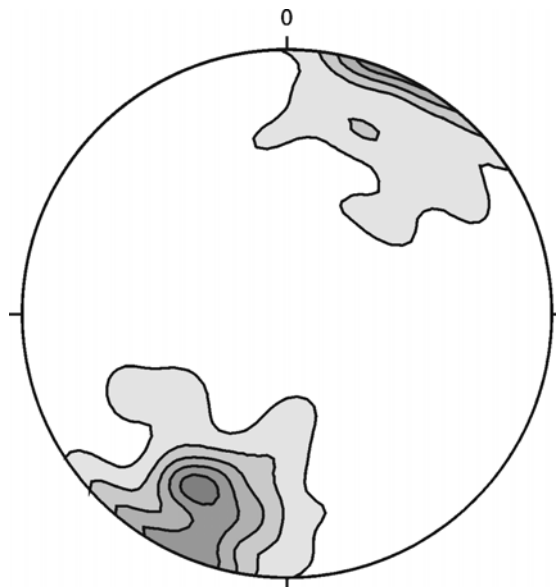


Fig. 4.13. Medium to low-T stretching lineations. $N = 102$, contours: 1, 3, 5... multiples of uniform distribution.

4.2.1.6. Other minor structures

S-C structures.

Sinistral S-C structures are a frequent feature in the deformed rocks of the area. In the syntectonic granites (Maldonado, Solis de Mataojo, Florencia), a C surface oriented 000° - 020° intersects an S surface marked by the shape-preferred orientation of feldspar megacrysts oriented 030° - 045° (Fig. 4.14).

Porphyroclasts

Porphyroclasts are a common feature in the granitic mylonites of the Sierra Ballena and Cordillera Shear Zones (Fig. 4.15). They range from millimetre to centimetre-sized depending on the texture of the protolith and show recrystallization tails with σ and δ shapes. They normally evidence a sinistral shearing sense when the shear zones strike NNE, while shearing sense is dextral when the shear zones strike ENE, pointing to the presence of a conjugate shear zones. From the colour of the feldspar it is usually possible to distinguish K-feldspar (pinkish) and plagioclase (white) porphyroclasts on the field.

In the ultramylonites where porphyroclasts are small and rounded, the sense of shearing can only be established at the microscopic scale.

Minor shear zones reworking older basement

At outcrop scale, and especially in the paragneisses of the eastern domain of the SBSZ, it is common to observe decimetre-wide high strain sinistral shear zones, which are oriented $030^{\circ}/90^{\circ}$, deflecting the previous high-T foliation (Fig. 4.16).

Asymmetric folds

Observed asymmetric folds of low T mylonitic foliation usually display an S shape and are consistent with a sinistral sense of shearing (Fig. 4.17). Some “asymmetrical” folds observed in aerial photographs need to be carefully examined because the low dip of the fold axis, combined with the topography, can lead to erroneous interpretations. In fact, an

outcrop inspection does not always confirm the asymmetric shape of the fold. The obliquity of the fold axis and shear zone is more reliable; at any rate, it confirms the sinistral sense for NNE shear zones.

Boudinage

Boudinage structures are not a common feature in the deformed rocks of the area, probably due to geometric and rheological factors. In the high T deformed rocks of the Sierra de Cabral Area, symmetric boudins were observed in banded amphibolite (Fig. 4.18), oriented consistently with measured stretching lineations ($13^{\circ}/075^{\circ}$). According to the classification proposed by Goscombe *et al.* (2004), they correspond only to tapering boudins with host influx.

Pseudotachylyte veins

Pseudotachylyte veins (1 to 25 mm thick) are a frequent feature in some areas. They display typical branching geometry and the main orientations are 030° and 330° . The former is sinistral while the latter is dextral, indicating conjugate directions (Fig. 4.19). At the microscopic scale these veins are composed of very fine-grained felsic material rich in opaque inclusions, a feature that could be ascribed to recrystallization of the original vitreous component of the pseudotachylyte

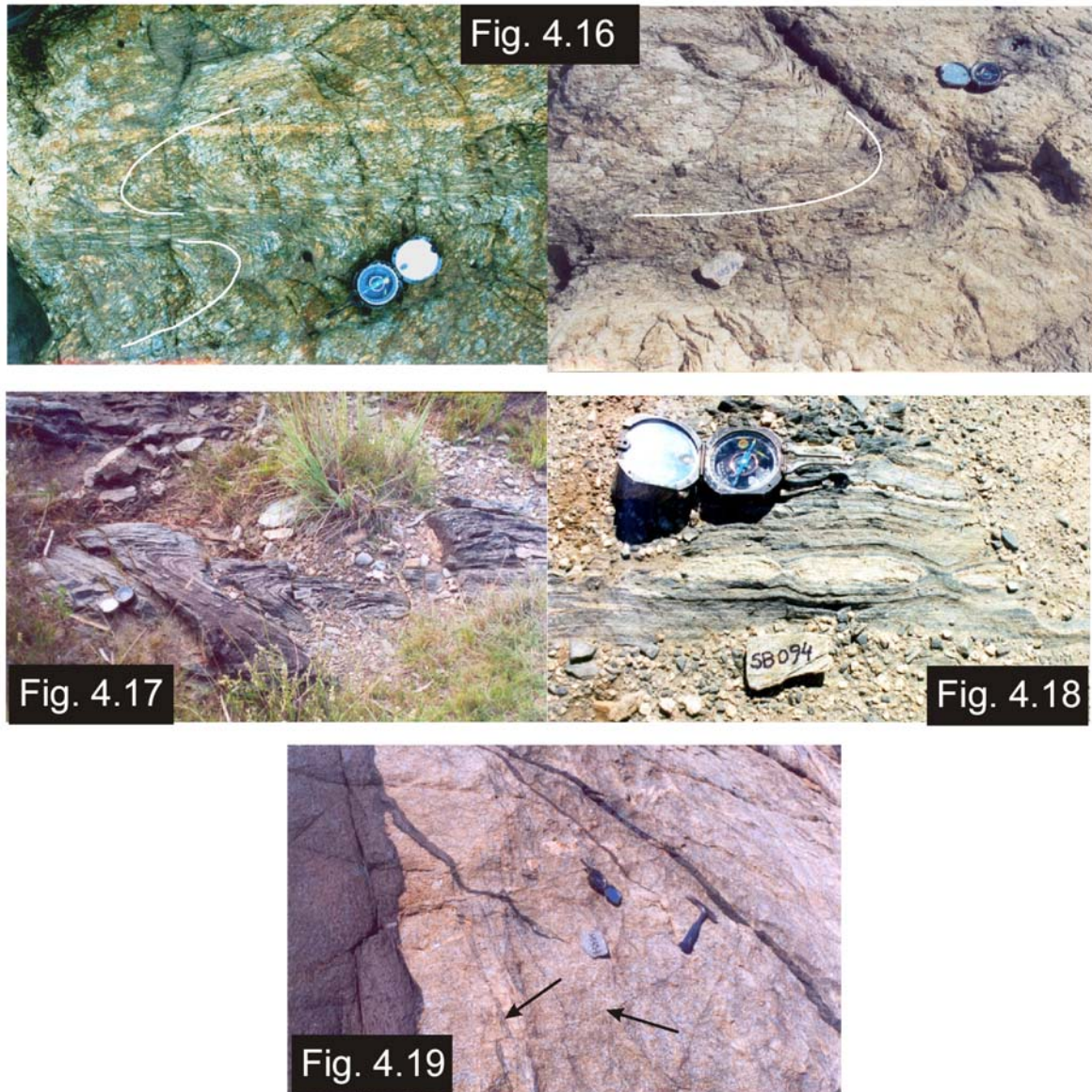


Fig. 4.16. Reworking of the high-T foliation by small shear zones with deflection of the foliation.

Fig 4.17. Asymmetric fold.

Fig 4.18. Boudins in banded amphibolite of Campanero Unit.

Fig. 4.19. Pseudotachylyte veins (arrows) and dolerite dikes in gneisses.

CHAPTER 5 THE PRE-BRASILIANO BASEMENT WEST OF THE SIERRA BALLENA SHEAR ZONE: CAMPANERO UNIT

5.1. Petrography of the main lithologies

During this investigation the following lithologies were identified and mapped in the Campanero Unit:

5.1.1. Orthogneisses and stripped orthogneisses

These felsic rocks are usually fine-grained, leucocratic, light-coloured, and weak to strongly foliated. Elongated feldspar and quartz aggregates define a stretching lineation. At microscopic scale they exhibit granoblastic texture, with feldspars frequently showing straight-grain boundaries and triple joints of nearly 120°.

Quartz is present in three forms: *i*) ribbons (aggregates of up to 30 x 0.5-1 mm of quartz grains with undulose extinction and subgrains); *ii*) coarser elongated grains, approx. 1 x 0.2 mm, with undulose extinction and subgrains; and *iii*) finer grains with nearly normal extinction.

Alkali feldspar is mainly orthoclase, in crystals with straight boundaries, and often with triple junctions of nearly 120°. Equant grains to short prisms of plagioclase (oligoclase ~An₂₀) normally do not display any evidence of significant intracrystalline strain. Myrmekites are sometimes developed in the contacts between plagioclase and alkali feldspar.

The main ferromagnesian minerals are biotite and, sporadically, amphibole. Biotite occurs as disseminated laths (0.2 x 0.05 mm) or as elongated aggregates. Sometimes it is partially altered to chlorite. Amphibole is green hornblende and also usually occurs as elongated aggregates.

Opaque minerals are euhedral magnetite, sometimes occurring in elongated opaque aggregates (trains), associated with sphene. This association may represent the metamorphic transformation of former ilmenite crystals.

These rocks seem to derive from strong deformation of a granitic protolith in medium to high-grade metamorphic conditions. A low-grade overprinting is also observed, represented by chloritization of biotite, neoformation of epidote, carbonate, and, occasionally, prehnite.

A U/Pb SHRIMP age determination on zircon (Mallman *et al.*, 2003) yielded an age of 1754 ± 6.8 Ma, interpreted as the magmatic age. Sánchez-Bettucci *et al.* (2003) reported a conventional U/Pb age determination on zircon with an upper intercept age of $1735 +32/-17$ Ma and a lower intercept age of $723 +240/-210$ Ma. Although these authors offer no interpretation, the first age could be considered the age of magmatic crystallization, while the second could be a rough approximation of the age of deformation-metamorphism.

5.1.2. Scapolite gneisses

These coarse-grained rocks are grey-coloured and display typical gneissic texture. Elongated holes in weathered outcrop surfaces are a characteristic field feature of these rocks.

At microscopic scale, they show granoblastic texture, sometimes with alkali feldspar megacrysts of up to 4 mm.

Biotite is the main ferromagnesian mineral, but in some outcrops ferromagnesian minerals are aegirin-augite and a pale-coloured clin amphibole (optically pargasite), both associated with sphene.

Plagioclase is very abundant and shows evidence of strain, such as tapering deformation twins and bent twins.

Scapolite is Na-rich (marialite) and locally very abundant. Zircon and apatite are the main accessories.

5.1.3. Amphibolites

Amphibolites are present in the central part of this high-grade assemblage, where they are associated with migmatites and BIFs.

They are foliated and sometimes display compositional layering. When they do show layering, dark green to black layers are interbedded with centimetre-scale light green ones. The texture is nematoblastic to grano-nematoblastic.

Euhedral hornblende is the main mineral and is found in grains of about 1-1.5 x 0.15-0.4 mm, with the following pleochroism: *Z* - bluish-green, *Y* - green, and *X* - greenish-yellow. Plagioclase is subhedral with An₅₀ (andesine-labradorite) composition. Anhedral quartz is also present in varying amounts. A pale green aegirin-augite is sometimes present, especially in the light-coloured layers of the banded amphibolites. Sphene occurs as euhedral to rounded grains of nearly 0.1 mm, disseminated in trains, while epidote and apatite are common accessories.

5.1.4. Micaschists

The micaschists have quartz-rich and mica-rich layers defining microlithons, with evidence of important tectonic transposition. Quartz is granoblastic, and straight contacts with mica indicate grain boundary migration. The mica-rich domains are composed of biotite with brownish pleochroism and muscovite. Polycrystalline mica fishes are observed. Garnet porphyroblasts display snowball inclusions indicating growth syntectonic with a first deformation phase (D_n), while porphyroblasts of staurolite are idioblastic, evidencing post-tectonic growth for said deformation event (D_n). Both kinds of porphyroblasts are wrapped by foliation (S_{n+1}), suggesting that they are post-tectonic for a D_{n+1} phase and that staurolite growth was inter-tectonic.

5.1.5. Banded iron formation

Isolated outcrops of magnetitic quartzites associated with the amphibolites were identified. They are coarse grained (0.5 - 2mm) and composed of quartz, magnetite, and pale green grunerite.

5.1.6. Migmatites

The migmatites have stromatitic structure and the leucosome stringers are complexly folded. Based on the definitions of Wimmenauer and Bryhni (2002) and on the

discrete nature of leucosome, melanosome, and mesosome, these migmatites can be classified as metatexites.

The mesosome is medium-grained with anhedral quartz (0.3 - 0.5 mm) displaying normal to slightly undulose extinction, plagioclase, and perthitic orthoclase. Zircon and apatite are the main accessories.

The melanosome is composed of elongated aggregates of biotite (0.5 - 5 mm) with brown to brownish-yellow pleochroism associated with fibrous sillimanite (fibrolite).

The leucosome is coarser-grained and composed of quartz, orthoclase, plagioclase, and small disseminated flakes of biotite.

5.2. Geochemistry of orthogneisses and stripped gneisses of the Campanero Unit

Analytical methods and the results of 19 samples are presented in Appendix 4 (see Table A.4.1).

These leucocratic orthogneisses normally have high SiO₂ contents ranging from 68 to 76%. Two samples yielded results outside this range: sample SB506, with 88% SiO₂, is probably affected by silica enrichment during deformation-metamorphism; and sample SB201, which corresponds to a scapolitic gneiss and has 55.7% SiO₂, displaying a very different composition. These two samples will not be considered in the following discussion of the characteristics of the gneisses.

Major elements

On the AFM diagram (Irvine and Baragar, 1971), the compositions plot in the calc-alkaline field (Fig. 5.1a). Total alkali content is high (Na₂O+K₂O = 6.25 - 9.26 %) and these orthogneisses classify as calc-alkaline in the TAS diagram (Fig. 5.1b), according to the limits set by Irvine and Baragar (1971). On the SiO₂ - K₂O diagram of Peccerillo and Taylor (1976), the compositions plot in the high-K₂O calc-alkaline field (Fig. 5.1.c). The alumina content is medium to high (Al₂O₃ = 11.6 - 16.3%) and most of the samples are slightly peraluminous (Fig. 5.1d). MgO content is very low in most of the samples (< 1%), and CaO content is low (normally <2%).

Trace elements

The pattern of trace elements is characterized by medium to high contents of large ion lithophile (LIL) elements (Ba is normally > 1000 ppm and Sr > 500 ppm), while contents of high field strength (HFS) elements are low (Nb is normally < 20 ppm and Y <16 ppm). The ORG-normalized spidergram (Fig. 5.2) demonstrates a pattern similar to some of the VAG presented by Pearce *et al.* (1984). Chondrite-normalized REE spidergrams are presented in Fig. 5.3. The patterns show slow continuous decrease from La to Lu, without significant Eu anomalies (Eu/Eu* = 0.68 - 1.08). The total content of REE and the LREE/HREE ratio are highly variable (Σ REE = 18 - 970 ppm and CeN/YbN = 74 - 3). The general pattern is comparable to REE patterns of mature active margin granites.

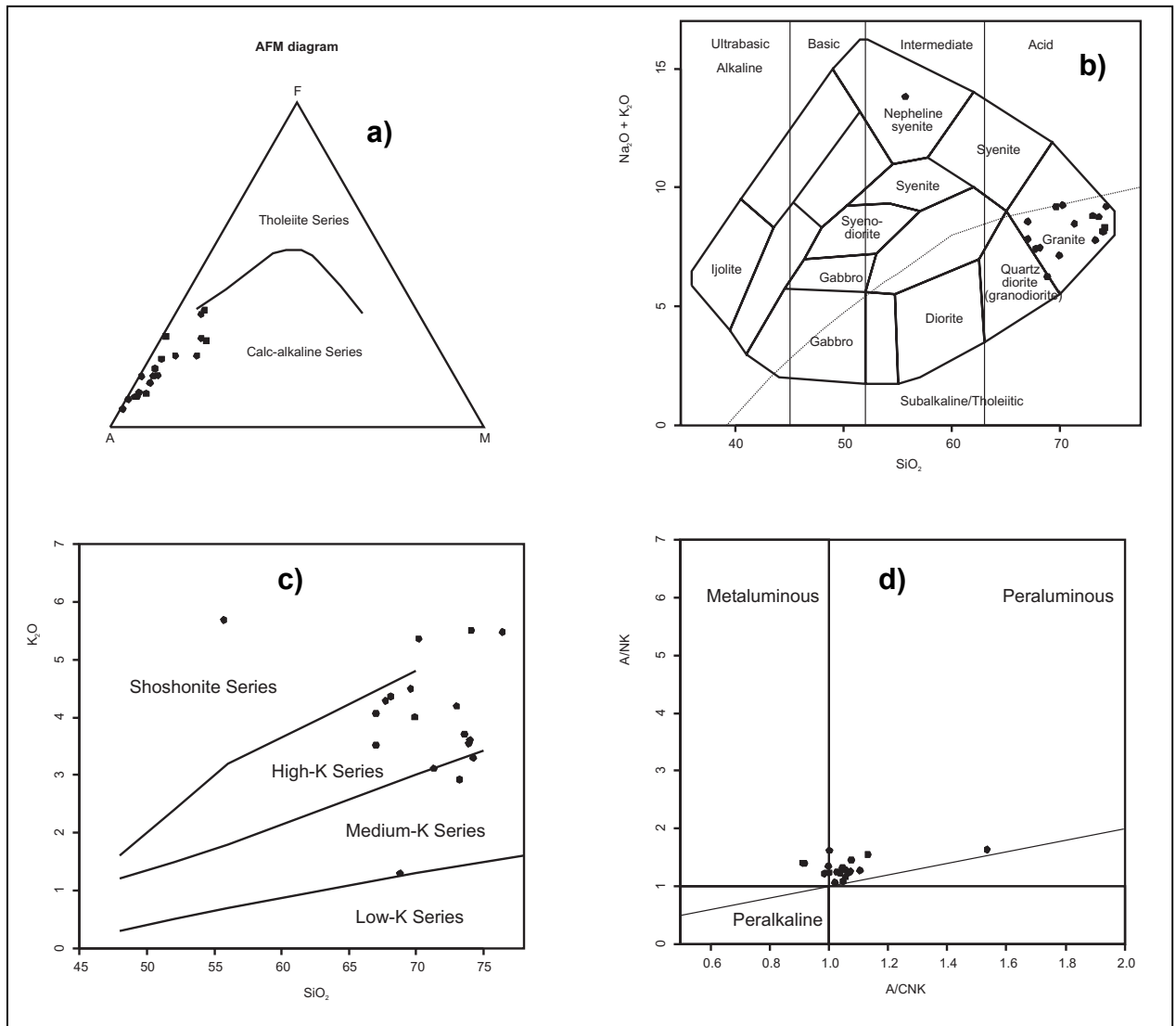


Fig. 5.1 - Chemical classification and nomenclature diagrams for the orthogneisses of the Campanero Unit. a) AFM diagram (after Irvine and Baragar, 1971); b) TAS diagram after Cox *et al.* (1979) with alkaline - subalkaline boundary after Irvine and Baragar (1971). c) K₂O vs. SiO₂ after Peccerillo and Taylor (1976), d) ANK vs. A/CNK diagram of molar ratios after Shand (1943). The outlier corresponds to the sample of scapolite gneiss.

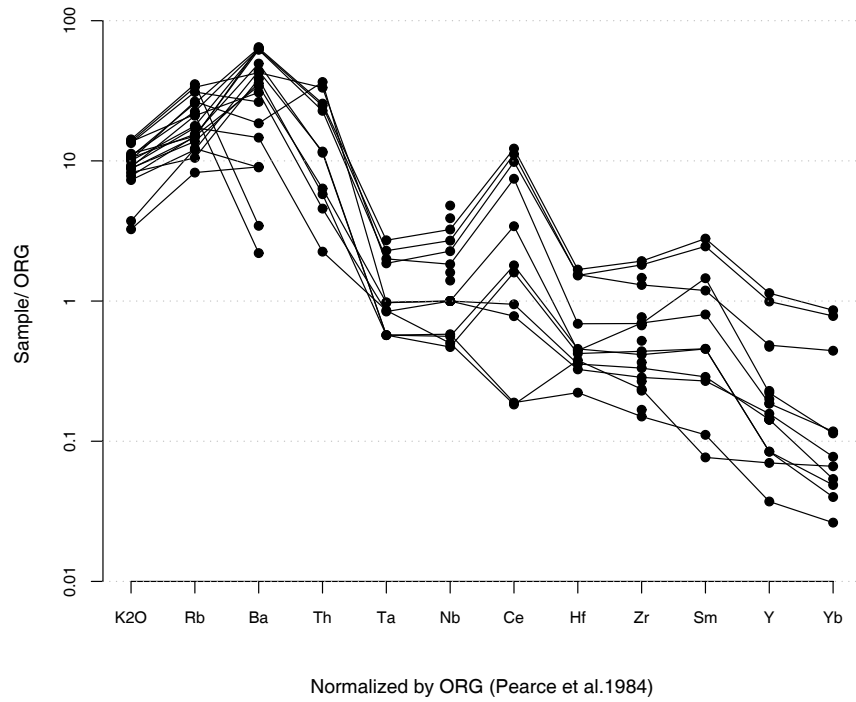


Fig. 5.2 - ORG-normalized spidergram for selected samples of the Campanero Unit orthogneisses.

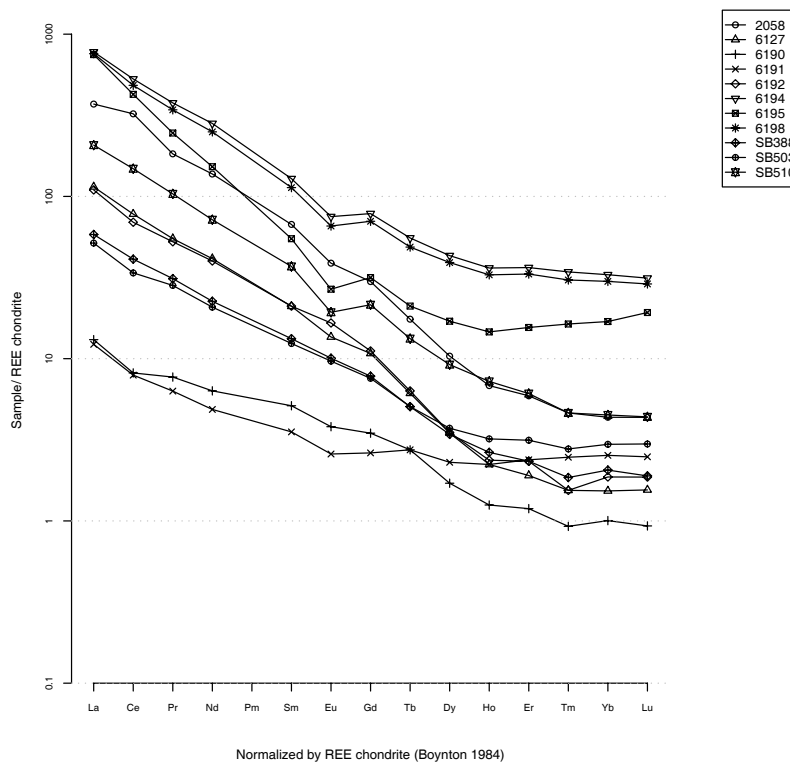


Fig. 5.3 - Campanero Unit orthogneisses: MORB-normalized spidergram for the REE.

Tectonic classification

Figure 5.4 shows the tectonic discrimination diagrams (after Pearce *et al.*, 1984) for the orthogneisses. These diagrams reveal a cluster in the volcanic arc granite field (VAG), and some of the samples plot in the within-plate granite field (WPG). Considering the geochemical affinity of the magmatism, it is concluded that the protoliths of the orthogneisses are granites related to a high K_2O calc-alkaline magmatic arc. The cluster between VAG and WPG in Pearce *et al.* (1984) diagrams probably indicates a post-collisional setting, considering the field for these kind of granites in the $Y+Nb$ vs. Rb diagram defined by Pearce *et al.* (1996).

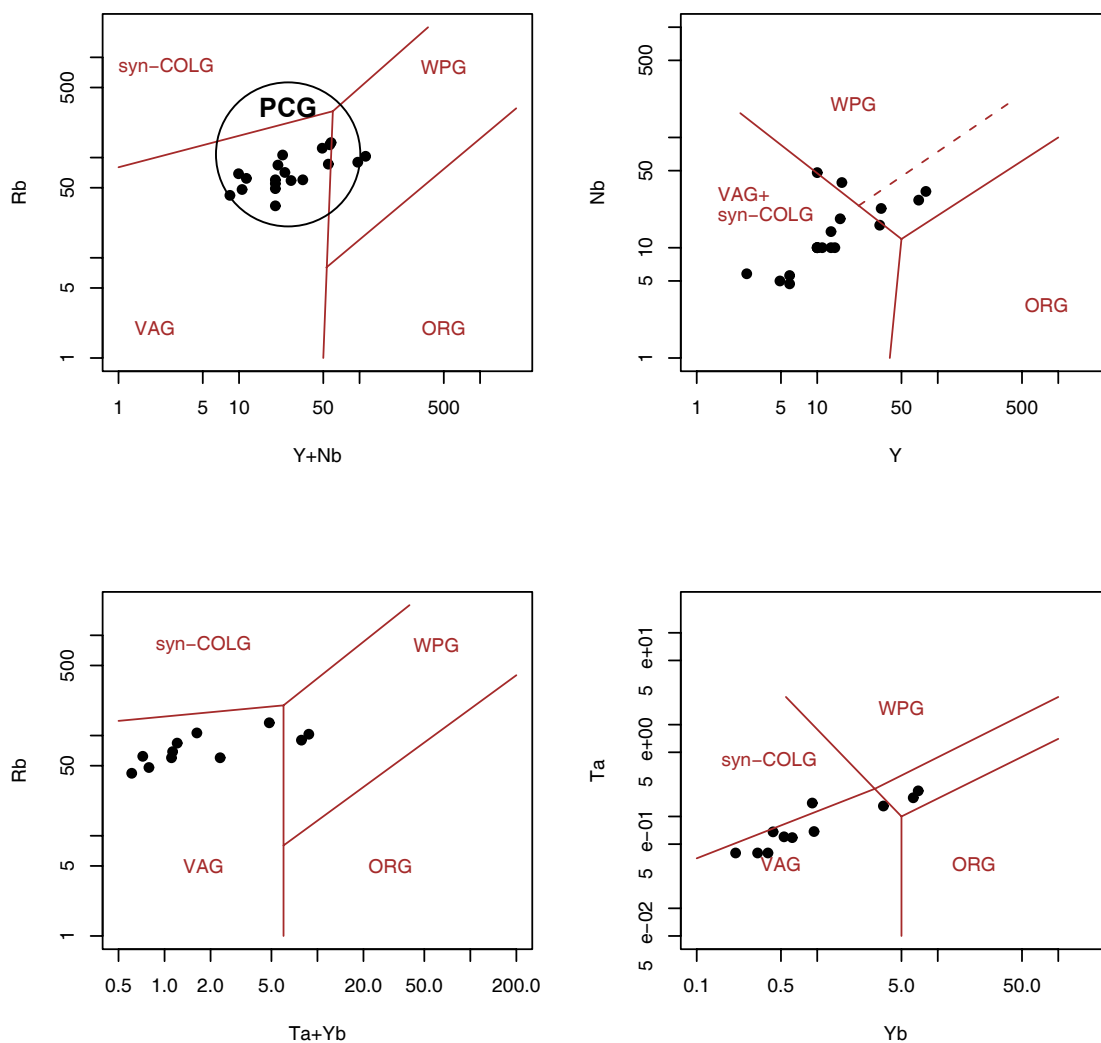


Fig. 5.4 Campanero Unit orthogneisses: tectonic discrimination diagrams after Pearce *et al.* (1984). Post-collision granites field (PCG) after Pearce (1996)

CHAPTER 6 BRASILIANO MAGMATISM: PETROGRAPHIC AND GEOCHEMICAL CHARACTERIZATION OF THREE INTRUSIONS AND ONE VOLCANIC ASSOCIATION

Three granitic plutons (Solís de Mataojo, Maldonado, and Pan de Azúcar), volcanics associated with the Las Ventanas supracrustal succession, and porphyries emplaced in the Sierra Ballena Shear Zone were investigated. A petrographical and a geochemical characterization are presented for each unit.

6.1. Solís de Mataojo Granitic Complex

This Granitic Complex is an elongate intrusive body of about 40 x 8 km, with major axis trending north-south, emplaced in the Sarandí del Yí Shear Zone. Mesozoic sediments cover the pluton to the north, while to the south the Río de la Plata River interrupts the outcrops. Umpierre and Halpern (1971) determined an Rb/Sr WR age of 560 ± 15 Ma, while a new U/Pb age on sphene (584 ± 13 Ma) is presented in this investigation (see chapter 9)

The pluton consists of three main lithological types: tonalites, porphyric granodiorites, and granites, distributed in several intrusive units sub-parallel to the long axis of the Complex (Fig. 6.1).

Tonalite facies occurs mainly in the western portion of the intrusion, forming an intrusive unit with maximum width of 3 km. The tonalite facies is grey and medium-grained, and contains euhedral plagioclase (An_{30} mean composition), quartz, biotite, hornblende, and occasional relicts of clinopyroxene. The most frequent accessories are sphene, zircon, apatite, and allanite. Microgranular enclaves with high aspect ratio are a common feature.

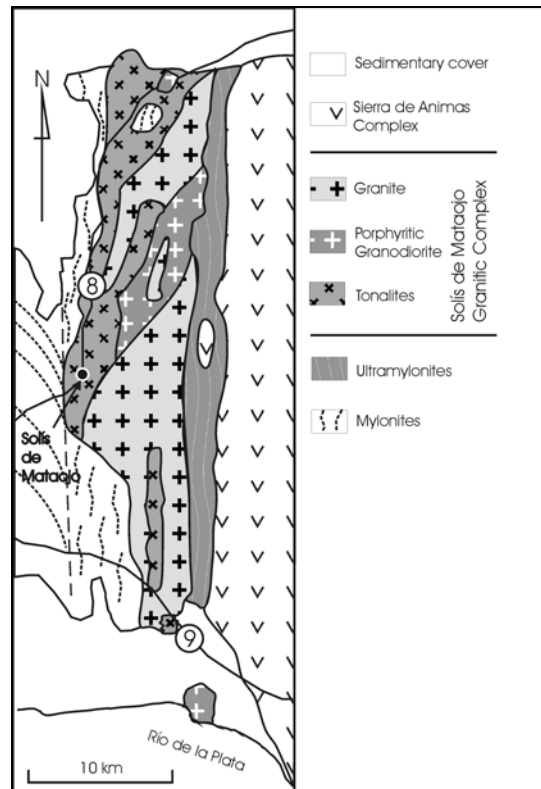


Figure 6.1 - Main petrographic facies of the Solis de Mataojo Granitic Complex.

Granodiorite facies appears in the central portion of the intrusion as discontinuous bands trending north-south. This facies is characterized by megacrysts of microcline 4-8 cm in length, in a medium-grained granular matrix. The mineral composition is oligoclase (An_{25} mean composition), microcline, quartz, biotite, and hornblende. Most frequent accessories are apatite, zircon, sphene, and allanite. Enclaves with high aspect ratios are common.

Granite facies occurs in the central and southern parts of the intrusion. The texture is medium to coarse grained, equigranular, and allotriomorphic. Protomylonitic textures are frequent. The mineralogy includes quartz, oligoclase, microcline, biotite, and muscovite, with apatite and zircon as the most frequent accessories. Where strongly deformed, neof ormation of sericite is observed.

Microgranular enclaves occur in tonalites and granodiorites, and are virtually absent in the granite. They display fine equigranular texture with strong shape-preferred orientation of plagioclase and ferromagnesian minerals. Their main components are plagioclase, biotite, hornblende, and quartz, and accessories are apatite, zircon, and sphene.

The composition of enclaves is quartz-dioritic in the case of tonalites, and tonalitic in the granodiorites.

The western country rocks comprise mylonites which belong to the Sarandí del Yí Shear Zone. Where the deformation is less intense, muscovite \pm biotite \pm quartz \pm garnet \pm staurolite schists, and plagioclase \pm hornblende \pm sphene amphibolites are recognized. Ultramylonites rich in quartz and sericite are also widespread. On the eastern side, rocks derived from the strong deformation of the Solís the Mataojo Complex, as well as quartz \pm sericite \pm chlorite ultramylonites, are observed. Within the SMGC, septa of country rock are frequently observed.

6.1.1. Geochemistry

Nine representative samples from the main facies, ranging from tonalite to granite, and from co-magmatic enclaves of quartz-diorite composition were analyzed at the University of Göttingen (see Appendix 4 for the details of the methods). The compositions are shown in Table A.4.2 (see Appendix 4).

The Harker diagrams (Fig. 6.2) show good negative correlation for TiO_2 , Fe_2O_3 , MgO , and CaO . The alkalis (Na_2O and K_2O) display a positive slope, while the $\text{K}_2\text{O}/\text{Na}_2\text{O}$ ratio, although scattered, increases with SiO_2 content.

Figure 6.3a presents the mesonormative compositions according to Mielke and Winkler (1979), plotted in a Q-ANOR diagram of Streckeisen and Le Maitre (1979). Most of the samples plot in the granodiorite and syenogranite fields in accordance with petrographic data.

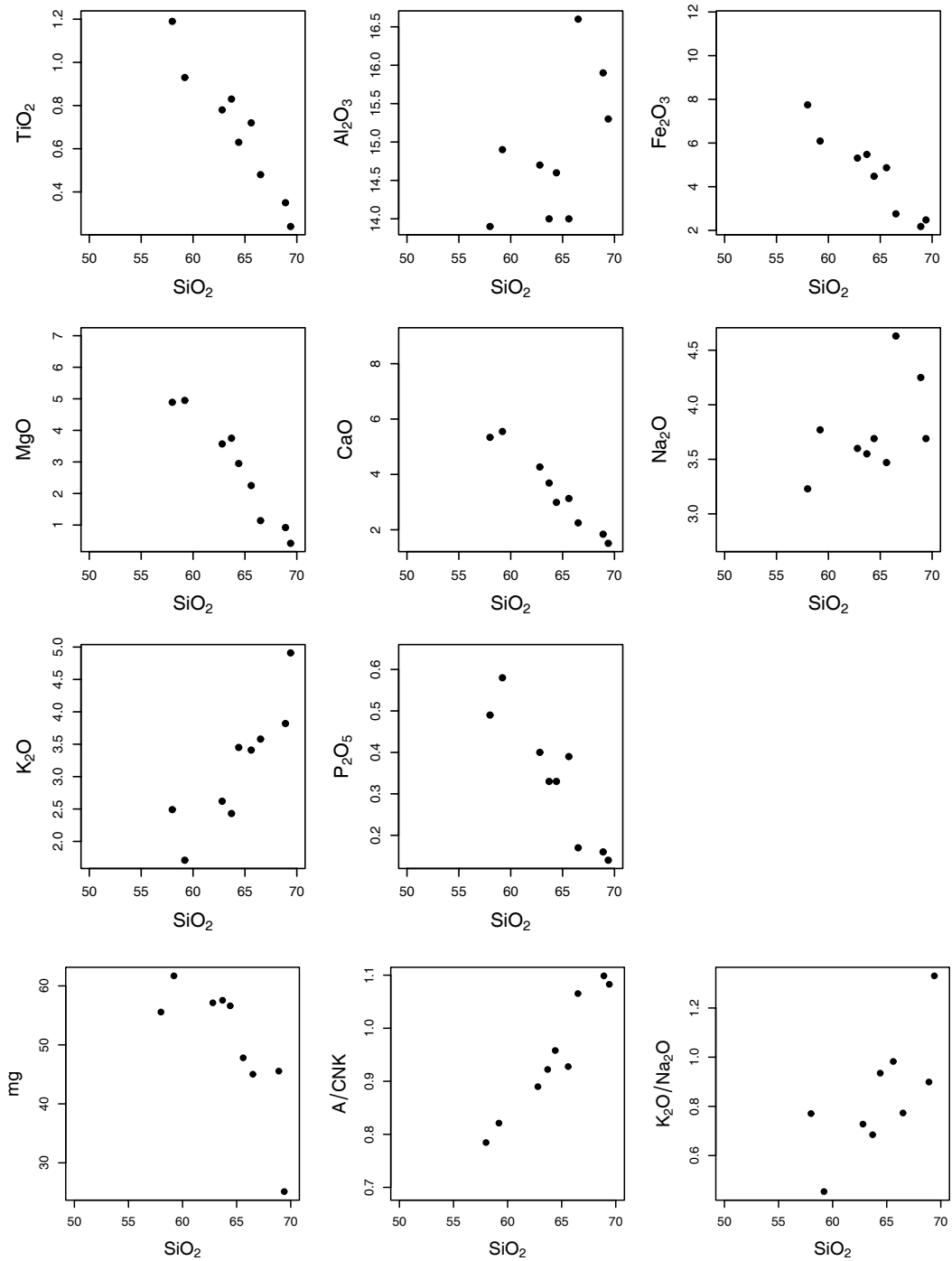


Fig. 6.2.- Solís de Matajo Granite: Harker plots for major elements and some ratios. Oxides in weight %.

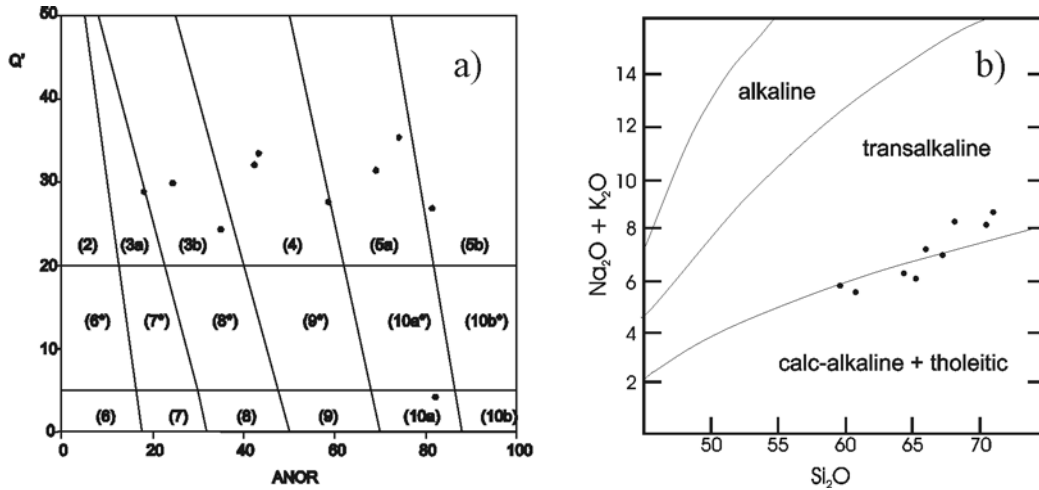


Fig. 6.3.- Solís de Mataojo Granitic Complex: a) Plot of the mesonormative compositions in Q-ANOR diagram after Streckeisen and Le Maitre (1979); b) Calc-alkaline to transalkaline affinity in TAS ($\text{Na}_2\text{O} + \text{K}_2\text{O}$) vs. SiO_2 (wt.%) plot. Fields after Middelmost (1997)

Total alkali content is medium to high (5.2 - 8.6 wt.%). In the TAS diagram ($\text{Na}_2\text{O} + \text{K}_2\text{O}$ vs. SiO_2), according to Middelmost fields (1997), the samples plot in the transition between calc-alkaline + tholeiitic and transalkaline fields (Fig. 6.3b). Na_2O and K_2O contents are approximately similar and in the SiO_2 vs. KO_2 diagram of Peccerillo and Taylor (1976) these granitoids classify in the transition from medium to high- K_2O calc-alkaline magma fields (Fig. 6.4a).

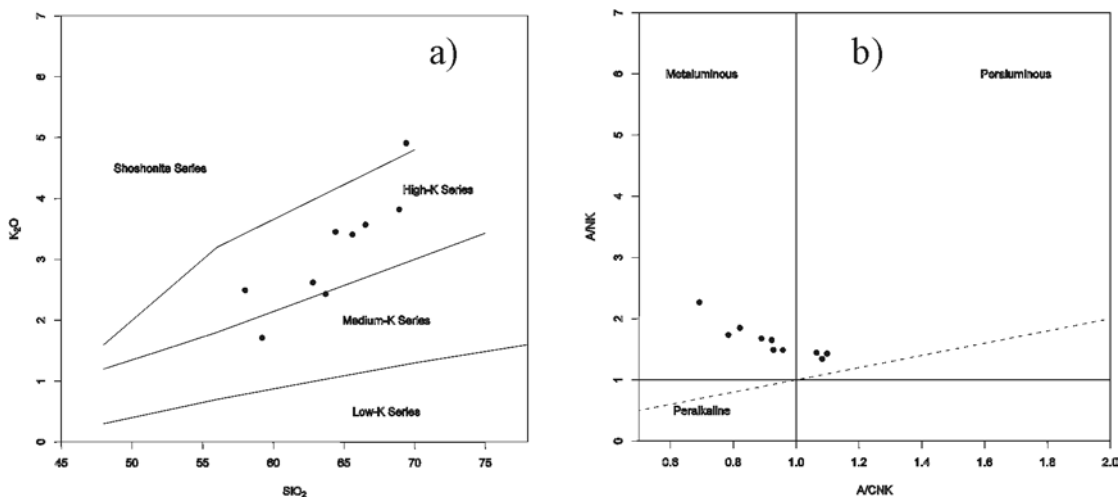


Fig. 6.4.- a) SiO_2 vs. K_2O , fields according to Peccerillo and Taylor (1976); b) Metaluminous character of most of the samples of the Solís de Mataojo Granite. Molar ratios of $\text{A/CNK} = \text{Al}_2\text{O}_3 / (\text{CaO} + \text{Na}_2\text{O} + \text{K}_2\text{O})$ and $\text{A/NK} = \text{Al}_2\text{O}_3 / (\text{Na}_2\text{O} + \text{K}_2\text{O})$, after Shand (1943).

A trend from metaluminous (most of the samples) to peraluminous compositions is observed in the Shand diagram (Fig. 6.4b).

Trace elements

Cr, Ni, Zr, and Y display negative discontinuous trends in the Harker diagrams while for Ba, Rb, and Sr the trends are variable and scattered (Fig. 6.5). The low Nb (9 - 13 ppm) and the high Ba (348 - 2390 ppm) contents are typical of calc-alkaline suites, according to the data presented by Brown (1982).

ORG-normalized spidergrams (after Pearce *et al.*, 1984) for three selected samples of tonalite, granodiorite and granite are presented in figure 6.6a. The most incompatible elements (Rb, Ba, Th) show enrichment while for Hf, Zr, Sm, Y, and Yb concentrations are low to very low. The pattern exhibits a regular decrease in the enrichment factor, with increasing compatibility, similar to the calc-alkaline granites of active continental margins and post-collision settings presented by Pearce *et al.* (1984). LIL and HFS element abundances, comparable to those presented by Brown *et al.* (1984), suggest a continental arc of normal maturity.

The RREE spidergrams normalized to chondrite display moderate REE contents ($\Sigma\text{REE} = 123\text{-}223$ ppm) and regular decrease from La to Lu without Eu anomalies (Fig. 6.6b). Ce_N ranges from 70 to 120, and the Ce_N/Yb_N ratio from 11 to 46. These parameters and the absence of Eu anomaly are similar to that indicated by Cullers and Graf (1984) for calc-alkaline granites of active continental margins.

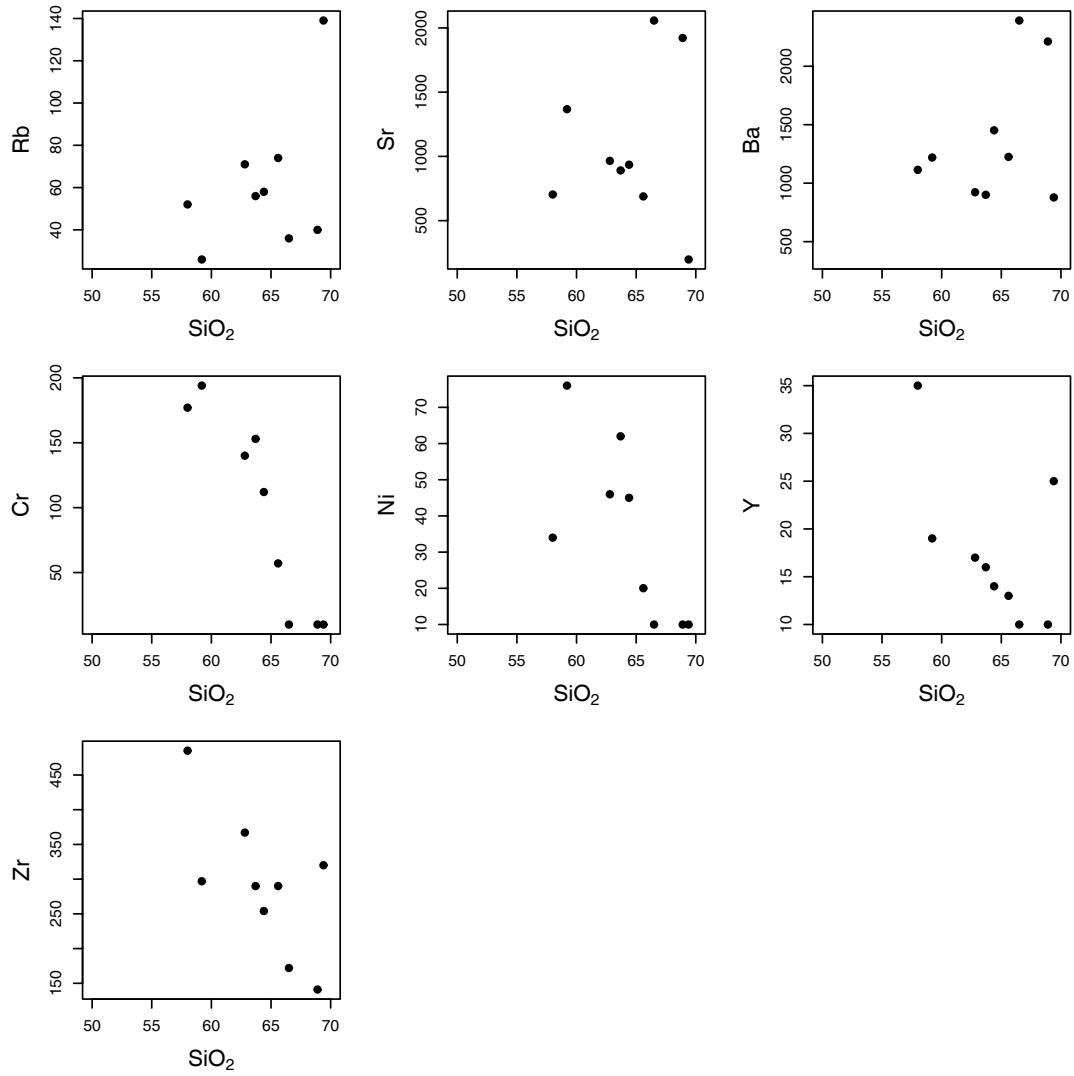


Fig. 6.5.- Solís de Mataojo: Harker diagrams for selected trace elements. SiO₂ in wt.%, trace elements in ppm.

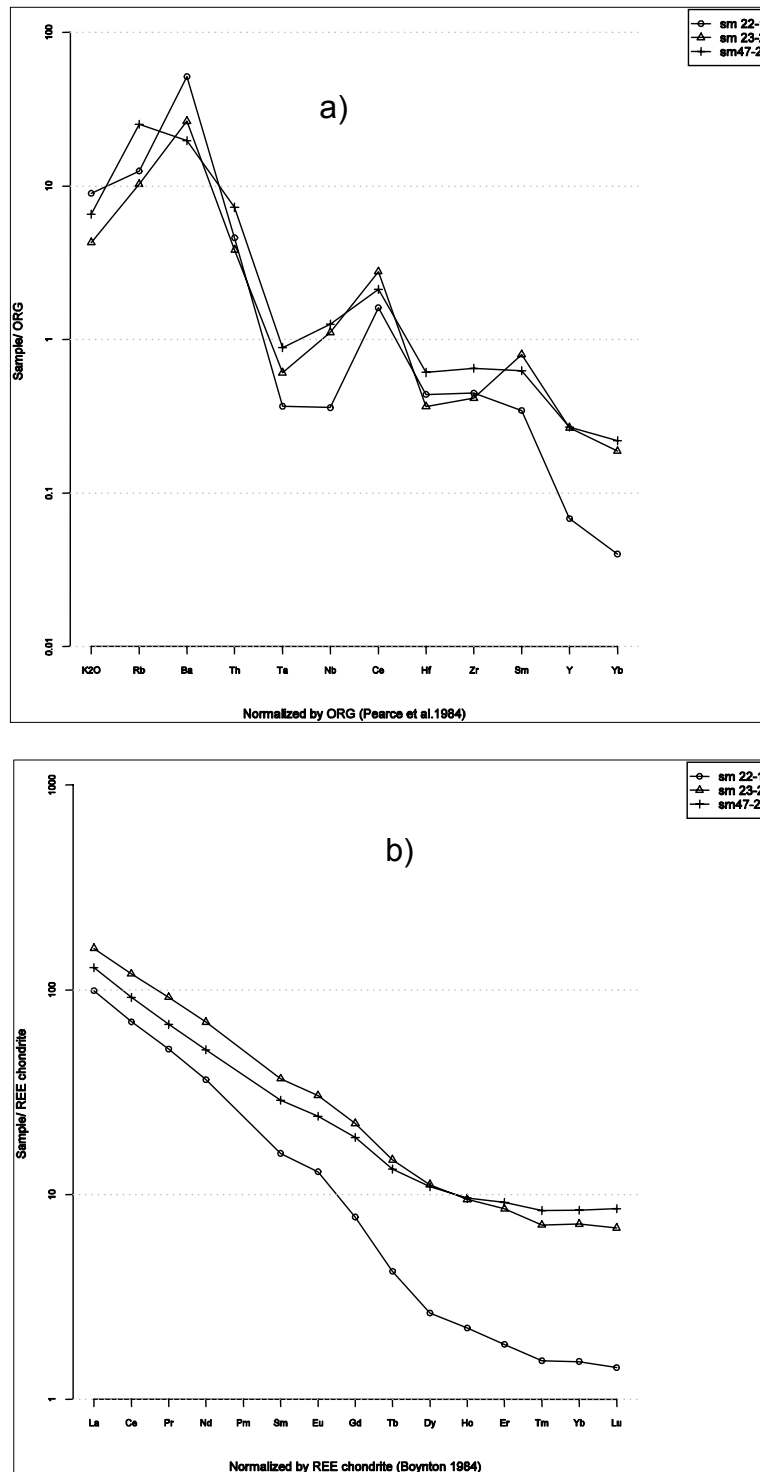


Fig. 6.6.- Solís de Matajojo: a) ORG-normalized spidergram. Normalization factors after Pearce *et al.* (1984); b) Chondrite-normalized REE abundances. Normalization factors after Boynton (1984).

In **summary**, the Solís de Mataojo Complex is a medium to high K₂O calc-alkaline granite. The high sum of K₂O + Na₂O, the high Ba and Sr contents and the REE pattern are typical of calc-alkaline granites of mature continental arcs.

6.2. Maldonado Granite

This granite is an elongated body emplaced between Sierra Ballena and Cordillera Shear Zones, in the southern part of the study area. Cenozoic sediments cover the outcrops in the north, while the Rio de la Plata River interrupts it in the south. The exposed area is nearly 10 x 7 km, with the major axis trending 020°. This pluton is probably one of the intrusive units that compose the Aiguá Batholith. The granite is weakly to strongly foliated with frequent S-C structures. Different facies have been recognized.

The porphyritic biotite granite facies is the most extended and contains alkali feldspar phenocrysts in a medium-grained matrix. The phenocrysts (microcline) are subhedral, are up to 20 mm in length, and display evidence of dynamic recrystallization (core and mantle structure). The matrix wraps the phenocrysts and it is medium-grained and composed of elongated aggregates of biotite, muscovite, and quartz, with development of subgrains. The coarse granoblastic texture of the matrix and the abundance of myrmekite in the foliation plane indicate deformation during high T sub-solidus conditions. Muscovite crystals are not deformed and frequently lie perpendicular to foliation, suggesting that they are probably secondary and related to a late thermal event.

The granodiorite facies shows petrographic features similar to those of the granitic one, but it is finer-grained and the phenocrysts are euhedral plagioclase (~An₁₅), showing bent twins, undulose extinction, and alteration to white mica. The matrix is granoblastic (~0.2 mm) and composed of anhedral microcline, perthitic orthoclase, quartz, and elongated mica aggregates.

A leucocratic granite facies is exposed directly in contact with the SBSZ. It is medium-grained (2 - 5 mm) and composed of quartz, orthoclase, microcline, apatite, and opaque minerals. Cataclastic overprinting of high T microstructures is related to the influence of the SBSZ and deformation at lower T conditions.

6.2.1. Geochemistry

Major elements

Figure 6.7 presents the Harker diagrams for the major elements of the Maldonado Granite. The SiO_2 range is restricted (71.6-76.4%), with four of the samples having silica contents of nearly 74%. Negative trends are observed for TiO_2 , Al_2O_3 , Fe_2O_3 , MgO , CaO , and P_2O_5 . The $\text{K}_2\text{O}/\text{Na}_2\text{O}$ ratio is high (1.66-1.91) and the alumina saturation parameter (A/CNK) is near 1 (Fig. 6.8).

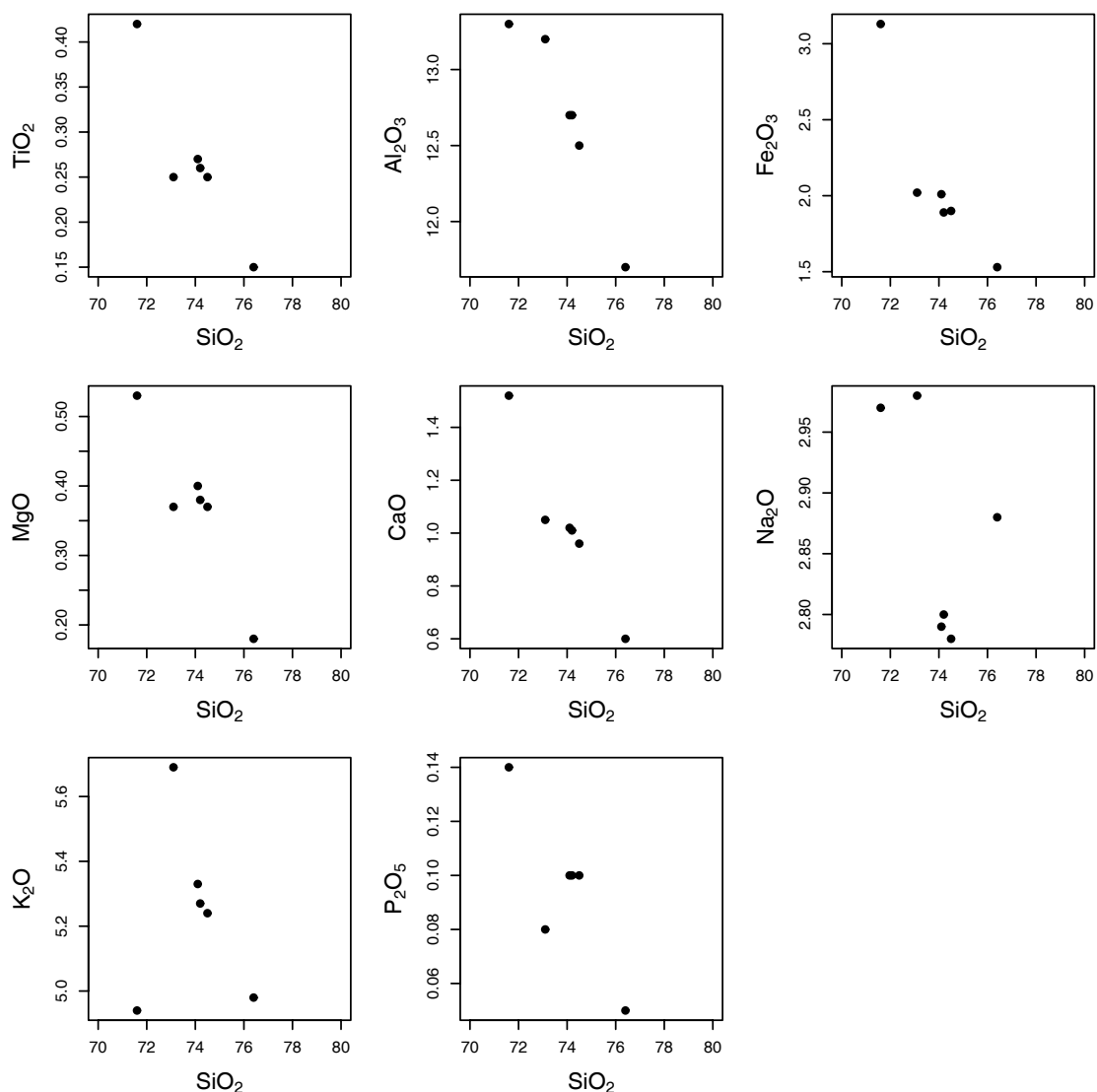


Fig. 6.7.- Maldonado Granite: Harker plots for major elements. Oxides in weight %.

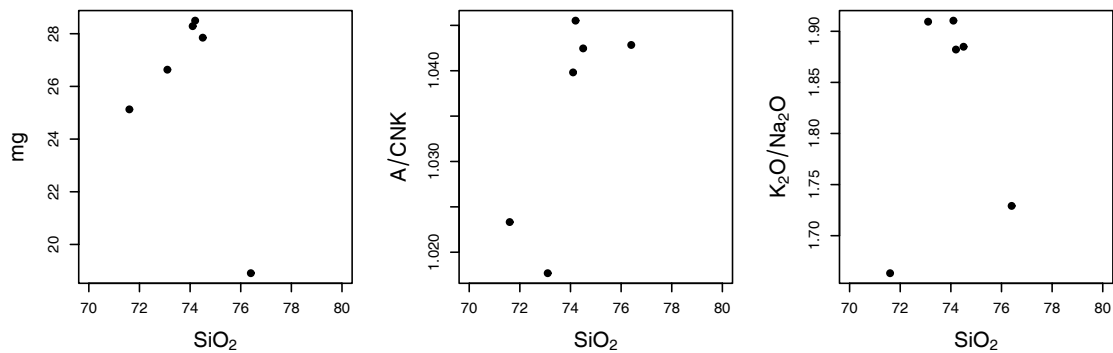


Fig. 6.8.- Maldonado Granite: Harker plots for some ratios. SiO_2 in weight %.

Alkalis content is high ($\text{Na}_2\text{O} + \text{K}_2\text{O} = 7.86 - 8.67$ wt.%) and, according to the limits proposed by Middelmost (1997), the samples classify near the transition between the calc-alkaline and transalkaline magma series (Fig. 6.9a). The SiO_2 vs. K_2O diagram (Peccerillo and Taylor, 1976) evidences a transitional character between the High K calc-alkaline and shoshonitic series (Fig. 6.9b).

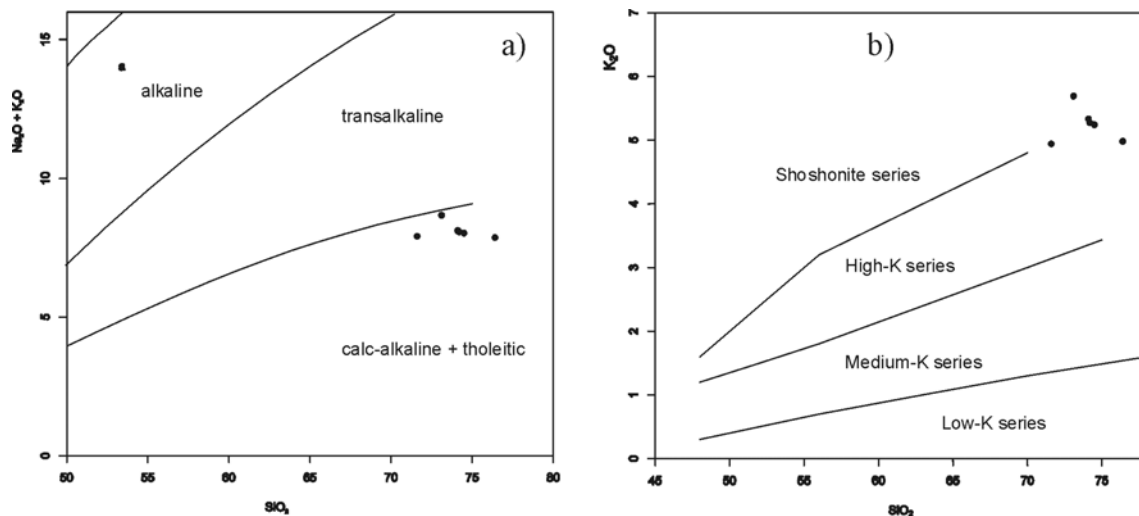


Fig. 6.9.- Maldonado Granite: a) SiO_2 vs. $\text{Na}_2\text{O} + \text{K}_2\text{O}$ diagram. Fields after Middelmost (1997); b) SiO_2 vs. K_2O diagram. Fields after Peccerillo and Taylor (1976). A/CNK and A/NK, see Fig. 6.4.

Shand's (1943) alumina and alkali saturation molar ratios indicate a slight oversaturation for both parameters (Fig. 6.10a), while the Sylvester diagram (1989), which discriminates alkaline from calc-alkaline and strongly peraluminous granites (Fig. 6.10b), classifies most of the samples as highly-fractionated calc-alkaline (HFCA).

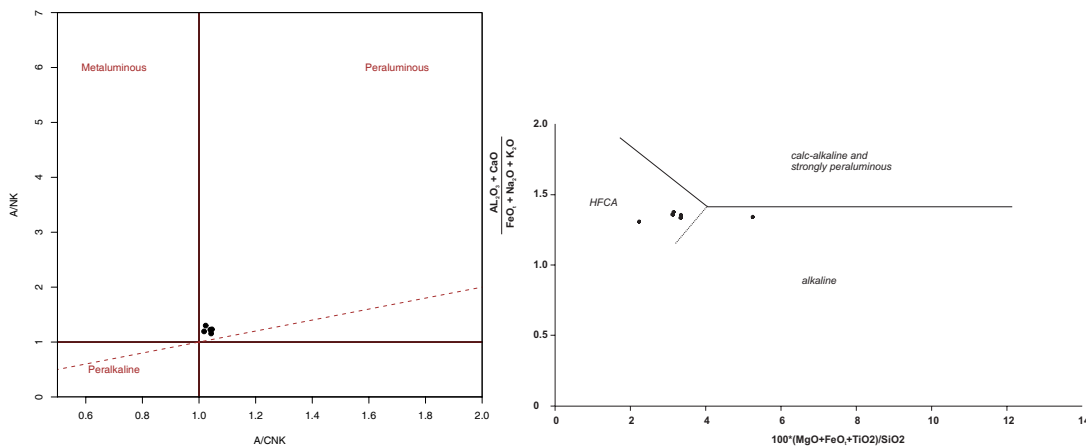


Fig. 6.10.- Maldonado Granite:

- Alumina and alkali-saturated nature of the Maldonado Granite in A/CNK vs. A/NK plot. Molar ratios after Shand (1943).
- Highly fractionated calc-alkaline character (HFCA): in $(\text{Al}_2\text{O}_3 + \text{CaO}) / (\text{FeO}_t + \text{Na}_2\text{O} + \text{K}_2\text{O})$ vs. $100 \times (\text{MgO} + \text{FeO}_t + \text{TiO}_2) / \text{SiO}_2$ (wt.%). Fields after Sylvester (1989).

The B vs. M milicationic diagram of Debon and Le Fort (1988) is useful for distinguishing between magnesian and ferriferous series. It indicates the ferriferous character of the Maldonado Granite, a feature that precludes shoshonitic affinity (Fig. 6.11).

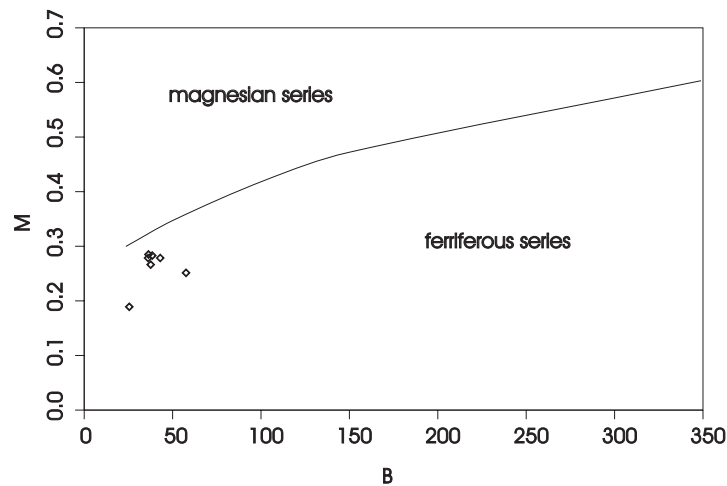


Fig. 6.11.- Ferriferous character of the Maldonado Granite in B (= Fe + Mg + Ti) vs. M (=Mg/(Mg+Fe)) milicationic diagram of Debon and Le Fort (1988).

Trace elements

Harker diagrams are not presented because of the limited SiO₂ range (71.6-76.4 %). In the ORG-normalized spidergrams (Fig. 6.12), with the normalization factors of Pearce *et al.* (1984), the patterns evidence enrichment in LIL elements.

Ba and Sr display low contents (39-334 ppm Ba, 11-89 ppm Sr), that are typical of alkaline granitic series, another characteristic that indicates that this granite does not have shoshonitic affinity. The ORG-normalized spidergrams (Fig. 6.12) show that enrichment decreases with increasing compatibility, and HFS elements (Hf, Zr, Y, and Yb) display low concentrations, a pattern observed in syn-collision and post-collision granites according to Pearce *et al.* (1984).

The REE diagram (Fig. 6.13) displays low fractionation from La to Lu (La_N/Yb_N ratio ranges from 7.5 to 9.8) and distinct negative Eu anomaly (Eu/Eu* = 0.08-0.3). The REE pattern is similar to the alkaline post-orogenic granites of Wisconsin (Anderson *et al.*, 1980) and typical of alkaline granites.

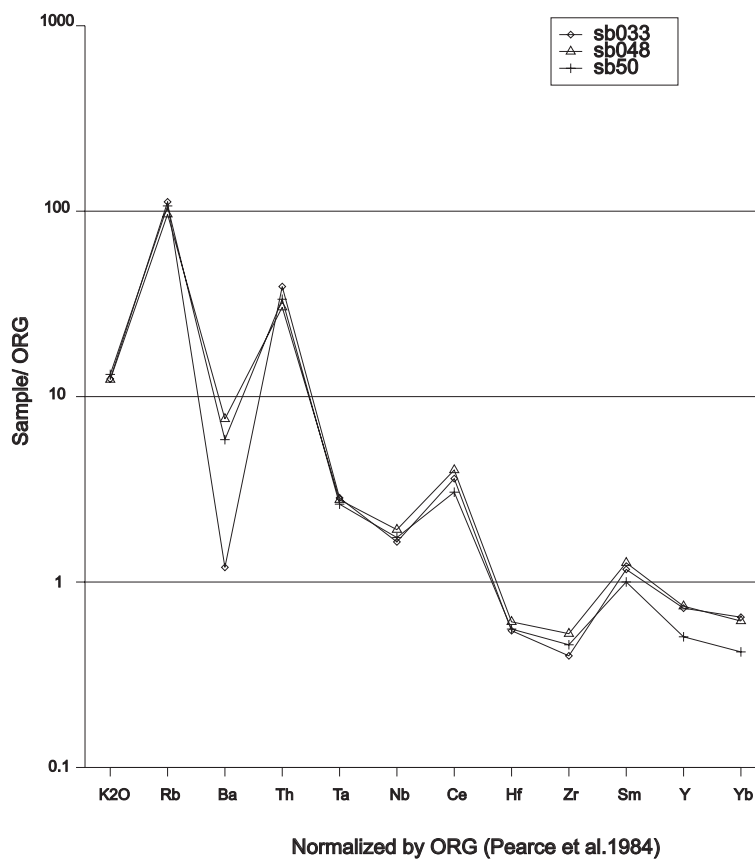


Fig. 6.12.- Maldonado Granite. Spidergram normalized to ORG.

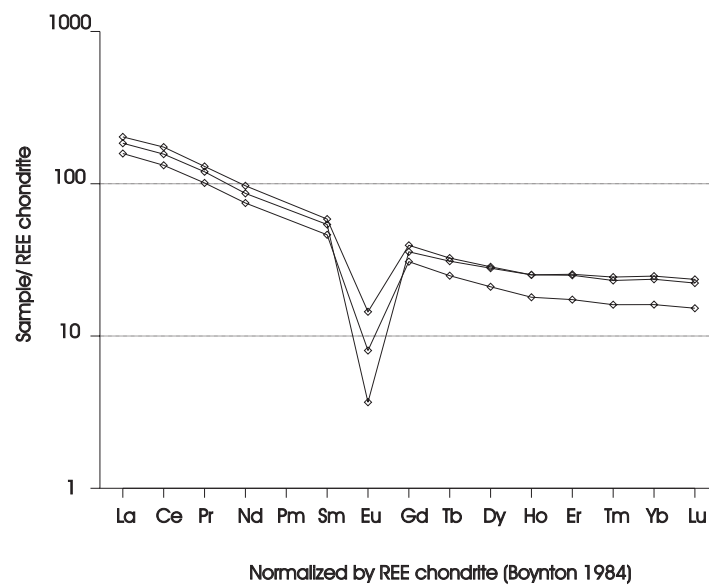


Fig. 6.13.- Maldonado Granite: REE spidergram normalized to Chondrite.

In **summary**, the Maldonado granite can be defined as a slightly metaluminous, highly-fractionated calc-alkaline to alkaline granite, with characteristics that are transitional between both types of series. The sum of $K_2O + Na_2O$ is high, but it plots neither in the transalkaline field of Middelmost (1997) nor in the alkaline field of Irvine and Baragar (1971). The low Ba and Sr and the REE pattern are typical of alkaline granites, but the abundance of HFS elements is not as high as in typical alkaline granites.

6.3. Pan de Azúcar Pluton (Sierra de las Animas Complex)

The Pan de Azúcar Pluton is a circular intrusion with a diameter of approximately 5 km. It is emplaced in Vendian to Cambrian volcanics of the Sierra de las Animas Complex. The crystallization age is probably ~ 550 Ma, taking into account a determination by Preciozzi *et al.*, 1985 (K/Ar in amphibole).

The pluton consists of three main lithologies: syenites, quartz-syenites (nordmarkites), and granites disposed more or less concentrically, forming a zoned pluton

with SiO₂-richer facies in the centre. The shape of the intrusion and the association with volcanics of similar age suggest a ring-complex structure for this pluton (Fig. 6.14).

Syenites are present in the marginal zone of the intrusion. They are grey to pink coloured and coarse-grained. The main mineral is perthitic orthoclase in subhedral crystals up to 4 cm in length. Albitization and rims of albite in orthoclase are common features. The main ferromagnesian minerals are pale green aegirin-augite and Na-amphibole, but interstitial biotite, tourmaline, and aggregates of stilpnomelane are also observed. Amphibole and biotite show dark pleochroism, and aegirin-augite shows distinct green pleochroism, indicating high FeO/(FeO+MgO) ratios. Accessory minerals include apatite and zircon.

Quartz-syenites (nordmarkites) crop out in the middle. They are medium-grained and the colours are highly variable, ranging from grey to brownish-pink to red. The mineral composition is similar to that of the syenites, but a small amount of interstitial quartz is present.

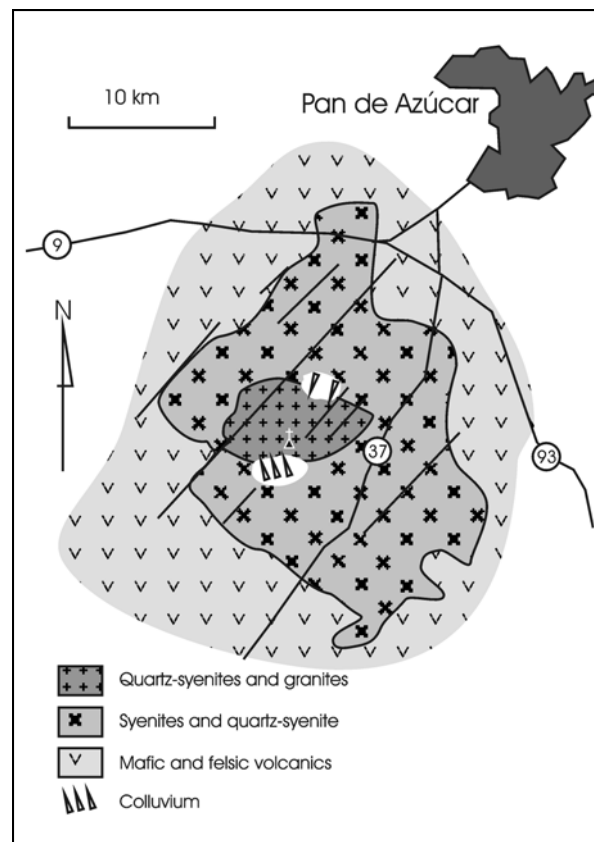


Fig. 6.14.- Geologic map of the Pan de Azúcar Pluton showing the distribution of the main petrographic facies.

Granite occurs in the central part of the intrusion. The texture is medium to fine-grained, equigranular to porphyritic, with small quartz and orthoclase phenocrysts and allotriomorphic. Development of micrographic texture is sometimes observed (granophyres). The main minerals are orthoclase and quartz, while ore minerals are the main accessories.

6.3.1. Geochemistry

Ten samples from the Pan de Azúcar Pluton, ranging from syenite to granite, were analyzed. The compositions are shown in Table A.4.4 (Appendix 4)

Major elements

Discontinuous and scattered trends are observed in the Harker diagrams of the major elements (Fig. 6.15). The syenites (samples 82, 83, 84, 85, and 29) have almost constant SiO₂ content at around 60%, with variations in most of the major elements and ratios (such as A/CNK, mg, and K₂O/Na₂O). The quartz-syenites and granites show negative trends for Al₂O₃, K₂O, and Na₂O, and a positive trend for the K₂O/Na₂O ratio.

Low contents are observed for TiO₂, MgO, and MnO (< 1 wt.%), while total alkali is high (Na₂O + K₂O = 7.3 - 11.4 %), and Al₂O₃ is variable but normally high (mean Al₂O₃ = 14.9%).

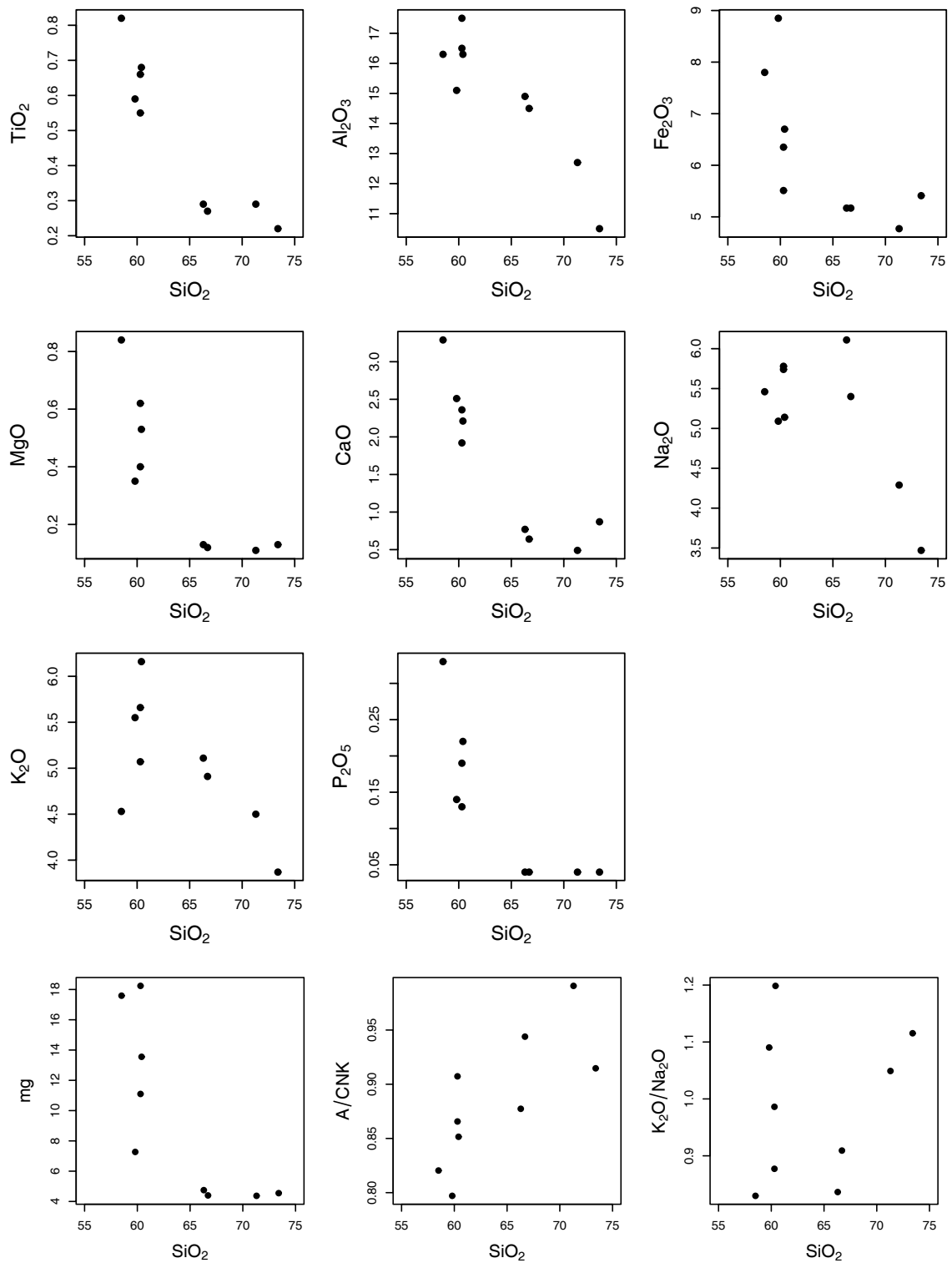


Fig. 6.15.- Harker diagrams for major elements and some ratios of the Pan de Azúcar Pluton (Sierra de las Animas Complex)

In an R1-R2 diagram (De la Roche *et al.*, 1980), the samples plot in syenite, quartz-syenite, and granite fields (Fig. 6.16).

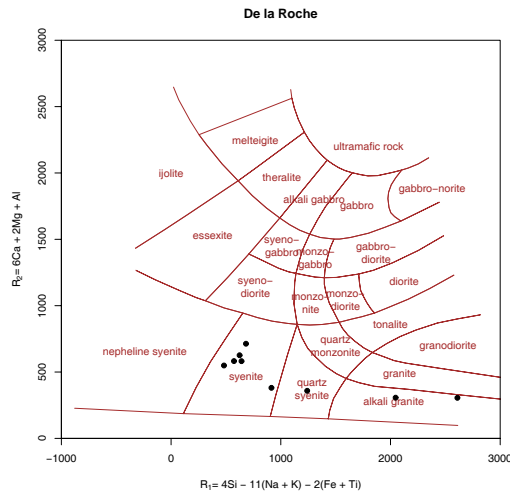


Fig. 6.16.- R1-R2 diagram of syenites and granites of the Pan de Azúcar Pluton (Sierra de las Animas Complex)

The mesonormative quartz content ranges from 0 to 37%, orthoclase content from 22 to 40%, and albite content from 29 to 48%, while normative anorthite is near 0%. Therefore the compositions plot at the AQ edge in a QAP diagram, ranging from syenites to alkali feldspar granites.

In the TAS diagram ($\text{Na}_2\text{O} + \text{K}_2\text{O}$ vs. SiO_2), most of the samples plot in the transalkaline field (Fig. 6.17), according to the Middlemost (1997) fields.

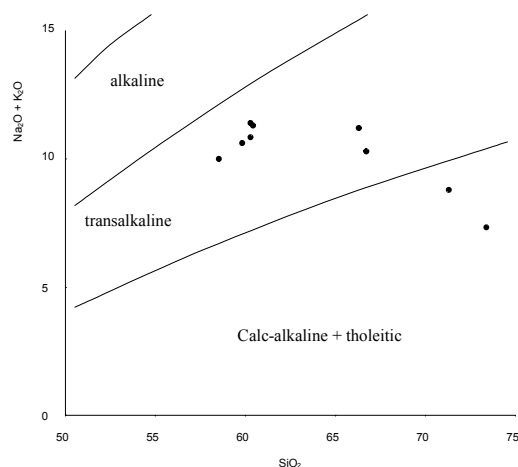


Fig 6.17.- Transalkaline affinity of the Pan de Azúcar Pluton (Sierra de Animas Complex) in the TAS: $\text{Na}_2\text{O} + \text{K}_2\text{O}$ vs. SiO_2 (wt.%) plot. Fields after Middlemost (1997).

Figure 6.18 shows that most of the samples plot in the transition between the metaluminous and peralkaline fields, a case that is typical of post-collisional alkaline granites (Sylvester, 1989).

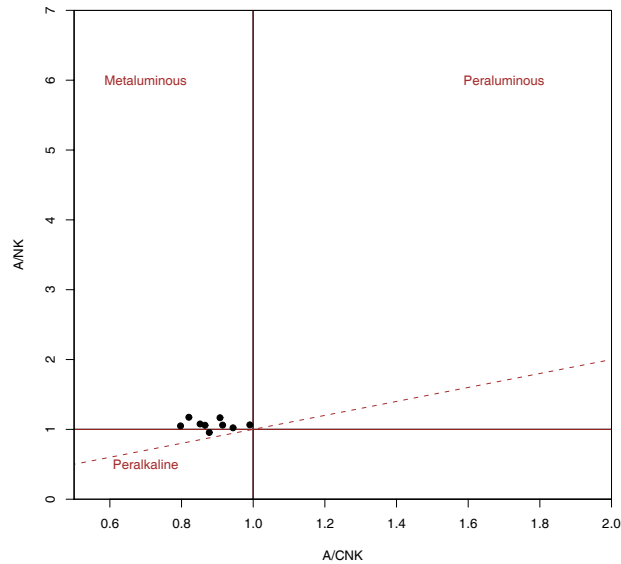


Fig 6.18.- A/CNK vs. A/NK diagram showing the metaluminous to slightly peralkaline nature of the Pan de Azúcar Pluton (Sierra de Animas Complex).

In the $100 \times (\text{MgO} + \text{Fe}_2\text{O}_3 + \text{TiO}_2) / \text{SiO}_2$ vs. $(\text{Al}_2\text{O}_3 + \text{CaO}) / \text{Fe}_2\text{O}_3 + \text{Na}_2\text{O} + \text{K}_2\text{O}$ diagram of Sylvester (1989), the samples plot in the field of alkaline post-orogenic granites (Fig. 6.19).

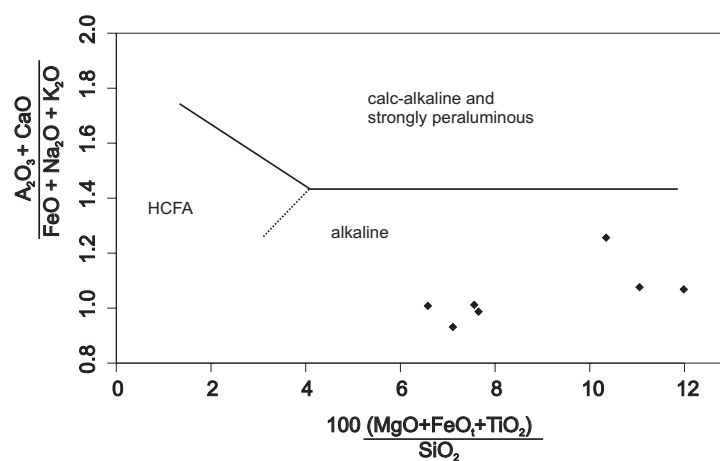


Fig. 6.19.- Alkaline affinity of the Pan de Azúcar Pluton in the diagram of Sylvester (1989). HCFA: highly-fractionated calc-alkaline.

Trace elements

Rb, Y, and Zr show positive discontinuous trends in the Harker diagrams (Fig. 6.20). Ba is normally low (< 500 ppm), except in three syenite samples (SA83, SA84, and SA85), where Ba contents rise to nearly 2000 ppm. Cr shows a negative trend in the case of granites and quartz-syenites ($\text{SiO}_2 > 65\%$ wt.), while the content of the syenites is very scattered. The variations observed in the composition of the syenites suggest that processes other than normal fractional crystallization are involved in the genesis of these rocks.

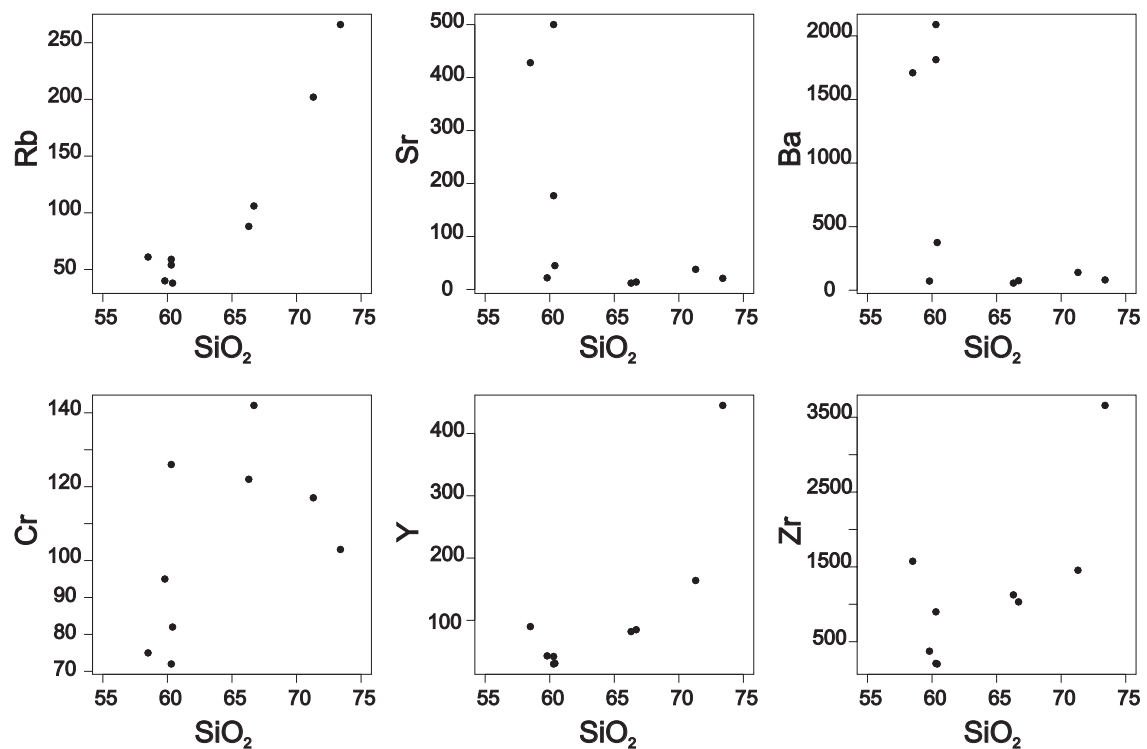


Fig. 6.20.- Harker diagrams for some selected trace elements of the Pan de Azúcar Pluton.

ORG-normalized spidergrams (after Pearce *et al.*, 1984) for three selected samples of syenite, quartz-syenite, and granite are presented in Figure 6.21. The quartz-syenite and the granite evidence a pattern typical of alkaline granites: negative anomaly of Ba and enrichment in HFS elements (Hf, Zr, Sm, Y, and Yb).

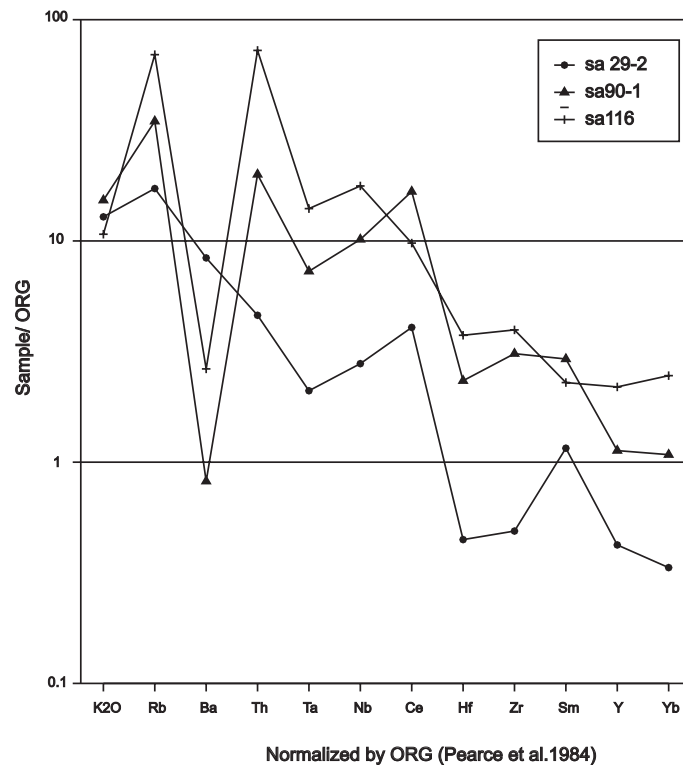


Fig. 6. 21.- Pan de Azúcar Pluton: ORG-normalized spidergrams. SA29-2: syenite, SA 90-1 : quartz-syenite, SA116: granite.

Total REE content is high to very high (Σ REE = 326-1239 ppm). The spidergrams of the quartz-syenite and granite samples (Fig. 6.22) display low fractionation from La to Lu, especially for the granite and quartz-syenite samples (La_N/Yb_N ratio ranges from 5.8 to 16), and a distinct negative Eu anomaly ($Eu/Eu^* = 0.09$). The REE pattern is similar to the alkaline post-orogenic granites of Wisconsin (Anderson *et al.*, 1980) and typical of alkaline granites. The pattern of the syenite (sample SA 29-2) is low in terms of total REE content, has a higher LREE/HREE ratio, and does not contain an Eu anomaly while the pattern of the granite (sample SA 116) shows enrichment in HREE, a fact probably associated to fluid activity during late magmatic stage as described for a peralkaline granite in the Midian Mountains of Saudi Arabia by Harris and Marriner (1980).

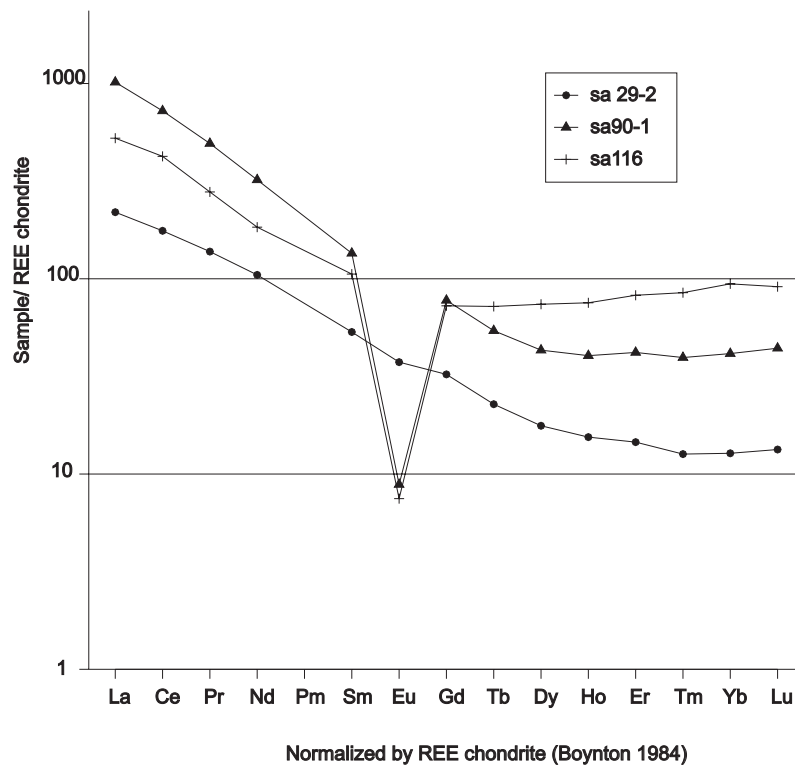


Fig. 6. 22 - Pan de Azúcar Pluton: REE spidergram normalized to Chondrite

In **summary**, the Pan de Azúcar Pluton is a metaluminous to peralkaline pluton with low Ba and Sr, and high contents of HFS elements, high REE content, and low LREE/HREE ratio, all characteristics typical of post-collisional alkaline granites.

6.4. Geochemical contrast between the Solís de Matojo, Maldonado and Pan de Azúcar Plutons.

Table 6.1 presents a summary of the main trace-element differences between the three plutons.

	Solís de Mataojo				Maldonado				Pan de Azúcar			
	n	Mean	Min	Max	n	Mean	Min	Max	n	Mean	Min	Max
Rb ppm	10	62	26	139	6	312	288	342	9	102	38	266
Sr ppm	10	1050	198	2057	6	55	11	89	9	140	12	500
Ba ppm	10	1266	348	2390	6	252	39	334	9	712	56	2089
Y ppm	10	18	10	35	6	41	31	53	9	112	30	445
Zr ppm	10	282	141	485	6	191	146	237	9	1170	202	3658
Nb ppm	3	9	3.6	12.6	3	18	16	19	3	102	28	177
Σ REE ppm	3		123	223	3		248	324	3		326	1239
La _N /Lu _N	3		15	70	3		7.8	10.4	3		5.8	23
Ce _N /Yb _N	3		11	46	3		6.3	8.2	3		4.5	17.5
Eu/Eu*	3		1.0	1.2	3		0.08	0.3	3		0.09	0.9
Ce _N	3		70	120	3		132	174	3		176	724

Table 6.1.- Mean, minimum and maximum contents of some selected trace elements and some REE ratios for the three plutons studied. Bold characters indicate high contents or ratios.

High Ba and Sr, and low Y, Nb, and Rb characterize the Solís de Mataojo Pluton. The REE contents are moderate (expressed by Σ REE or Ce_N), while the LREE/HREE ratio (La_N/Lu_N or Ce_N/Yb_N) is variable but high, and no Eu anomalies are present.

High Rb, low Sr and Ba, and moderate Y and Nb contents characterize the Maldonado granite. The REE abundances are moderate, while the LREE/HREE ratio is low, and the patterns display negative Eu anomalies.

Samples of the Pan de Azúcar Intrusion exhibit high Nb, Zr, and Y, moderate Sr, and low Rb. The Ba contents are low in the granites (< 500 ppm), but highly variable, from low to high, in the syenites (56 - 2089 ppm). The contrast between the three plutons, graphically presented in the boxplots of Figure 6.23, confirms the geochemical classification of each.

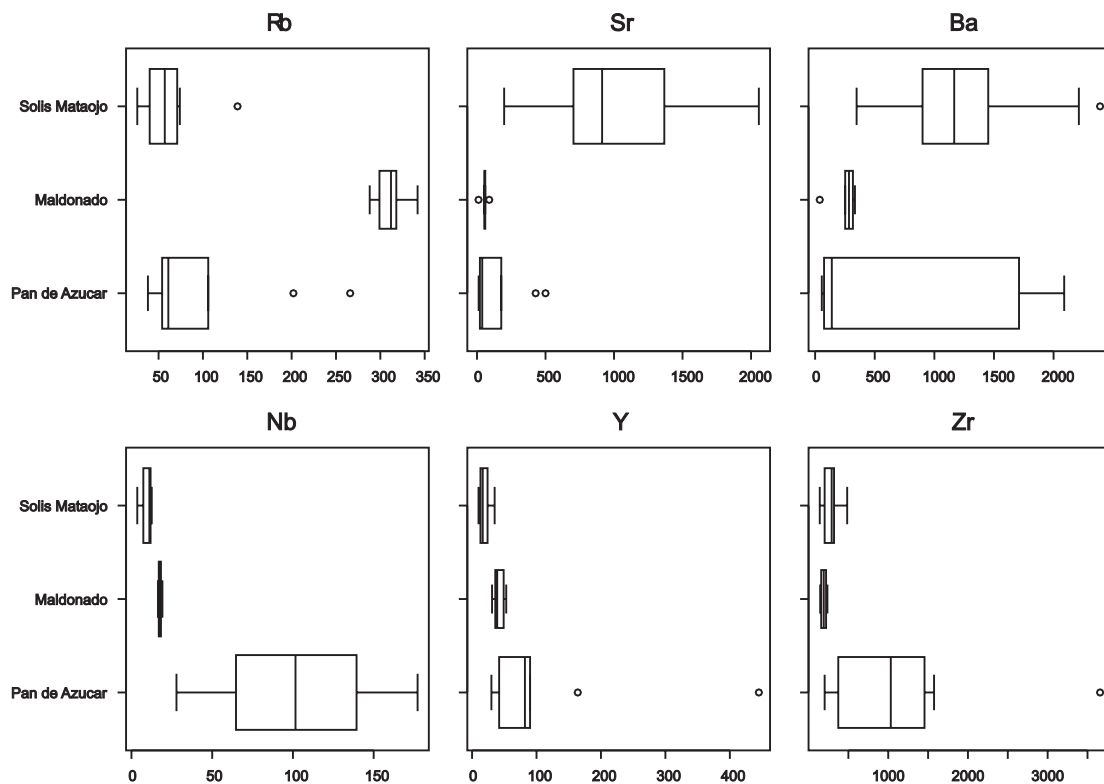


Fig. 6.23.- Boxplots of some LIL elements (Rb, Sr, and Ba) and HFS elements (Nb, Y, and Zr) for the Solís de Mataojo, Maldonado and Pan de Azúcar Intrusions. Concentrations in ppm.

The ORG-normalized spidergrams (Fig. 6.24) show similar patterns for the Maldonado and Pan de Azúcar intrusions, with characteristically low Ba anomaly, while the Solís de Mataojo evidences very low Ta, Nb, Y, and Yb, and high Ba, when compared with the ORG-normalization parameters of Pearce *et al.* (1984).

The REE spidergrams of Figure 6.25 evidence the difference in REE pattern between Maldonado and Pan de Azúcar -with high REE contents, low LREE/HREE ratios, and distinct Eu anomalies (typical of alkaline granites)- and Solís de Mataojo -with medium REE contents, higher LREE/HREE ratios, and no Eu anomalies (characteristic of calc-alkaline granitoids of active continental margins).

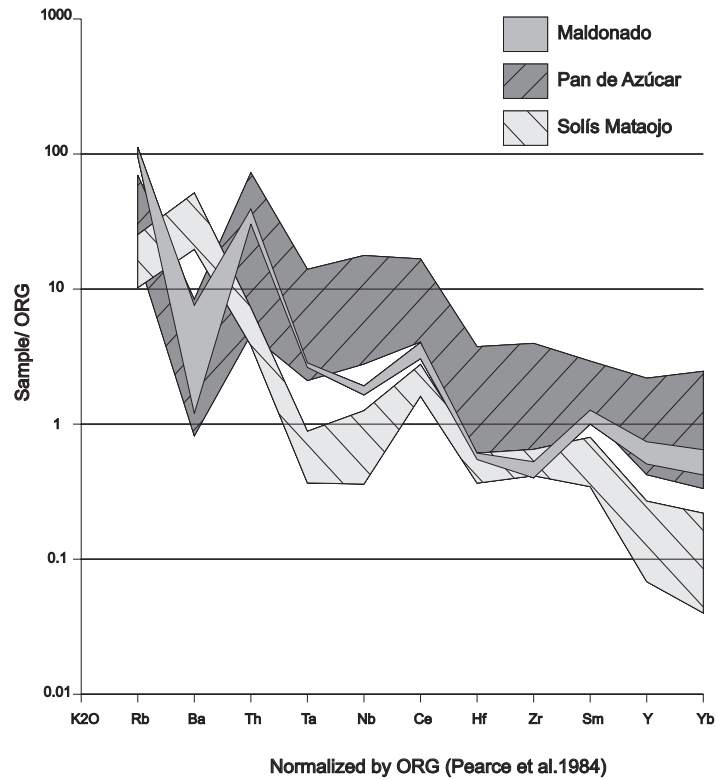


Fig. 6.24.- Fields for the ORG-normalized spidergrams of the three plutons studied.

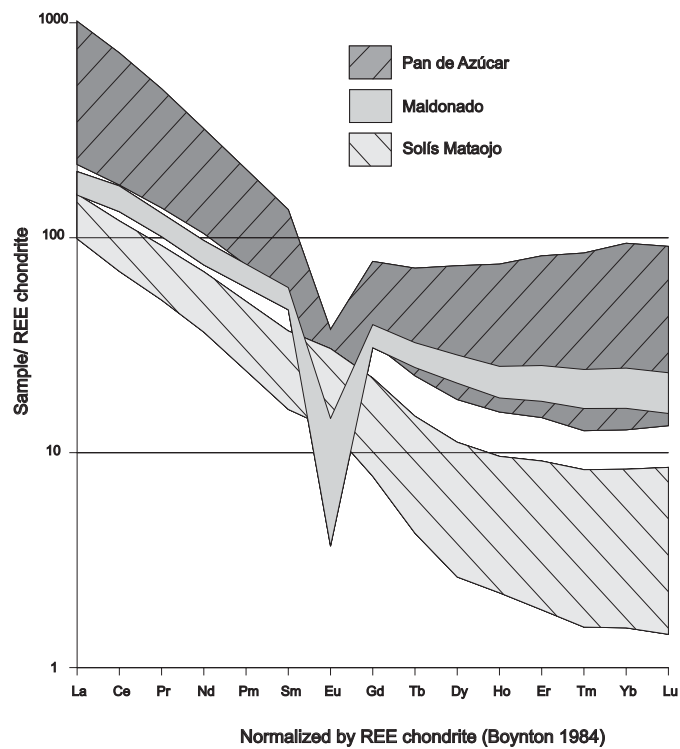


Fig. 6.25.- REE fields of the Chondrite-normalized spidergrams for the three plutons studied.

In **summary**, the Solís de Mataojo Pluton is a medium to high K₂O calc-alkaline granitoid with a mature continental arc signature, the Maldonado Granite is a highly fractionated calc-alkaline (HFCA) to alkaline granite, with characteristics transitional between both types of series, and the Pan de Azúcar intrusion exhibits typical characteristics of post-collisional alkaline granites.

6.5. Tectonic setting considerations

The possibility of discriminating the tectonic setting of magmatism on the basis of the geochemical signature is a matter of debate. The main limitation of such an approach is that magmas from different sources can coexist in the same tectonic setting. Förtser *et al.* (1997), in an evaluation of the Rb vs. (Y+Nb) diagram of Pearce *et al.* (1984), conclude that there is a good correlation between tectonic setting and trace element composition. Nevertheless, they point out that discrimination diagrams are not foolproof, and emphasize that they must be used together with other geological pieces of evidence.

Figure 6.26a presents the K₂O x Rb / MgO vs. Na₂O x Zr x Y discrimination diagram of Tischendorf and Förster (1992). The Solís de Mataojo Granite samples plot in the field where volcanic arc and collisional granites overlap. The Maldonado Granite samples plot in the field of collisional granites, while the Pan de Azúcar Granite samples plot in the “within plate” field.

In the R1-R2 diagram with the fields defined by Batchelor and Bowen (1985) the Pan de Azúcar Pluton samples plot in the anorogenic field, and the Maldonado Granite samples in the transition between the syn-collision and post-orogenic fields. The Solís de Mataojo Complex, it is in a not very well-defined location between pre-plate collision and post-collision uplift (6.26b).

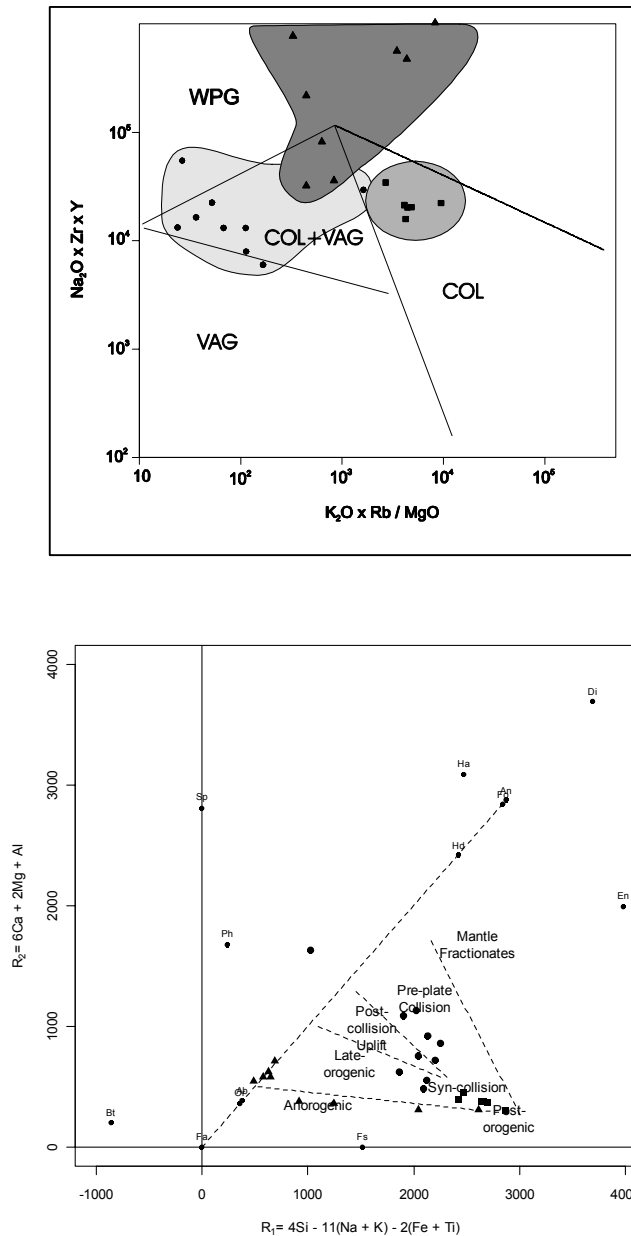


Fig. 6.26.- a) Discrimination diagram $\text{Na}_2\text{O} \times \text{Zr} \times \text{Y}$ vs. $\text{K}_2\text{O} \times \text{Rb} / \text{MgO}$ (Tischendorf and Förster, 1992); b) R1-R2 diagram with tectonic setting fields, after Batchelor and Bowen (1985). WPG: within-plate granites; COL: collision granites; syn-COLG: syn-collision granites; VAG: volcanic arc granites. References: circles - Solís de Mataojo; squares - Maldonado; triangles - Pan de Azúcar.

A comparable result is observed using the discrimination diagrams of Pearce *et al.* (1984). Samples of the Solís de Mataojo Complex plot in the field of volcanic arc granites, mainly in the area defined by Pearce (1996) as post-collisional granites. The Pan de Azúcar Pluton samples plot in the within-plate granite area, and the Maldonado Granite samples in the boundary region between WPG, syn-COLG, and VAG (Fig. 6.27; see Fig. 6.26 for

abbreviations). Given the available data concerning the age of these three plutons (see Chapter 8), and the conclusions of the geochemical characterization, there seems to be an evolution from medium to high-K calc-alkaline (Solís de Mataojo) to highly fractionated calc-alkaline (Maldonado) and finally to alkaline magmatism (Pan de Azúcar). This evolution is evident in the tectonic discrimination diagrams as an increase in the magmatism of the “within-plate component” (in the sense given by Brown *et al.*, 1984). The characteristics of these three intrusions and the association with shoshonitic volcanics (see section 6.7) indicate that the most probable tectonic setting is post-collisional shifting to anorogenic, with thermal boundary layer detachment (Black and Liegeois, 1993; Liegeois *et al.*, 1998) or slab breakoff (Davies and von Blanckenburg, 1995) as probable mechanisms for magma generation.

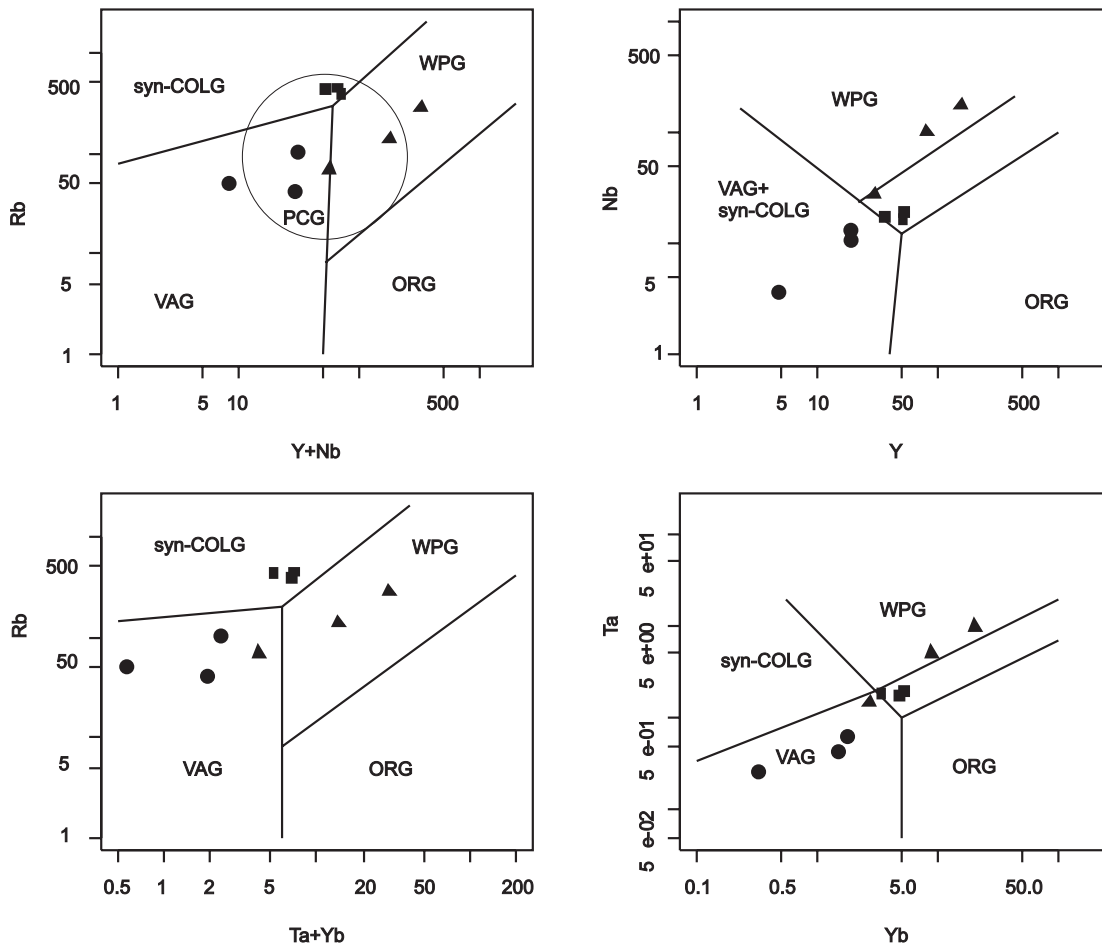


Fig. 6.27.- Tectonic discrimination diagrams of Pearce *et al.* (1984). Field of post-collision granites (PCG), after Pearce (1996). Symbols, see Fig. 6.26.

6.6. Geochemistry of the mylonitic porphyries of Sierra Ballena Shear Zone

The composition of four samples of these mylonites is available. Analytical methods are described in appendix 4 and the results are shown in table A.4.5 (see Appendix 4). Only immobile elements will be taken into consideration, because of the possibility of chemical changes during mylonitization. The mylonitic porphyries are peralkaline, manifested in the modal occurrence of aegirin-augite and Na-amphibole, and they may represent the same magmatic event as the Sierra de las Animas Complex, but emplaced in high-strain zones (in the Sierra Ballena Shear Zone).

Figure 6.28 shows that the mylonitic porphyries plot in the peralkaline rhyolite (Com/Pant) and trachy-andesite fields. The high SiO₂ content (71-76 wt.%) of these rocks suggests the possibility of silica enrichment during mylonitization. The Nb/Y ratio is high (0.6-1.5) and similar to the Pan de Azúcar magmatism, thus pointing to the alkaline nature of the protolith of these mylonites.

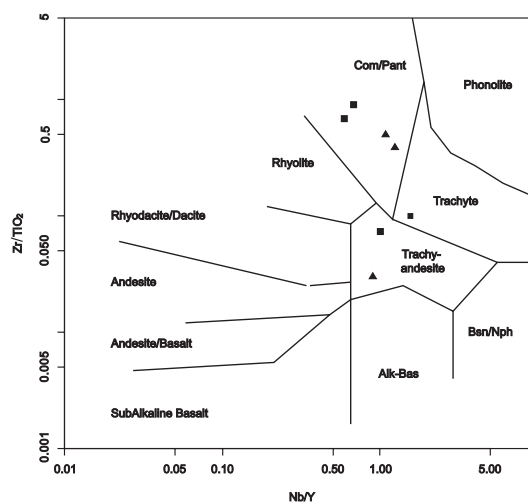


Fig. 6.28.- Nb/Y vs. Zr/TiO₂ diagram of Winchester and Floyd (1977). Symbols: squares - mylonitic porphyries; triangles - Pan de Azúcar Pluton.

In the Rb vs. Y+Nb and Nb vs. Y diagrams of Pearce *et al.* (1984), the mylonites plot in a scattered region, two in VAG field and two in WPG field (Fig. 6.29).

Considering the mobility of several elements during mylonitization and the fact that only data from four samples is available, the characterization as alkaline and the relation with the Sierra de las Animas magmatism is feasible but further investigations are necessary to confirm this hypothesis.

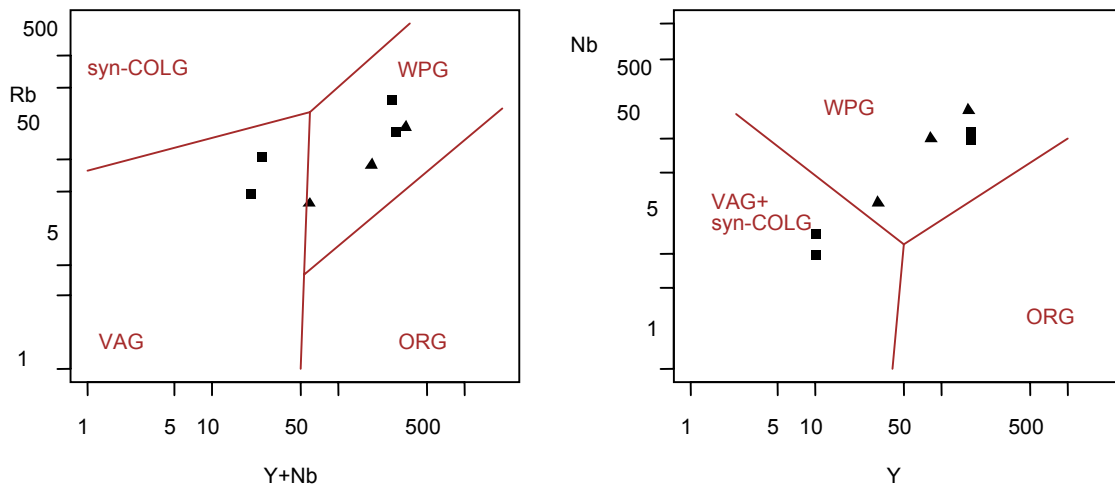


Fig. 6.29.- Pearce *et al.* (1984) diagrams for the mylonitic porphyries and the Pan de Azúcar Pluton. Symbols see fig. 6.28.

6.7. Las Flores basic volcanics

These basic volcanics are associated with the Maldonado Group, and in particular with the Las Ventanas Formation, a volcano-sedimentary succession of Lower Vendian age (see Chapter 3). The classification of this basic magmatism and the characterization of its tectonic setting is of interest because a transtensional basin was proposed for this succession, and geochemical data can help to constrain the setting. Available age determinations are not very conclusive and the crystallization ages of these rocks may range from 615 to 565 Ma, based on a reinterpretation of data presented by Sánchez-Bettucci and Linares (1996).

The mafic association of Las Flores basalts includes amygdaloidal basalts, dolerite dikes, and hyaloclastic breccias. The basalts are normally dark green and fine-grained. Plagioclase phenocrysts are very abundant in a normally glassy groundmass. Clinopyroxene phenocrysts are also frequent. The composition of the plagioclase ranges from oligoclase to andesine and it normally displays saussuritization. The fine-grained matrix contains plagioclase laths and interstitial glass altered to chlorite. The glassy groundmass sometimes displays perlitic cracks that evidence very rapid cooling. The amygdules are rounded and up to 1 cm in diameter, and are filled with epidote, chlorite, carbonate, quartz, pumpellyite, and prehnite. The dolerites have ophitic texture and are composed mainly of plagioclase and clinopyroxene.

A frequently associated lithology is a breccia where basalts clasts are cemented by silica, chlorite, and epidote.

The perlitic cracks in the groundmass and the presence of basic breccias in basic volcanics associated with sediments suggest contact of magma with water. Fisher and Schmincke (1984) point out that this is the most likely formation mechanism for pyroclastic rocks from basic magmas that are normally poor in volatiles.

The abundance of chlorite and epidote, and the occurrence of pumpellyite and prehnite suggest that these rocks are overprinted by very low to low-grade metamorphism, as indicated in chapter 3.

6.7.1. Geochemistry

Analytical methods are described in appendix 4 and the results are shown in table A.4.5 (see Appendix 4). Diagrams presented in figures 6.30a to 6.30d indicate that this is a metaluminous, calc-alkaline to alkaline and high K_2O to shoshonitic magmatism. In the Ti/Zr vs. Nb/Y diagram, these rocks classify as trachy-andesites. The Nb/Y ratio is medium to high indicating an affinity transitional between alkaline and subalkaline series (Fig. 6.30e).

The Pearce and Norry (1979) diagram suggests a within-plate setting for these basalts regarding the very high Zr/Y ratio (Fig. 6.30f).

Morrison (1980) pointed out the following characteristics of the shoshonitic associations: high total alkalis ($Na_2O+K_2O > 5\%$), low TiO_2 ($< 1.3\%$), high but variable alumina (14-19%), low enrichment in iron in the AFM diagram, and enrichment in LIL elements (P, Rb, Sr, Ba). The Las Flores basalts present high alumina contents (14.9 - 18.9 %), high total alkalis (5 - 7 %), very high Ba (1086 - 1839 ppm), and high Rb (25 - 69 ppm) contents. TiO_2 is low for alkaline basalts (0.19 - 1.44 %).

These facts together with the location of the samples in SiO_2 vs. K_2O , AFM, Nb/Y vs. Zr/ TiO_2 , AFM, and Zr vs. Zr/Y diagrams, and combined with the petrographic characteristics indicate a shoshonitic affinity for these mafic rocks. The characterization should be considered preliminary until more data is available. In southern Brazil (Taquarembó Plateau - *Río Grande do Sul*), Gastal (1999) describes a shoshonitic association, including basalts and trachy-andesites, that predates the alkaline magmatism by 10-40 Ma, and that can be correlated with the Las Flores basalts.

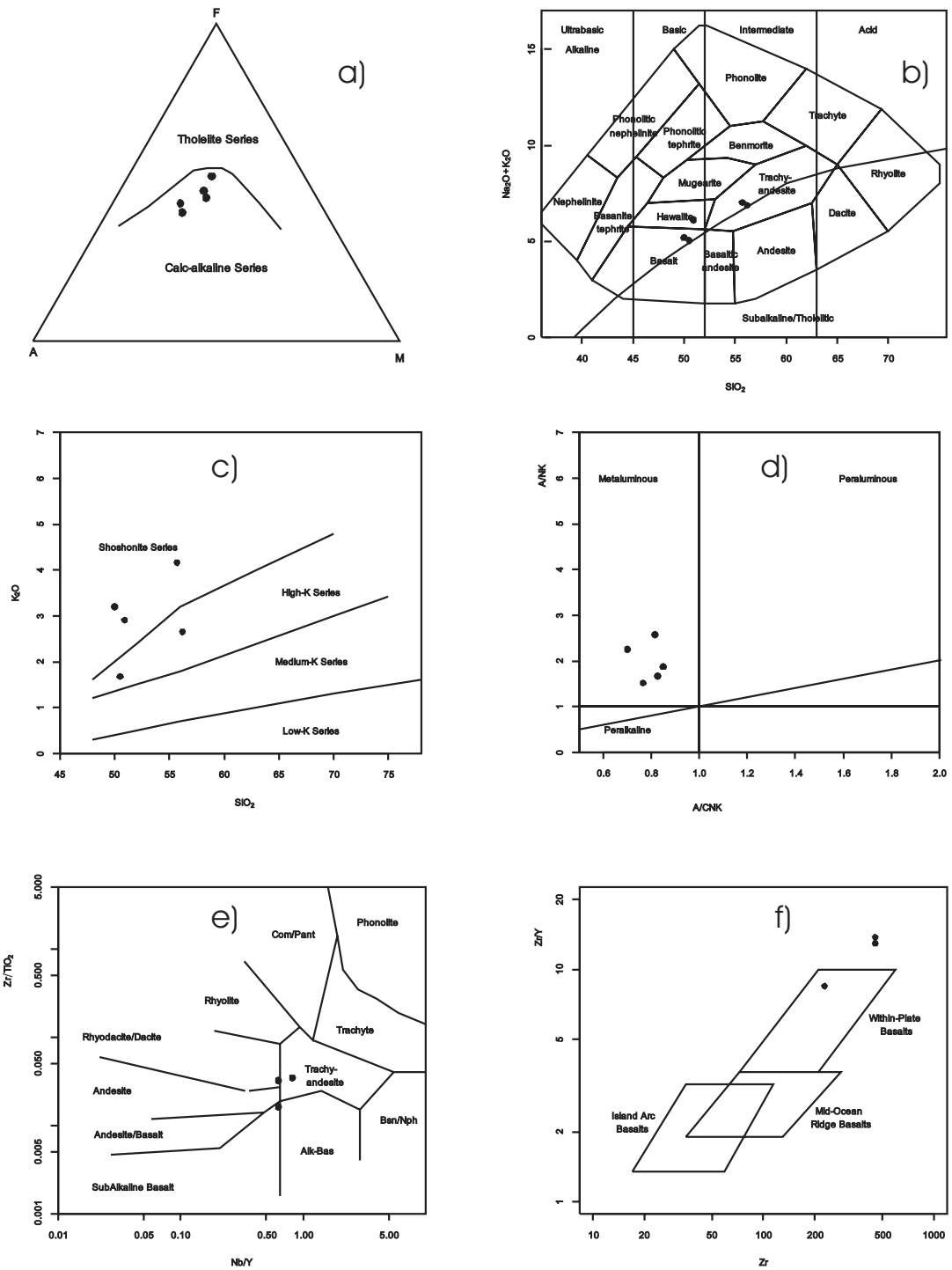


Fig. 6.30 - Diagrams of Las Flores basalts.

a) AFM diagram indicating non-tholeiitic character; b) TAS diagram after Cox *et al.* (1979): subalkaline to alkaline character; c) SiO₂ vs. K₂O diagram, after Peccerillo and Taylor (1979): high K₂O to shoshonitic character; d) A/CNK vs. A/NK, parameters: metaluminous character; e) Nb/Y vs. Zr/TiO₂ diagram, after Winchester and Floyd (1977): trachy-andesite and mild alkaline classification; f) Zr vs. Zr/Y diagram, after Pearce and Norry (1977): within-plate tectonic setting.

CHAPTER 7 MICROSTRUCTURAL AND TEXTURAL ASPECTS OF MEDIUM-LOW AND HIGH-T TECTONITES

7.1. Microstructures

7.1.1. Low to medium-T tectonites

Four different main types of mylonites were identified in the Sierra Ballena Shear Zone: granitic mylonites, phyllonites, quartz-mylonites, and mylonitic porphyries.

Granitic mylonites

These mylonites have a very foliated matrix wrapping alkali feldspar and plagioclase porphyroclasts. The porphyroclasts have σ -type morphology and recrystallized tails that in most cases indicate a sinistral sense of shear.

Feldspar shows fractures, bent twins, and undulose extinction. The fractures are usually filled with quartz (Fig. 3.1c).

Quartz exhibits dynamic recrystallization to elongated ribbons with dominant subgrain rotation recrystallization. In the highly-strained mylonites, coalescence of quartz leads to the segregation of continuous layers of quartz.

Plagioclase evidences no significant alteration, but abundant epidote (probably associated with the action of fluids during shearing) is present. The anorthite content of comminuted plagioclase seems to have contributed to epidote neoformation. The plagioclase porphyroclasts have rounded shapes, a fact that could be associated with a high vorticity strain regime.

The described microstructures observed in feldspar and quartz are typical of deformation in greenschists conditions (Paschier and Trow, 1996, pp. 49 and 50, and Tullis *et al.*, 2000). The occurrence of ribbon quartz with important subgrain rotation indicates deformation in dislocation regime 2 of Hirth and Tullis (1992).

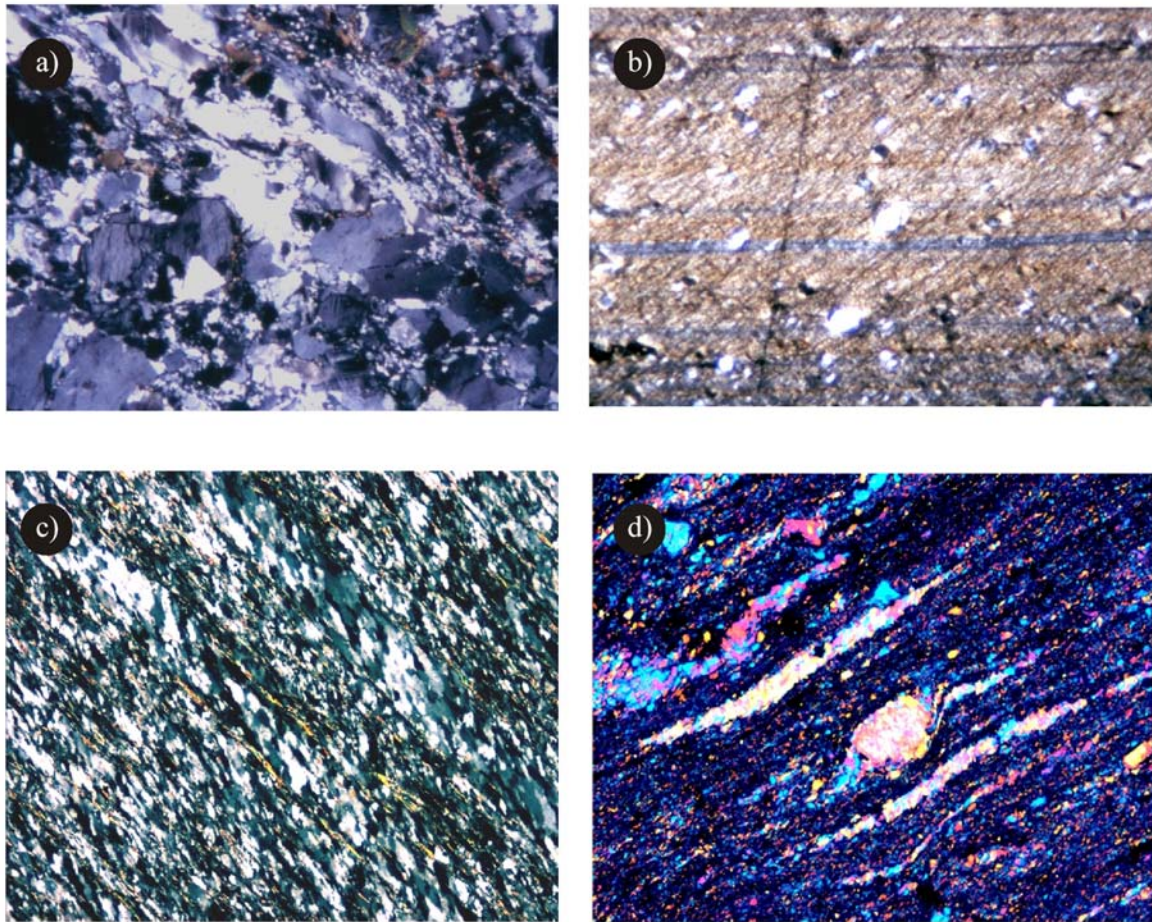


Fig. 7.1 Microstructural features of low-medium T tectonites

All photomicrographs in crossed polarized light.

All photomicrographs width of view 3 mm

a) Granitic mylonite. Subgrain rotation recrystallization in quartz (dislocation creep regime 2)

b) Phyllonite. Mica rich matrix generated by breakdown of feldspar

c) Quartz mylonite. Mica grains pin the boundary migration of quartz.
Transition to dislocation creep regime 3.

d) K-feldspar porphyroblast in mylonitic porphyry. Recrystallization of quartz phenocrysts.
Tails of recrystallized feldspar phenocryst.

Phyllonites

Phyllonites are characterised by a mica rich matrix displaying millimetre-wide compositional layering. Very well-rounded plagioclase and K feldspar porphyroclasts “float” in this matrix. Porphyroclasts are nearly 0.1 mm in size, and the asymmetric distribution of mica around them, evidenced by different extinction positions, is a kinematic indicator of sinistral shearing (Fig. 7.1). In other cases, asymmetric pressure shadows of carbonate indicate the same kinematics. In some layers, epidote porphyroclasts, frequently with allanite cores, are a common feature. The porphyroclasts display little intracrystalline deformation and most of the strain seems to be accommodated by the very weak matrix.

Muscovite mica fish (nearly 0.2 mm) also display a sense of shearing consistent with that of the porphyroclasts.

Very fine-grained quartz layers are observed and interpreted as the result of mechanical segregation during deformation. They display quartz subgrains and an SC structure.

An extensional crenulation cleavage (Platt and Vissers (1980) or C' band cleavage (Berthé *et al.* 1979) is also present at low angle with layering.

All the microstructures mentioned are consistent with sinistral shearing during low-grade conditions.

As pointed out in Chapter 3, the protolith of these rocks is probably a granitic rock in which the breakdown of K-feldspar contributed to the mica-rich matrix and the breakdown of plagioclase to neoformation of epidote.

Quartz mylonites

These rocks correspond to quartz dikes emplaced in the Sierra Ballena Shear Zone during deformation stage 3 probably in releasing zones. They are composed mainly of quartz with accessory sericite, tourmaline, and opaques.

Quartz normally displays a distinct SC structure, where elongated quartz grains (0.2 x 0.04 mm) form the S, which is cut by a C surface, evidencing sinistral shearing. Sericite

is concentrated in these discrete C surfaces. Tourmaline crystals are wrapped by the foliation and sometimes boudinaged, thus indicating the stretching direction.

Quartz displays subgrain rotation recrystallization and grain boundary migration. The latter process determines that quartz grains are coarser in sericite-poor layers.

When these quartz dikes are folded, the foliation determined by the orientation of quartz grains (S_{myl_n}) is also folded, and an axial plane foliation is observed. This new foliation ($S_{myl_{n+1}}$) is a millimetre-spaced fracture cleavage with sericite (Fig. 7.1).

The characteristics observed are similar to the microstructures described by Hirth *et al.* (1998) in sheets 3 through 6 of Heavitree quartzite, and are evidence of recovery brought on by subgrain rotation and grain boundary migration (transition from regime 2 to regime 3 of Hirth and Tullis, 1992), in upper greenschist conditions.

Mylonitic porphyries

These rocks correspond to deformed dikes of porphyry emplaced in the Sierra Ballena Shear Zone during deformation stage 3, probably in releasing zones. These mylonitic porphyries are characterized by alkali feldspar phenocrysts (about 1 x 0.5 mm) in a fine-grained felsic matrix. The rheological properties of these phenocrysts determined their behaviour as the “strong phase” (in the sense of Handy, 1994), isolated in an “interconnected weak” (in the sense given by Handy, 1994) matrix (Fig. 7.1).

In most of the cases, the original euhedral shape of the phenocrysts is very well preserved. When the strength contrast with the matrix is lower or the strain is higher, the phenocrysts evolve to porphyroclasts with σ and δ shapes. The δ shape is considered an indication of an important component of simple shear, in view of the axial ratio ($n \sim 2$) of the porphyroclasts.

Quartz phenocrysts are normally transformed into elongated aggregates, which are coarser-grained than the matrix. The quartz of the phenocrysts is dynamically recrystallized; the subgrains display negative elongation and form an S-C structure in relation to the outline of the elongated phenocrysts that are parallel to the mylonitic foliation.

Phenocrysts of quartz with chessboard texture (Kruhl, 1996) are also sometimes observed. This texture is evidence of high T subsolidus deformation.

Feldspar phenocrysts sometimes display tension boudins and a core and mantle structure with asymmetric tails.

Aegirine-augite, sometimes observed in pressure shadows of phenocrysts, is considered an indication of synmagmatic deformation.

The fabric of these mylonitic porphyries seems to result from magmatic flow in a non-coaxial strain regime, simultaneous with strike-slip movement in the Sierra Ballena Shear Zone. The microstructures described above indicate that deformation of these mylonitic porphyries began in the magmatic stage and continued in the sub-solidus stage.

7.1.2. High T tectonites

Tectonites related to high temperature deformation are observed in the basement at both sides of the Sierra Ballena Shear Zone. In the western side they correspond to orthogneisses and stripped orthogneisses of the Campanero Unit, and in the eastern side to paragneisses and granulites of the Cerro Olivo Complex.

The orthogneisses of the Campanero Unit are fine-grained and normally leucocratic, usually displaying a banded structure with alternating quartz and feldspar aggregates. A stretching lineation is defined by quartz, feldspar, and biotite aggregates. The texture is granoblastic, and sub-equant feldspar grains with common straight boundaries and triple joints of nearly 120° are observed. Quartz shows chessboard extinction (see Fig. 7.2), which is evidence of high temperature conditions of deformation, according to Kruhl (1996). Given these features, the texture could also be defined as granulitic (in the sense given by Martelat *et al.*, 1999).

When strain increases, the phase boundaries between elongated quartz grains and feldspar-rich domains cusp in the direction of the foliation, a feature that according to Gower and Simpson (1992) is associated with diffusional creep at high T (~ 600°). Evidence of partial melting can be observed in some of the orthogneisses as interstitial micrographic intergrowths of quartz and feldspar (probably eutectic compositions). These partial melts can enhance deformation by diffusional creep, as described by Dell'Angelo *et al.* (1987). Garlick and Gromet (2004) described microstructures in high temperature mylonites of New England (USA) that are very similar to those observed in the

orthogneisses of the Campanero Unit and ascribed to diffusional creep associated with partial melting.

Quartz forms polycrystalline ribbons (Types III and IV of Boullier and Bouchez, 1978) that could be considered equivalent to the “plattenquarz” of the German nomenclature. In highly-deformed rocks, complete segregation of quartz and feldspar is attained and “stripped gneisses” are formed. In these “stripped gneisses,” straight ribbons up to several centimetres long separate feldspar-rich domains with evidence of high T recrystallization, such as mosaic texture, straight grain boundaries, and triple joints of nearly 120°. According to Hippertt *et al.* (2001), this kind of microstructure could be related to plastic deformation and coalescence of scattered quartz grains associated with enhanced grain boundary mobility in a high-grade metamorphic environment. Other postulated origins for this kind of structures, such as crack and seal (fracture and injection of quartz veins) parallel to the mylonitic foliation (Vollbrecht *et al.*, 1997 and references therein), apparently do not apply to our study area, as all intermediate cases, from elongated quartz grains to straight ribbons, can be observed, such as the case described by Hippertt *et al.* (2001). Nevertheless, in order to reach a more definitive conclusion regarding this genetic aspect, more detailed fabric analyses are necessary.

The temperature conditions of the deformation in the western side of the SBSZ could be constrained between 650° and 750° by the association quartz + muscovite and by the presence of chessboard texture in quartz. Also, the regional association with migmatites containing sillimanite in the paleosome indicates regional high temperature.

In the eastern side of the Sierra Ballena Shear Zone, the occurrence of hypersthene is diagnostic of granulite facies conditions. Using Opx-Cpx and Hbl-Plag geothermometers, Masquelin *et al.* (2001) bracketed the T conditions between 768° and 850°C during deformation-metamorphism in the Cerro Olivo Complex.

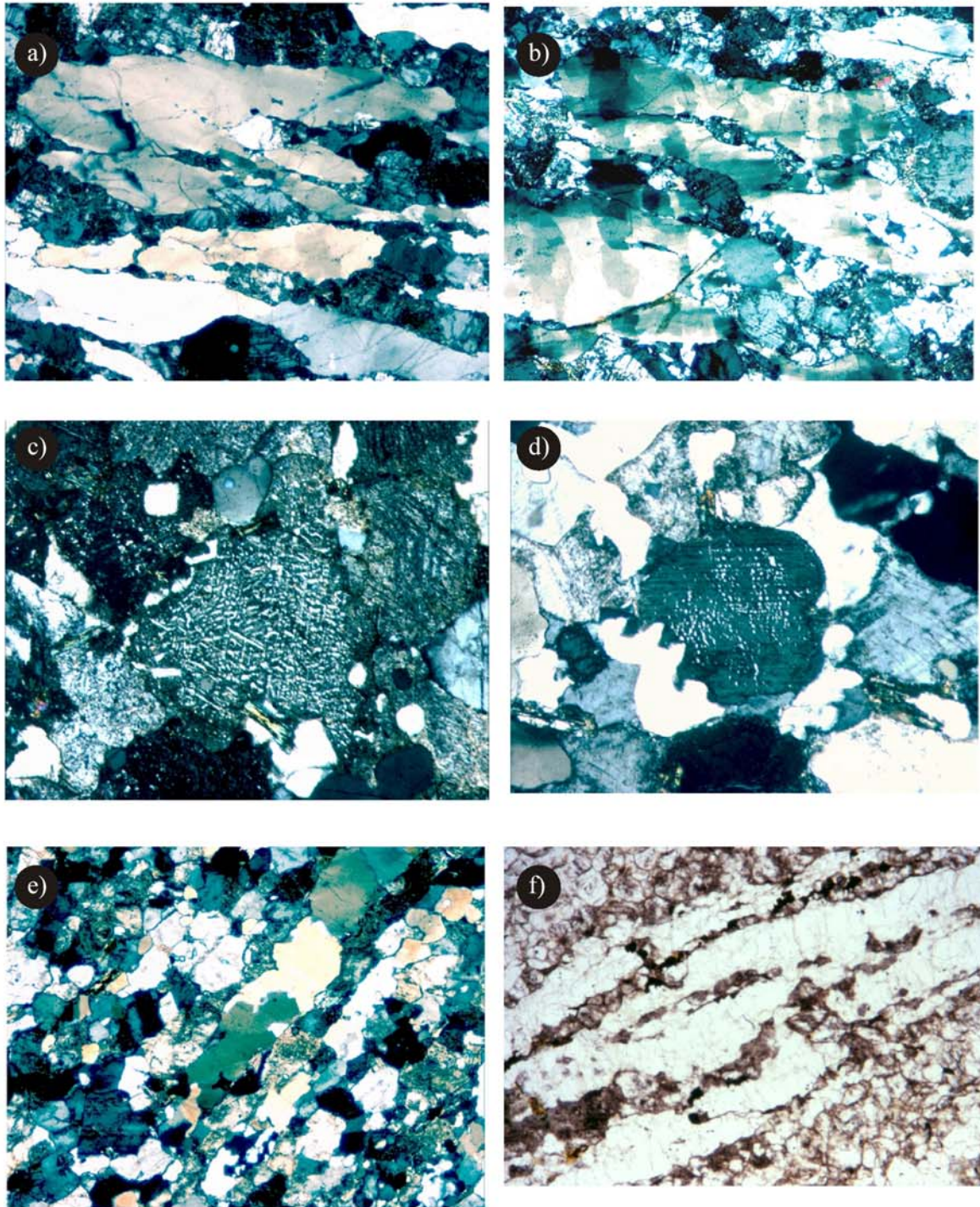


Fig. 7.2 Microstructural features of High T tectonites

a) Diffusional creep. Cusps of feldspar point in the direction of foliation. CPL

b) Chessboard structure in quartz. CPL

c) Interstitial graphic intergrowths of plagioclase and quartz, evidence of partial melting. CPL

d) Grain boundary migration. CPL

e) Quartz ribbons in stripped gneiss. CPL

f) Quartz ribbons in stripped gneiss. PPL

Width of view in all Photomicrographs 3 mm.

CPL = crossed polarized light. PPL = plane polarized light.

7.2. Texture investigation

Texture (crystallographic-preferred orientation) analyses were conducted at the Forschungszentrum Jülich of the University of Bonn (Germany), using neutron diffraction on samples of mylonites from the Sierra Ballena Shear Zone and the syntectonic Maldonado Granite. The principles of the method and the equipment used are described in Schäfer (2002). Neutron texture measurements and experimental pole figures were recalculated to ODF by Jens Walter, using the program Beartex.

The use of neutron diffraction for textural studies offers several advantages. Complete texture analysis is possible, in contrast with the U-stage method where only the orientation of c-axis is obtainable in quartz. Furthermore, the high penetration capability of neutrons determines that, unlike with X-ray based methods, large samples can be investigated and thus better statistics are obtained.

The pol-figures are represented in the standard XZ section and the trace of the foliation plane is indicated in each projection.

Granitic mylonites

Two samples of granitic mylonite from Cordillera shear zone were selected for textural analysis. Cordillera shear zone is less affected by deformation stage 3 than Sierra Ballena shear zone and then the textures of stage 2 should be better preserved. Figure 7.3 presents the recalculated pol-figures for quartz and biotite in granitic mylonites. Contour lines were interrupted whenever the recalculated shape was not reliable or interferences of reflections from other minerals occurred.

Two different patterns were observed for quartz. Sample SB 180 is a slightly asymmetric Type I crossed girdle, suggesting the alignment of rhomb slip planes. The asymmetry indicates a component of dextral shearing in the deformation. In the case of SB 318, the pattern resembles an oblique single girdle. The inclination of the girdle and the position of the single a-maxima are consistent with dextral shearing. This shearing sense is consistent with meso and macrostructure indications. The textures are interpreted to be an evidence of dominant activity of rhomb $\langle a \rangle$ slip system.

The pole figures of biotite indicate strong alignment in the foliation plane.

The microstructures described above and the patterns of the pol-figures suggest that the granitic mylonites were deformed in conditions of middle greenschist facies, at lower temperature than the quartz mylonites.

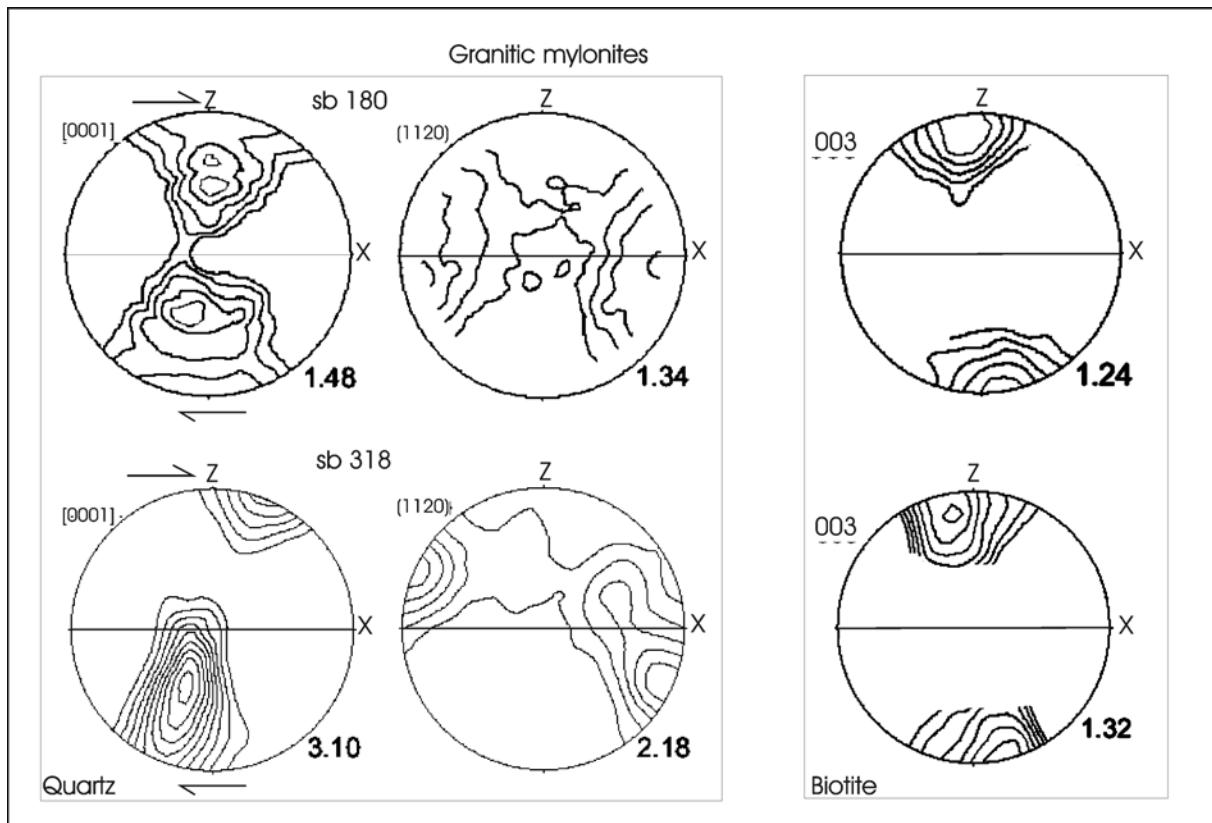


Fig. 7.3.- Recalculated pol-figures of granitic mylonites from Cordillera shear zone. Maximum densities are indicated in the bottom left-hand side of each pol-figure. Diagrams are contoured at multiples of uniform distribution.

Quartz mylonites

Figure 7.4 presents the pol-figures of the quartz-mylonites of Sierra Ballena shear zone. The most outstanding point is the misalignment of the texture with respect to the external reference frame (foliation and lineation). This kind of deviation had already been detected by Simpson (1980) and MacCready (1995). The reason for the discrepancy could be either that the final strain is not consistent with finite strain, that an older fabric is inherited, or that some $\langle c \rangle$ slip occurred (MacCready, 1996 and references therein).

Ullemeyer and Weber (1999) also found this kind of deviated textures in the Moldanubian Zone in Australia, where transpressive deformation is well-documented. These authors suggested that the ductile behaviour of quartz determines that its texture changes, while other minerals of the rock are already brittle and their textures remain unchanged. They also proposed that this different rheological behaviour could explain the misfit in a transpressive deformation regime.

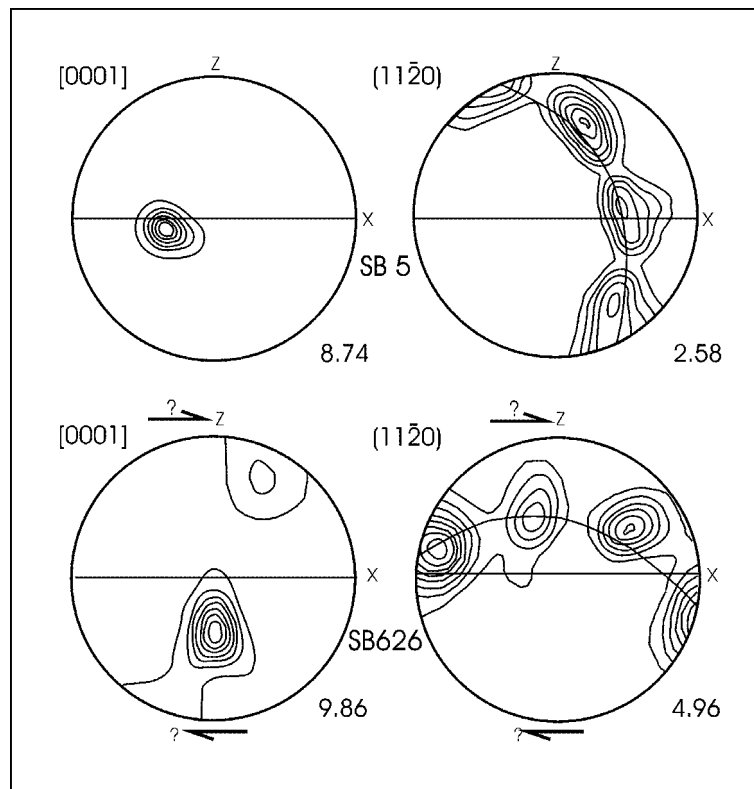


Fig. 7.4 Recalculated pol-figures of quartz-mylonites of Sierra Ballena shear zone. Maximum densities are indicated in the bottom left-hand side of each pol-figure. Diagrams are contoured at multiples of uniform distribution. Contour intervals for $\{0001\}$: 1, 2, 3...; for $(11\bar{2}0)$: 0.5, 1, 1.5 ... times.

Another feature of the pol-figures of quartz-mylonites is the near Y cluster of the c-axis. Texture patterns with Y-maximum have been reported in tectonites deformed in upper greenschist to amphibolite facies (Schmid and Casey, 1986 and references therein) and are related to prism $\langle a \rangle$ slip. The observed asymmetric disposition of a-axis maxima indicates a rotational component in the deformation, according to the criteria indicated by Schmid and Casey (*op. cit.*).

Mylonitic porphyries

Two samples of mylonitic porphyry emplaced in Sierra Ballena shear Zone were investigated. The pol-figures of quartz and biotite are presented in Figure 7.5. Sample SB 2 resembles the pattern of SB 5 (quartz mylonite). The c-axis maximum of quartz is slightly displaced from Y and the preponderance of one a-axis maximum is a sign of a sinistral component of rotational deformation. The slip system is prism $\langle a \rangle$. As indicated for the quartz mylonites, the departure from the external reference frame could be considered an indication of transpressive deformation regime. Sample SB 612 is similar, but a rhomb $\langle a \rangle$ slip system is also present, and deviation from external reference frame is small.

The patterns for biotite indicate strong alignment parallel to the foliation plane. In the case of sample S B2, a divergence with the external texture frame is observed.

The textures analysed are consistent with the microstructures described and suggest medium to high-T deformation, probably during sub-solidus cooling of the porphyries emplaced in the shear zone.

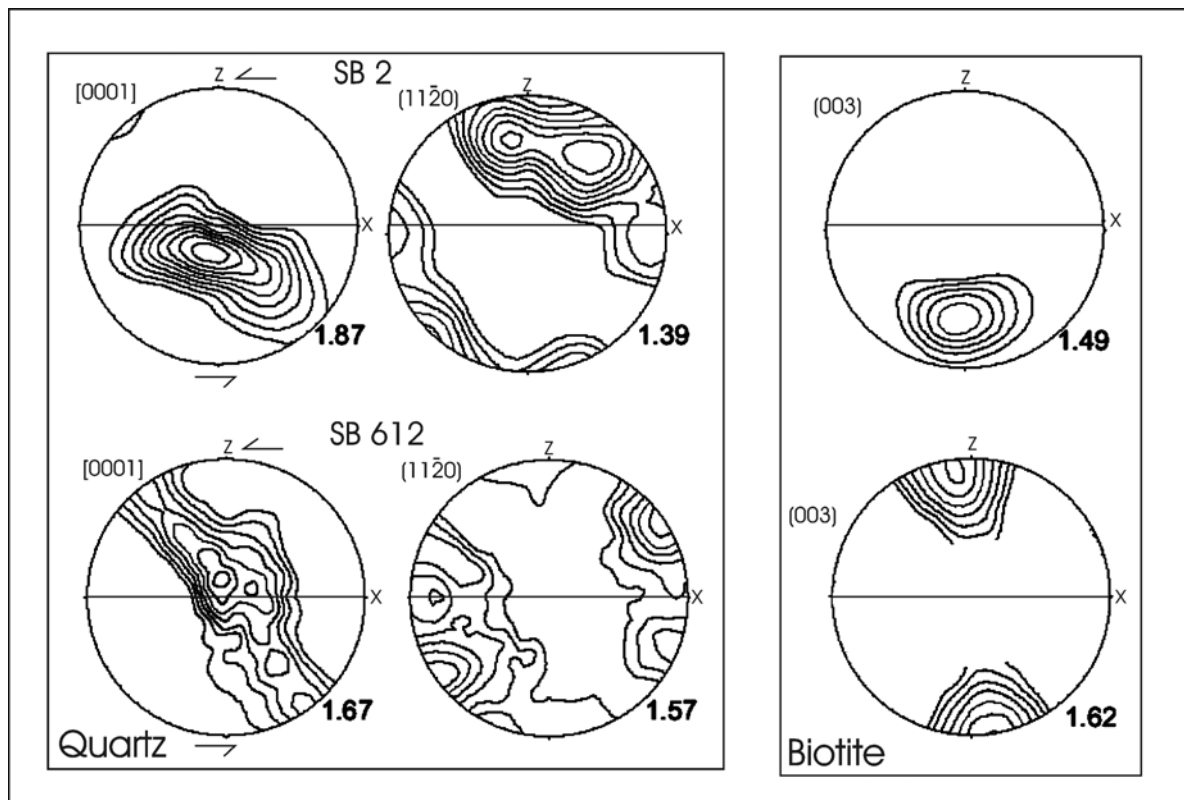


Fig. 7.5.- Recalculated pol-figures of mylonitic porphyries of Sierra Ballena shear zone. Maximum densities are indicated in the bottom left-hand side of each pol-figure. Diagrams are contoured at multiples of uniform distribution. Contour intervals for $\{0001\}$: 1, 2, 3...; for $(11\bar{2}0)$: 0.5, 1, 1.5 ... times.

Maldonado Granite

The quartz pol-figure of the Maldonado Granite displays a classic Y-maximum c-axis pattern (Fig. 7.6). Asymmetric distribution of a-axis maxima imply a component of sinistral rotational deformation, according to the criteria of Schmid and Casey (1986), and the misfit with the external reference frame suggests a transpressive strain regime (Ullemeyer and Weber, 1999).

These textures are consistent with microstructural evidence of high T deformation, such as dynamic recrystallization of feldspar (core and mantle structure), and with abundance of myrmekite in the foliation plane. The prolate shape of co-magmatic enclaves and their axial ratios suggest an important flattening component, also consistent with transpression.

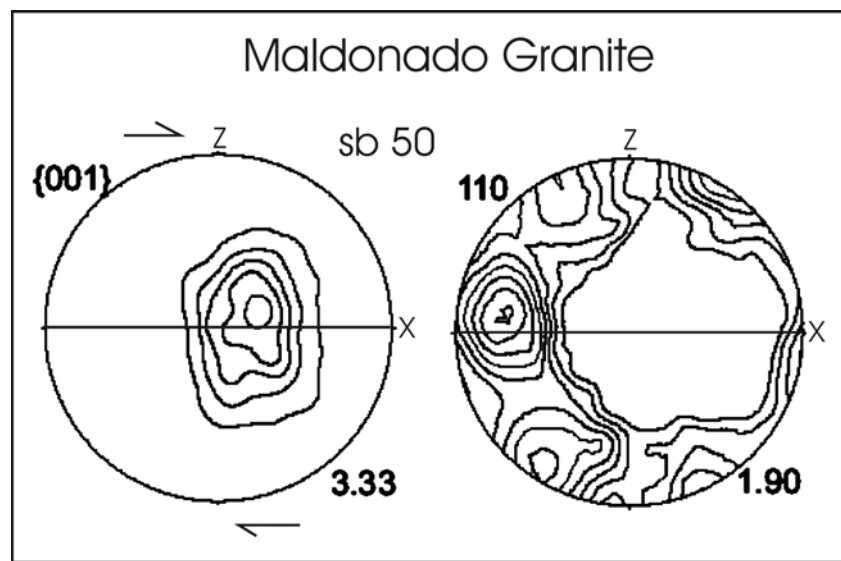


Fig. 7.6- Recalculated pol-figures of Maldonado granite. Maximum densities are indicated in the bottom left-hand side of each pol-figure. Diagrams are contoured at multiples of uniform distribution. Contour intervals for $\{0001\}$: 1, 2, 3...; for (1120): 0.5, 1, 1.5 ... times.

7.3. Conclusions

The microstructures observed and the textures measured indicate that deformation took place in low T conditions (middle greenschist facies) in the case of the granitic mylonites and at medium to high-T (upper greenschist to lower amphibolite facies) in the case of quartz mylonites and mylonitic porphyries.

The microstructures present in quartz depend on the dislocation regime, which is in turn conditioned by the strain rate and temperature (Hirth and Tullis, 1992). At medium strain rates and temperatures, subgrain development predominates (regime 2); if the temperature increases or the strain rate decreases, grain boundary migration is preponderant. In a recent detailed study of the eastern Tonale Fault, Stipp *et al.* (2002) established that the transition between single or crossed girdle patterns and Y single maximum occurs at $\sim 500^{\circ}\text{C}$, near the transition from subgrain rotation (SGR) to grain boundary migration (GBM) recrystallization mechanism. They also indicated that the strain rate in Tonale mylonites is within the range of most natural shear zones, concluding that the microstructural type and texture pattern can be used to estimate the temperature in mylonites when syntectonic parageneses are not present.

With respect to the microstructures of quartz observed in this investigation, the granitic mylonites predominantly display subgrain rotation recrystallization (regime 2 of Hirth and Tullis, 1992), while in quartz mylonites and mylonitic porphyries, grain boundary migration indicates transition to dislocation creep regime 3. This variation is consistent with differences observed in the patterns of quartz textures. Quartz mylonites and mylonitic porphyries display Y-maximum patterns for c-axis, indicating a prism $\langle a \rangle$ slip system, while in the granitic mylonites the main slip system appears to be rhomb $\langle a \rangle$. Taking these elements into account, the temperature for the deformation of the Sierra Ballena Shear Zone quartz mylonites can be estimated at around 500° , considering the pattern of the pol-figures and the coexistence of SGR and GBM.

The heat added to the shear zone by syn-kinematic intrusions can explain the occurrence of medium to high-T mylonites (upper greenschist to amphibolite facies) in a shear zone where regional lower greenschist conditions are well constrained by the parageneses of metasediments in genetically associated basins (the Maldonado Group and the San Carlos Formation). These medium to high-T mylonites are thus the result of

deformation during contact metamorphism or during sub-solidus cooling (mylonitic porphyries).

In the Maldonado Granite, deformation took place at high temperatures, close to the granite solidus. The presence of prism- $\langle a \rangle$ slip provides evidence that solid-state deformation occurred at temperatures higher than 500°C, while the asymmetry of the fabrics and the microstructures indicate a non-coaxial flattening deformation regime.

CHAPTER 8 GEOCHRONOLOGY

Available geochronological data (including data gathered in this investigation) is presented in Table 8.4. Some selected ages are exposed in Figure 8.1. The respective age frequency histograms are shown in Figures 8.2 and 8.3. The first conclusion arrived at is that there is insufficient age data for the pre-Brasiliano Basement, with high temperature age determinations being particularly scarce.

The suggestion by Preciozzi *et al.* (1999) of a Namaqua/Greenville Terrane (the Punta del Este Terrane) is not confirmed by Hartmann *et al.* (2002), who gave a 2058 ± 11 Ma SHRIMP age determination in the core of zircon grains in an orthogneiss, which are interpreted as inherited from the Basement. Further research is needed to prove the actual presence of basement related to the Namaqua Province of Africa in the eastern crystalline of Uruguay.

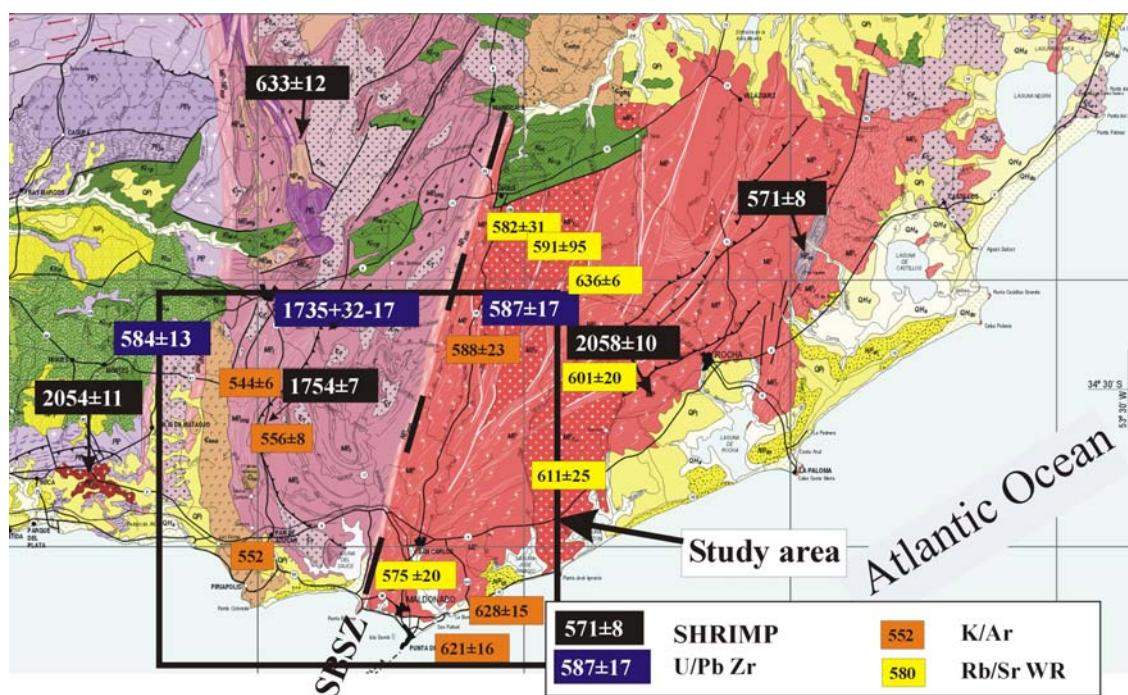


Fig 8.1.- Location of selected age determinations in the southeastern crystalline of Uruguay. Details of age determinations are given in table 8.4. Geology after Bossi and Ferrando (2001). Geographic grid: 50 km.

The other main determination is the high frequency of ages in the 500-600 Ma range. They include crystallization, probably metamorphically overprinted, as well as cooling ages, and correspond to what Silva *et al.* (2005) defined as Brasiliano III

(equivalent to Pan-African III). The abovementioned lack of robust zircon ages determines the impossibility of accurately recognizing the different Brasiliano/Pan-African events postulated for southern Brazil (Brasiliano I and II of Silva *et al.*, 2005), or the earlier episodes (900-750 Ma) that Porada (1989) recognized in southern and equatorial Africa.

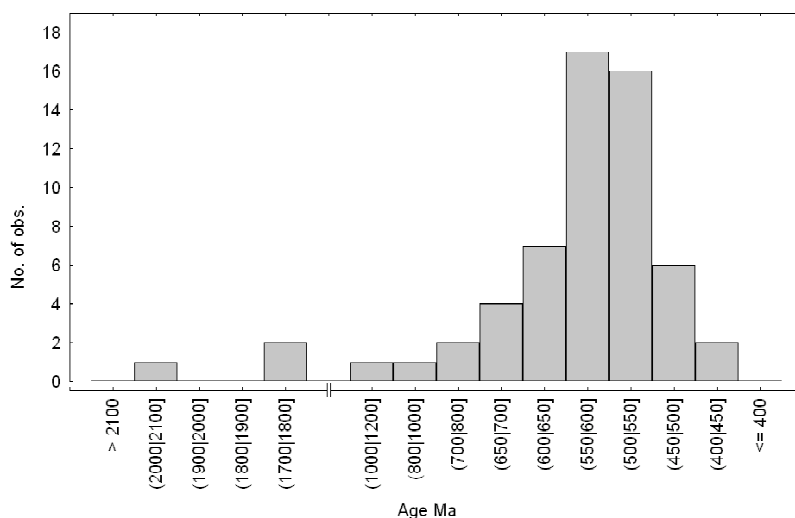


Fig. 8.2.- Histogram of age determinations for the southeastern crystalline of Uruguay.

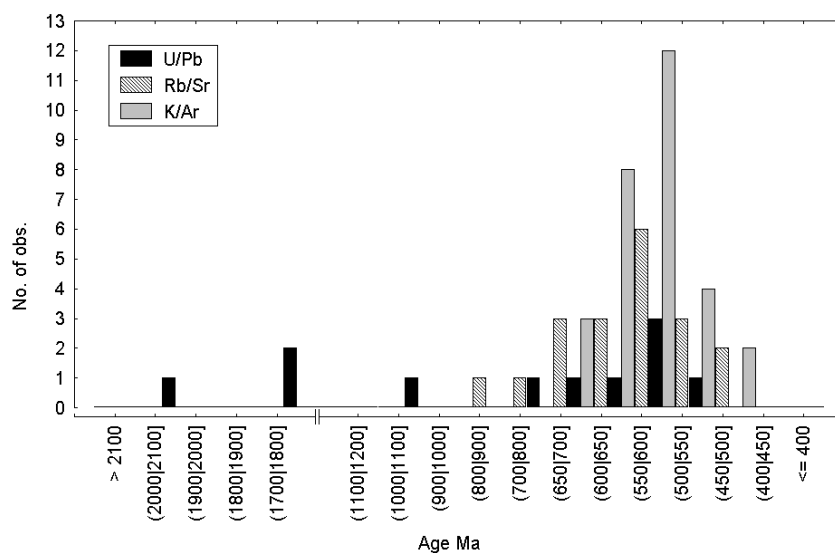


Fig. 8.3.- Histogram of age determinations according to different methods, for the southeastern crystalline of Uruguay.

8.1. New geochronological data

This investigation produced fifteen new age determinations. Dr. Klaus Wemmer and assistants conducted the isotopic analysis (for the K/Ar and Rb/Sr ages) at the laboratories of the Geowissenschaftliches Zentrum, Georg-August Universität, Göttingen. The coordinates of the samples are presented in Appendix 3.

8.1.1. Solis the Mataojo Granitic Complex

During a geochronological reconnaissance of Uruguay, Umpierre and Halpern (1971) presented a first Rb/Sr age determination of 560 ± 15 Ma, assuming an $^{87}\text{Sr}/^{86}\text{Sr}$ initial ratio of 0.704. The lithology originally described as migmatite was later redefined by Oyhantçabal *et al.* (1993b) as the granodiorite facies of an elongated syntectonic intrusion emplaced in the Sarandí del Yí Shear Zone.

Prismatic sphene crystals of a tonalite sample from the Solis de Mataojo Complex were used to obtain a $^{207}\text{Pb}/^{206}\text{Pb}$ isochron. The analytical data is shown in Table 8.1.

acid	time	$^{206}\text{Pb}/^{204}\text{Pb} \pm 2s^+$	$^{207}\text{Pb}/^{204}\text{Pb} \pm 2s^+$	$^{208}\text{Pb}/^{204}\text{Pb} \pm 2s^+$	r_1^*	r_2^{**}			
mix	20'	18.772	0.027	15.574	0.023	38.752	0.061	0.978	0.962
1N HBr	1h	19.285	0.031	15.559	0.026	41.483	0.072	0.980	0.969
4N HBr	3h	45.246	0.153	17.138	0.059	69.902	0.240	0.994	0.994
8.8N HBr	12h	93.651	0.238	20.003	0.052	117.849	0.308	0.992	0.987
8.8N HBr	48h	124.568	0.136	21.848	0.025	152.635	0.187	0.980	0.967
14N HNO ₃	12h	101.585	0.320	20.461	0.065	128.723	0.415	0.994	0.987
residue	24h	108.852	0.447	20.916	0.087	136.799	0.572	0.994	0.988

* $r_1 = ^{206}\text{Pb}/^{204}\text{Pb}$ vs. $^{207}\text{Pb}/^{204}\text{Pb}$ error correlation
** $r_2 = ^{206}\text{Pb}/^{204}\text{Pb}$ vs. $^{208}\text{Pb}/^{204}\text{Pb}$ error correlation
+ Errors are two standard deviations absolute

Table 8.1. U-Pb data of the Solís de Mataojo Granitic Complex.

The age obtained is 584 ± 13 Ma, with an MSWD of 1.7, and is interpreted as the age of crystallization of the rock. The source of Pb shows an age *ca.* 1450 Ma (see Fig. 8.4). The age obtained is not far from the first approximation by Umpierre and Halpern (1971).

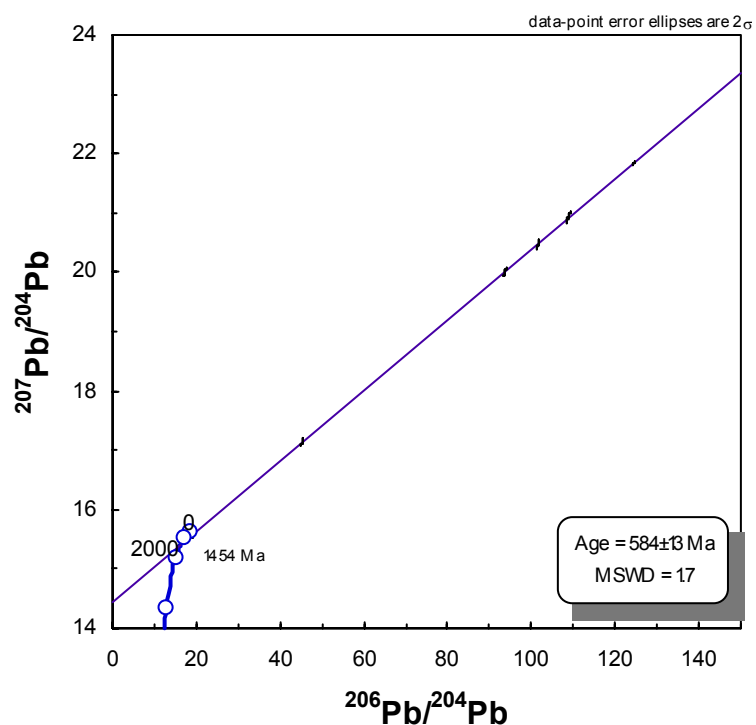


Fig. 8.4.- Lead-Lead Isochron: Titanite from the Solís de Mataojo Granitic Complex.

K/Ar ages were also determined in biotite and hornblende from the same tonalite sample (SB 632). Results are shown in Table 8.2. Biotite ages are scattered between 501.4 and 578.4 Ma, a fact probably associated with alteration (chloritization). The age obtained in hornblende (553.2 Ma) is considered to low and can not be explained only by the cooling rate of the pluton, bearing in mind that the blocking temperature for U/Pb in sphene is approximately 700°C , while for K/Ar in hornblende is about 550°C .

Sample	Mineral	K ₂ O [Wt.%]	⁴⁰ Ar * [nl/g] STP	⁴⁰ Ar * [%]	Age [Ma]	2s-Error [Ma]	2s-Error [%]
SB 632	Hornblende	1.58	32.99	98.83	553.2	17.0	3.1
SB 632	Biotite	9.41	206.91	99.59	578.4	5.8	1.0
SB 632	Biotite	9.41	175.40	95.56	501.4	5.0	1.0

Table 8.2.- K-Ar data of the Solis de Mataojo Granitic Complex.

The geochronological data obtained confirms the reactivation of the Sarandí del Yí Shear Zone, with emplacement of syntectonic granites during the late Brasiliano, as suggested by Oyhantçabal *et al.* (1993b).

8.1.2. Cooling ages

Table 8.3 presents a set of new K/Ar data, interpreted as cooling ages. The 588.2 Ma age for the Arroyo de los Píriz Granite is considered a good approximation to its minimal crystallization age, taking into account the close age of 587 Ma (U/Pb - zircon) available for a granitoid that according to field data is genetically related (see Table 8.4 age determination Nr. 24: Aiguá - Las Cañas).

Sample	Unit	Lithology		K ₂ O Wt. %	⁴⁰ Ar * nl/g STP	⁴⁰ Ar * %	Age Ma	2s- Error Ma	2s- Error
UY 10-04	C° Olivo	Pegamatite	Musc	10.30	249.30	98.37	627.5	10.1	1.6
SB 042	C° Olivo	Pegamatite	Musc	10.32	246.87	97.24	621.3	11.6	1.9
UY 3-04	Lavalleja Gr.	Metabasalt	WR /2	1.27	24.33	78.62	513.6	9.2	1.8
UY 3-04		Metabasalt	WR /2	1.27	24.33	78.62	513.6	9.2	1.8
UY 4-04	Lavalleja Gr.	Metapelite	<2µm	3.59	73.61	94.73	544.7	5.9	1.1
UY 5-04	Lavalleja Gr.	Metapelite	<2µm	2.27	47.69	76.14	556.1	7.9	1.4
SB 527	Campanero	Pegamatit	Musc	10.60	222.66	97.67	556.1	9.8	1.8
SB 553	A° Piriz granite	Pegamatit	Musc	10.67	239.28	98.61	588.2	6.0	1.0

Table 8.3.- K-Ar cooling age data for different lithologies of the study area.

Cooling ages in pegmatites of the Basement east of Sierra Ballena (Cerro Olivo Complex) are older (621-628 Ma) than cooling ages of samples in the eastern Basement.

The 556 Ma K/Ar age in muscovite from a pegmatite that cuts the mylonitic foliation of the Campanero Unit orthogneisses establishes a minimum age for the deformation associated with this foliation.

The cooling ages obtained in the Lavallega Group (metabasalt and metapelite) can be related to thermal overprint associated with granitic intrusions, as indicated by Cingolani *et al.* (1990), and/or to exhumation.

8.2. Conclusions

The 584 Ma age obtained in the Solis de Mataojo Granitic Complex is an important reference to constrain the chronology of the transpressive stage of deformation (deformation stage 2), considering the non-coaxial strain regime recorded in this intrusion during the magmatic stage (Oyhantçabal *et al.*, 2001a).

The higher K/Ar cooling ages in the eastern side of the Sierra Ballena Shear Zone may reveal a difference in exhumation between both sides of the shear zone. In view of the stretching lineations in the shear zone that dip to the southwest, together with the sinistral sense of shearing, higher cooling ages are expected in the eastern side of the shear zone. More data is needed to confirm this possible difference in exhumation rate.

Table 8. 4.- Summary of geochronological data available from eastern Uruguay. (Abreviatons: next page)

Number	Basement	Cover	Migmatism	T	Loation	Stratigraphic Unit	Rock type	Method	Age	+/-	R ₀	Interpretation	Reference	Number
1				W	Soca	Soca Gr.	Granite	U/Pb SHRIMP Zr	2054	11		Crystallization	Bossi <i>et al.</i> (2001)	1
2				E	Rocha	syn-tectonic granite	Syenogranite	U/Pb SHRIMP Zr (core)	2058	10		Inherited zircon	Hartmann <i>et al.</i> (2002)	2
3				W	N of Pan de Azúcar	Campanero Unit	Orthogneiss	U/Pb SHRIMP Zr	1754	6.8		Crystallization	Mallmann <i>et al.</i> (2003)	3
4				W	N of Pan de Azúcar	Campanero Unit	Orthogneiss	U/Pb (UI) Zr	1735	+32/-17		Crystallization	Sánchez-Bettucci <i>et al.</i> (2003)	4
5				E	Rocha	Cerro Olivo Cx.	Orthogneiss	U/Pb (UI) Zr	1006	37		Crystallization	Preciozzi <i>et al.</i> (1999)	5
6				W	Minas SE	Campanero Unit ?	Orthogneiss	Rb/Sr WR	844	91	0.7035	?	Preciozzi <i>et al.</i> (1993)	6
7				W	Penitente	syn-tectonic granite	Granite	Rb/Sr WR	779	24	0.7036	Crystallization	Preciozzi <i>et al.</i> (1993)	7
8				E	Rocha	syn-tectonic granite	Syenogranite	U/Pb SHRIMP Zr (rim)	762	8		Crystallization	Hartmann <i>et al.</i> (2002)	8
9				W	S ^a de los Caracoles	S ^a de los Caracoles gr.	Granite	Rb/Sr WR	681	48	0.7162	Crystallization	Preciozzi <i>et al.</i> (1993)	9
10				E	Rocha	Rocha gr.	Granite	Rb/Sr WR	678	14	0.7075	Crystallization	Preciozzi <i>et al.</i> (1993)	10
11				W	N of Pan de Azúcar	Lavalleja Gr.	Metabasalt	U/Pb (UI) Rut	670			Metamorphism ?	Sánchez-Bettucci <i>et al.</i> (2003)	11
12				E	Alferez	Alferez gr.	Granite	Rb/Sr WR	670	59	0.7120	Crystallization	Preciozzi <i>et al.</i> (1993)	12
13				E	Valdivia	Valdivia gr.	Granite	Rb/Sr WR	636	6	0.7094	Crystallization	Preciozzi <i>et al.</i> (1993)	13
14				W	N of Minas	Ptas. del Santa Lucía gr.	Granite	U/Pb SHRIMP Zr	633	8		Crystallization	Hartmann <i>et al.</i> (2002)	14
15				E	La Barra	Cerro Olivo Cx.	Pegmatite	K/Ar Musc	628	10.1		Cooling age	This investigation	15
16				E	La Barra	Cerro Olivo Cx.	Pegmatite	K/Ar Musc	621	11.6		Cooling age	This investigation	16
17				W	Las Flores	Sierra de Animas Cx	Trachybasalt	K/Ar WR	615	30		?	Sánchez and Linares (1996)	17
18				E	José Ignacio	Garzón gr.	Granite	Rb/Sr WR	611	25	Ass	Crystallization	Umpierre and Halpern (1971)	18
19				E	Garzón	Garzón gr.	Granite	Rb/Sr WR	601	20	0.7071	Crystallization	Preciozzi <i>et al.</i> (1993)	19
20				W	Aguas Blancas	Sarandí del Yí SZ	Mylonite	K/Ar Musc	594	13.4		Cooling age	This investigation	20
21				E	Florencia	Florencia gr.	Granite	Rb/Sr WR	591	95	0.7047	Crystallization	Preciozzi <i>et al.</i> (1993)	21
22				E	José Ignacio	Garzón gr.	Granite	Rb/Sr WR	590	25	0.708	Crystallization	Umpierre and Halpern (1971)	22
23				W	N of San Carlos	A° Piriz gr.	Pegmatite	K/Ar Musc	588	6		Cooling age	This investigation	23
24				E	Maldonado	Aiguá Batholith	Granite	U/Pb (UI) Zr	587	16		Crystallization	Basei <i>et al.</i> (2000)	24
25				W	Solís de Mataojo	Solís de Mataojo	Tonalite	U/Pb Sph	584	13		Crystallization		25
26				E	Aiguá	Aiguá Batholith	Granite	Rb/Sr WR	582	31	0.7232	Crystallization	Preciozzi <i>et al.</i> (1993)	26

Table 8. 4.- Summary of geochronological data available from eastern Uruguay (cont.). Cx: Complex; Fm: Formation; Gr: Group; gr: granite; LI: lower intercept; UI: upper intercept; WR: whole rock; Zr: zircon; Rut: rutile; Ass.: assumed 0.704.

Number	Basement	Cover	Migmatism	T	Location	Stratigraphic Unit	Rock type	Method	Age	+/-	R ₀	Interpretation	Reference	Number
27				W	Solis de Mataojo	Solis de Mataojo gr.	Tonalite	K/Ar Bio	578	5.8		Cooling age	This investigation	27
28				E	San Carlos	Maldonado gr	Granite	Rb/Sr WR	575	20	Ass.	Crystallization	Umpierre and Halpern (1971)	28
29				E	Cerro Aguirre	Sierra Aguirre Fm.	Dacite	U/Pb SHRIMP Zr	571	8		Crystallization	Hartmann <i>et al.</i> (2002)	29
30				W	Barriga Negra	Barriga Negra gr.	Granite	Rb/Sr WR	565	59	0.7136	Crystallization	Preciozzi <i>et al.</i> (1993)	30
31				W	Las Flores	Sierra de Animas Cx	Basalt	K/Ar WR	565	30		Cooling age	Sánchez and Linares (1996)	31
32				W	Minas	Solis de Mataojo gr	Granodiorite	Rb/Sr WR	560	15	Ass	Crystallization	Umpierre and Halpern (1971)	32
33				W	N of Pan de Azúcar	Lavalleja Gr.	Metapelite	K/Ar Sericite	556	7.9		Cooling age	This investigation	33
34				W	N of Pan de Azúcar	Campanero Unit	Pegmatite	K/Ar Musc	556	9.8		Cooling age	This investigation	34
35				W	Solis de Mataojo	Solis de Mataojo gr.	Tonalite	K/Ar Bio	553	17		Cooling age	This investigation	35
36				W	C° Pan de Azúcar	Sierra de Animas Cx	Syenite K-Feld	K/Ar Amp	552			Cooling age	Preciozzi <i>et al.</i> (1985)	36
37				W	N of Pan de Azúcar	Lavalleja Gr.	Metapelite	K/Ar Sericite	545	5.9		Cooling age	This investigation	37
38				E	Rocha	Santa Teresa gr.	Granite	Rb/Sr WR	537	7	0.7082	Crystallization	Umpierre and Halpern (1971)	38
39				W	18 km E of Polanco	A° del Soldado Gr.	Metapelite	K/Ar Sericite	532	16		Cooling age	Cingolani <i>et al.</i> (1990)	39
40				W	Polanco	A° del Soldado Gr.	Granodiorite	Rb/Sr WR	530	15	0.708	Crystallization	Umpierre and Halpern (1971)	40
41				W	N of Minas	A° del Soldado Gr.	Metapelite	K/Ar Sericite	530	16		Cooling age	Cingolani <i>et al.</i> (1990)	41
42				W	Las Flores	Sierra de Animas Cx	Basalt	K/Ar WR	525	15		Cooling age	Sánchez and Linares (1996)	42
43				W	Playa Verde-Piriápolis	Sierra de Animas Cx	Porphyries	Rb/Sr WR	520	5	0.7065	Eruption age	Bossi <i>et al.</i> (1993)	43
44				W	C° San Antonio	Sierra de Animas Cx	Rhyolite	K/Ar WR	519			Eruption age	Preciozzi <i>et al.</i> (1985)	44
45				W	N of Pan de Azúcar	Lavalleja Gr.	Metabasalt	K/Ar WR	519	9.4		Cooling age	This investigation	45
46				W	13 km SE of Polanco	A° del Soldado Gr.	Metapelite	K/Ar Sericite	518	15		Cooling age	Cingolani <i>et al.</i> (1990)	46
47				W	N of Pan de Azúcar	Lavalleja Gr.	Metabasalt	K/Ar WR	514	9.2		Cooling age	This investigation	47
48				W	Rocha	Cerro Olivo Cx.	Migmatite/Leucosome	U/Pb (LI) Zr	510	130		Migmatization	Preciozzi <i>et al.</i> (1999)	48
49				W	C° Pan de Azúcar	Sierra de Animas Cx	Syenite K-Feld	K/Ar WR	508			Cooling age	Preciozzi <i>et al.</i> (1985)	49
50				W	18 km E of Polanco	A° del Soldado Gr.	Metapelite	K/Ar Sericite	506	15		Cooling age	Cingolani <i>et al.</i> (1990)	50
51				W	Solis de Mataojo	Solis de Mataojo gr.	Tonalite	K/Ar Bio	501	5		Cooling age	This investigation	51

Number	Basement	Cover	Magmatism	T	Location	Stratigraphic Unit	Rock type	Method	Age	+/-	R ₀	Interpretation	Reference	Number.
52				W	C° Pan de Azúcar	Sierra de las Animas Cx	Syenite K-Feld	Rb/Sr WR	499	72	0.7063	Crystallization	Preciozzi <i>et al.</i> (1993)	52
53				E	Aiguá	Aiguá gr.	Granite	Rb/Sr WR	497	21	0.7092	Crystallization	Umpierre and halpern 1971	53
54				W	N of Minas	A° del Soldado Gr.	Metapelite	K/Ar Sericite	492	14		Cooling age	Cingolani <i>et al.</i> (1990)	54
55				W	Las Flores	Sierra de Animas Cx	Basaltic dike	K/Ar WR	490	15		Cooling age	Sánchez and Linares (1996)	55
56				W	N of Pan de Azúcar	Lavalleja Gr.	Metapelite	K/Ar Sericite	489	6.1		Cooling age	This investigation	56
57				W	C° Pan de Azúcar	Sierra de Animas Cx	Syenite	K/Ar K-Feld	487			Cooling age	Preciozzi <i>et al.</i> (1985)	57
58				W	Las Flores	Sierra de Animas Cx	Basalt	K/Ar WR	434	14		Cooling age	Sánchez and Linares (1996)	58
59				W	Las Flores	Sierra de Animas Cx	Gabbro	K/Ar WR	410	30		Cooling age	Sánchez and Linares (1996)	59

Table 8.4.- Summary of geochronological data available from eastern Uruguay (cont.).

Cx: Complex; Fm: Formation; Gr: Group; gr: granite; LI: lower intercept; UI: upper intercept; WR: whole rock; Zr: zircon; Rut: rutile. Ass.: assumed 0.704.

CHAPTER 9 GEOTECTONIC EVOLUTION AND RELATION TO OTHER PAN-AFRICAN-BRASILIANO BELTS OF SOUTH AMERICA AND AFRICA

9.1. Geotectonic evolution.

9.1.1. Paleoproterozoic basement

The oldest geological record of the study area is the pre-Brasiliano basement. This basement is represented in the western side of the Sierra Ballena Shear Zone by the Campanero Unit and in the eastern side by the Cerro Olivo Complex. Both basement units comprise orthogneisses, high-grade supracrustals, and migmatites. Age determinations are scarce, but Paleoproterozoic ages have been obtained for both units. Data presented in this study indicate that the leucocratic orthogneiss of the Campanero Unit has a geochemical signature characteristic of mature continental arcs. The age of this arc according to SHRIMP and conventional U/Pb determinations on zircon is *ca.* 1750 Ma. The micaschists and BIFs may be interpreted as relicts of a platform sequence of unknown age.

As for the Cerro Olivo Complex, the nature of the protoliths has not been studied yet, but taking into account that the Sierra Ballena Shear Zone displaced the units, a correlation with the Campanero Unit cannot be discarded. The age of this Complex is still a matter of debate, but inherited zircons in Brasiliano gneisses have been interpreted as an indication of the Proterozoic age of the basement (Hartmann *et al.*, 2002).

9.1.2. First deformation stage (Neoproterozoic high temperature deformation-metamorphism).

High temperature deformation, metamorphism, and migmatization have been documented in the Cerro Olivo Complex (Masquelin, 2004), while in the present study these features have been recognized on both sides of the Sierra Ballena Shear Zone (Campanero Unit and Cerro Olivo Complex).

In the basement of the Dom Feliciano Belt in southern Brazil, based on U-Pb SHRIMP dating on zircon, Leite *et al.* (2000) established the age of the high-K calc-

alkaline protolith of the gneisses at around 2.08 Ga and the age of the deformation associated with low angle shear zones in the 800-590 Ma range. Preciozzi *et al.* (1993) also proposed that the migmatization affecting the Cerro Olivo Complex is of Brasiliano age, taking into account the 510 Ma age (U-Pb zircon, lower intercept) they obtained in leucosomes of migmatites of this unit. High temperature deformation of Neoproterozoic age has been recognized elsewhere in Brazil (Egido-Silva *et al.*, 2002; Hippertt *et al.*, 2001).

Given the available data for the region and the correlation with similar Neoproterozoic events in southern Brazil, it is suggested that the high temperature deformation that affected the pre-Brasiliano basement of the study area is of Neoproterozoic age. The regional extent of this high temperature deformation in Uruguay and Brazil indicates that it is probably related to a collision between large plates (Leite *et al.*, 2000).

In the study area, this high temperature foliation is associated to stretching lineations inclined approximately 30 degrees towards NW or SW. The observed vergence of this deformation stage is towards the south - southwest (Fig. 9.1). The symmetry of boudinage and the lack of asymmetric structures suggest that this phase was pure shear-dominated.

The high temperature mylonitic foliation of the basement was rotated as a consequence of the activity of the dextral Sarandí del Yí Shear Zone (Fig. 9.1). If the assumed age of the foliation were correct, it would mean that the dextral event of the Sarandí del Yí Shear Zone is Neoproterozoic.

9.1.3. Basement cover relationships

The pre-Brasiliano basement is covered by two allochthonous successions of unknown age: the Lavallega Group and Zanja del Tigre Formation. Neoproterozoic as well as Mesoproterozoic ages have been indicated for these units. In the case of the Lavallega Group, a back-arc basin setting was proposed (Fernandes *et al.*, 1992, Sánchez-Bettucci *et al.*, 2001), related to subduction of the Adamastor Ocean towards the west.

Basement and cover were probably similarly deformed during the development of the high-temperature foliation of the basement and do not help to constrain the age of these

supracrustal units. Additionally, the contact between basement and cover was reworked during late Brasiliano events, with vergence towards the northwest.

9.1.4. Second deformation stage (Vendian low temperature deformation-metamorphism).

This stage is characterized by the development of high angle transcurrent shear zones and is responsible for the final architecture of the belt. Strike slip basins associated with shoshonitic magmatism were formed and volcano-sedimentary successions of Vendian age were deposited (Las Ventanas and San Carlos Formations).

Stretching lineations related to this stage are near horizontal and parallel to the belt, trending $\sim 020^\circ$. The transpressional character of this stage is documented in west vergent folds with fold axis sub-parallel to the strike slip planes, in flat and ramp structures in the supracrustals with vergence to the northwest, and in the fabric of mylonites and syn-transcurrent intrusions (see Chapter 7). During this stage, the Sierra Ballena Shear Zone was formed as an important boundary between eastern and western domains of the area. The intrusion of the Solís de Mataojo Granitic Complex (~ 584 Ma), with an important flattening component in the magmatic strain, corresponds to this stage. The D2 folding structures described by Rossini and Legrand (2003) in the Zanja del Tigre Formation are associated with this stage. Sinistral as well as dextral shear zones were developed and the Sarandí del Yí Shear Zone was reactivated with sinistral sense (Fig. 9.1). Towards the late-Vendian, a foreland basin developed to the northwest, with deposition of the Arroyo del Soldado Group.

9.1.5. Third deformation stage (Late Vendian-Cambrian low temperature deformation-metamorphism).

The final stage is related alkaline dikes emplaced in releasing bends of the Sierra Ballena Shear Zone, and to folding and strike-slip faults that affect the different supracrustal units, including the Arroyo del Soldado Group, which is the youngest, of upper Vendian age, according to Gaucher *et al.* (2004). It also coincides with the D3 deformation event described by Rossini and Legrand (2003) in the supracrustals of the Zanja del Tigre Formation.

The age of this deformation stage is constrained between 550 and 500 Ma taking into account: a) the proposed age for the Arroyo del Soldado Group; b) the assumed age of the mylonitic porphyries, which is thought to be co-magmatic of the Sierra de las Animas Complex (550-520 Ma); and c) the fact that no Brasiliano intrusives are known to cut the Sierra Ballena Shear Zone. The deformation is sinistral and seems to be simple shear-dominated.

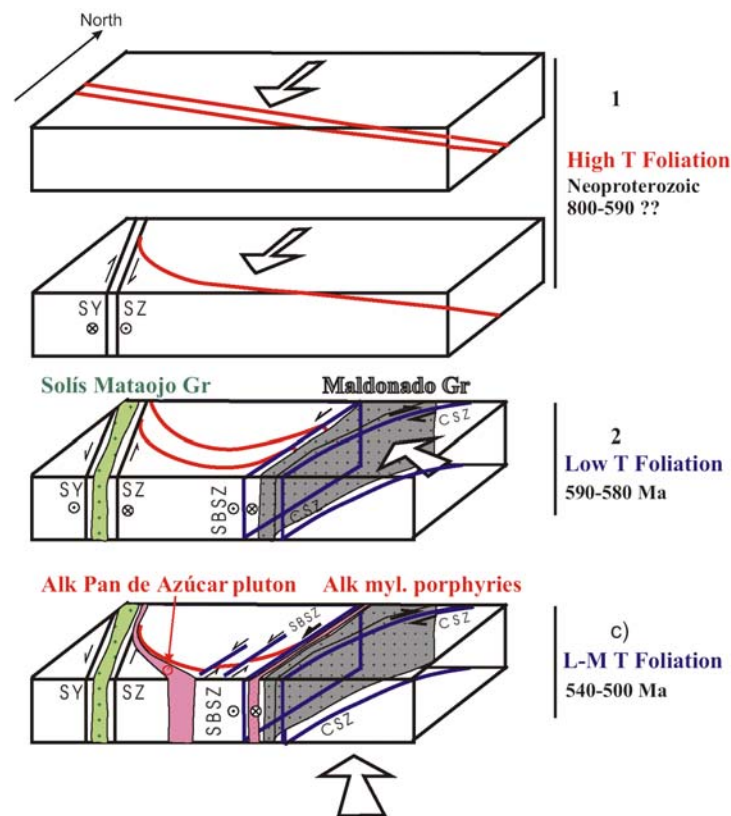


Fig. 9.1.- Schematic block diagrams illustrating the structural relationships between the main shear zones. a) First deformation stage: high temperature mylonitic foliation with vergence to the south and dextral shearing related to the Sarandí del Yí Shear Zone (SYSZ); b) Second deformation stage: transposition with development of conjugate shear zones at ~ 590-580 Ma; c) Third deformation stage: simple shear-dominated transposition associated with strike-slip at ~ 540 – 500 Ma.

9.2. Correlation with Brazil and South Africa

Porada (1979) defined the Upper Proterozoic - Lower Paleozoic “Damara-Ribeira Orogen” and interpreted its evolution in terms of continental collision. The coastal branch of this Orogen in Africa, represented by the Gariiep and Kaoko belts, was correlated by this author with the Ribeira belt of South America.

Fragoso-Cesar (1980) defined the Dom Feliciano belt as a different geotectonic unit, separated from the Ribeira belt by the Luiz Alves Craton. A relationship between the Dom Feliciano belt of South America and the Kaoko belt of Africa has been indicated by most of the authors (Fernandes *et al.*, 1992; Trompette, 1994; Dürr and Dingeldey, 1996; and Basei *et al.*, 2000). A key interesting similitude between the Kaoko and Dom Feliciano belts is the presence of a central major shear zone that controls the architecture of the orogen: the Purros Shear Zone in the Kaoko belt and the Sierra Ballena-Canguçu Shear Zone in the Dom Feliciano belt. Several investigations on the geology of the Kaoko belt and the Purros Shear Zone have been published recently (Goscombe *et al.*, 2003; Paschier *et al.*, 2002; and Konopásek *et al.*, 2005) and it is possible to compare its evolution with that of the Sierra Ballena Shear Zone of Uruguay and the Canguçu and Major Gercino Shear Zones of southern Brazil. In spite of the deficient geochronological database and the possibility of a diachronic evolution, similar evolution stages are recognized in the shear zones of the Kaoko and Dom Feliciano belts (Table 9.1). In view of the similitude in the deformation stages and the ages of the events, it is considered feasible that the Purros Shear Zone of Namibia may represent the continuity of the Sierra Ballena and Dorsal de Canguçu Shear Zones of Uruguay and Brazil.

<u>Kaoko belt</u>			Dom Feliciano belt	
Purros Shear Zone			Canguçu and Major Gercino SZs	Sierra Ballena SZ
Goscombe <i>et al.</i> , 2003	Paschier <i>et al.</i> , 2002	Konopásek <i>et al.</i> , 2005	Brazil	Uruguay (this study)
Early thermal ~ 656 Ma	D1 : E-W shortening	D1 : oblique thrusting. HT metamorphism kin indicators rare and ambiguous Migmatization ~575-550 Ma	Low angle deformation ~700 Ma Leite <i>et al.</i> (2000) Syn-transcurrent granites in MGSZ 602-590 Ma Chemale <i>et al.</i> (2003)	D1: High T deformation (800 ? – 590 Ma). Pure shear dominated. Migmatization D2: transpression (590 – 540 Ma) Aiguá Granite 587 Ma
Trans-pressional 580-550 Ma	D2 : trans-pression (>530 Ma)	D2: sinistral transpression ~527-530 Ma *	Syn-transcurrent granites to DCSZ (Frantz <i>et al.</i> , 2003): 658-625 Ma transpressive period 625-600 Ma transtractive period	Solís de Mataojo Granite 585 Ma Maldonado Granite 575 Ma
Post-trans-pression shortening 530-510 Ma	D3 sinistral trans-pression	D3: sinistral strike-slip 442-479 Ma *		D3: sinistral strike slip (~ 550 – 500 Ma) Intrusion of alkaline porphyries (~ 550 – 520 Ma)

Table 9.1.- Main evolution stages of the Purros Shear Zone of Namibia, the Major Gercino (MGSZ) and the Dorsal do Canguçu (DCSZ) Shear Zones of Brazil, and Sierra Ballena Shear Zone of Uruguay. * = K/Ar. cooling ages

CHAPTER 10 CONCLUSIONS

The study area is the southernmost exposure of the Dom Feliciano Belt. Different shear zones converge in the area and play a key role in its evolution. The Sarandí del Yí Shear Zone is the boundary between the Paleoproterozoic Piedra Alta Terrane (where there is no isotopic record of Neoproterozoic events), and the Nico Pérez Terrane and the Neoproterozoic Dom Feliciano Belt. The former may represent a reworked craton during Brasiliano times (metacraton).

The Sierra Ballena Shear Zone (SBSZ) is a high-strain central zone that divides the Dom Feliciano Belt into two domains and controls its evolution and architecture. This belt in the study area includes a pre-Brasiliano basement, supracrustal successions of different ages, and Brasiliano magmatism.

A first deformation stage (D1) recognized in the study is recorded in a high temperature mylonitic foliation associated with migmatization. The age of this event is not very well constrained in Uruguay, but based on regional data available from southern Brazil, the 800-600 Ma interval is considered as an initial approximation. The similitude in the high-T deformation and the lithologies at both sides of the Sierra Ballena Shear Zone do not support the idea advanced by Bossi and Gaucher (2004) that the shear zone is a terrane boundary resulting from the docking of two plates by tangential collision at 530 Ma.

An evolution is observed in the Brasiliano magmatic suites studied, beginning with highly-fractionated calc-alkaline granites (Solis the Mataojo Granitic Complex ~584 Ma), followed by mildly alkaline granites and shoshonitic volcanics (Maldonado granite ~575 Ma, and Las Flores basalts), and concluding with peralkaline intrusions and volcanics (Sierra de las Animas Complex ~540-520 Ma). Contrary to previous proposals, which considered this magmatism to be the root of a continental arc, it is proposed here that it occurred in an environment transitional from orogenic to anorogenic, during post-orogenic uplift and collapse. The Sierra Ballena Shear Zone was active in this post-collisional environment, and the shear system played a major role in magma ascent and in the emplacement of granitic plutons.

The deformation observed in the Sierra Ballena Shear Zone took place in regional low-grade conditions, as indicated by metasediments of associated strike-slip basins and by microstructures typical of these conditions, observed in granitic mylonites and phyllonites.

The second and third deformation phases recognized are related to high-angle fabrics. An important strain partitioning during these phases determined the development of several high-strain subvertical shear zones (the Sierra Ballena and Cordillera), which are the boundaries separating low-strain domains.

The second deformation phase was transpressional, pure shear dominated, and is associated with conjugate dextral and sinistral shear zones. Thrust structures with vergence to the northwest are associated with this stage. Granites emplaced during this phase show magmatic fabrics with evidence of important flattening. The age of these intrusions allow us to estimate an interval of 590 to 540 Ma for this event.

The granitic mylonites of the SBSZ and Cordillera shear zone were probably formed during this stage. The microstructures observed in quartz of these granitic mylonites are characteristic of the dislocation creep regime 2 of Hirth and Tullis (1992), and fabric pol-figures observed are asymmetric crossed girdles and asymmetric single girdles with rhomb - $\langle a \rangle$ as the active slip system. These features indicate middle greenschist facies conditions during transpressional deformation.

The third stage is a strike-slip tectonic event, with evidence of an important component of simple shear in the strain regime. Alkaline porphyries emplaced in the shear zone have characteristics similar to those of post-orogenic alkaline volcanics and intrusives emplaced in the low strain domain, with ages ranging from 550 to 520 Ma. The lack of Brasiliano granitic intrusions cutting the shear zone and the assumed age of the mylonitic porphyries bracket the age of this third event between 550 and 500 Ma.

Quartz dikes and said alkaline porphyries were emplaced in the SBSZ during the third deformation stage, probably in releasing zones, and latter transformed into quartz mylonites and mylonitic porphyries. Both mylonitic rocks display quartz microstructures in the transition between regime 2 and regime 3 of Hirth and Tullis (1992), and these microstructures indicate that grain boundary migration was an important recovery mechanism. The fabric pol-figures display Y maximum patterns, with prism - $\langle a \rangle$ being the main slip system. These characteristics indicate deformation in upper greenschist to

lower amphibolite facies (~500 °C), according to the criteria of Stipp *et al.* (2002). This medium to high temperature of deformation in a regional low-grade crust level is ascribed to heat provided by emplacement of the porphyries.

Correlation of the above-described evolution with the stages illustrated by Konopásek *et al.* (2005) for the Kaoko Belt of Namibia indicates that the Sierra Ballena Shear Zone represents the continuation of the Purros Shear Zone of the Kaoko Belt.

REFERENCES

- Almeida F.F.M. de, Amaral, G. Cordani, U.G. and Kawashita, K. (1973) The Precambrian evolution of the South American cratonic margin south of Amazonas River. **In:** Nairn and Stille (eds.) The ocean basin and margins. **1:** 411-446, Plenum, New York.
- Anderson, J.L., Cullers, R.L.V. and Schmus, W.R. (1980) Anorogenic metaluminous and peraluminous granite plutonism in the Mid-Proterozoic of Wisconsin, USA. *Cont. Mineral. Petr.* **74:** 311-328.
- Basei, M.A. Siga Jr., O. Masquelin, H. Harara, O. M. Reis Neto, J. M. and Preciozzi, F. (2000) The Dom Feliciano Belt (Brazil-Uruguay) and its Foreland (Rio de la Plata Craton): Framework, tectonic evolution and correlations with similar terranes of southwestern Africa. **In:** Cordani, U. Milani, E. Thomaz Filho, A. and Campos, D. (eds.) Tectonic evolution of South America. 311-334, *31 IGC*. Rio de Janeiro, Brazil.
- Batchelor, R.A. and Bowden, P. (1985) Petrogenetic interpretation of granitoid rock series using multicationic parameters. *Chem. Geol.* **48:** 43-55.
- Berthé, D. and Brun, J.P. (1980) Evolution of folds during progressive shear in the south Armorican Shear Zone, France. *Jour. Struct. Geol.* **2:** 127-133.
- Berthé, D. Choukroune, P. and Jegouzo, P. (1979) Orthogneiss, mylonite and non-coaxial deformation of granites: the example of the South Armorican shear zone. *Jour. Struct. Geol.* **1:** 31-42.
- Bitencourt, M. F. and Nardi L.V.S (2000) Tectonic setting and sources of magmatism related to the southern Brazilian Shear Belt. *Rev. Bras. Geoc.* **30(1):** 186-189.
- Black, R. and Liegeois, J. P. (1993) Cratons, mobile belts, alkaline rocks and continental lithospheric mantle: the Pan-African testimony. *Jour. Geol. Soc. London* **150:** 89-98.
- Blanco, G. and Gaucher, C. (2004) Stratigraphy, paleontology and age of Las Ventanas Formation (Neoproterozoic, Uruguay). *1st Symp. Neoproterozoic-Early Paleozoic Events in SW-Gondwana Ext. Abstracts, IGCP Project 478*, 8-9. Brazil.
- Bossi, J. (1983) Breve reseña sobre el conocimiento geológico del Escudo Predevoniano en Uruguay, Sud América. *Zentralbl. Geol. Paläont.* **1(3/4):** 417-429.
- Bossi, J. and Campal, N (1992) Magmatismo y tectónica transcurrente durante el Paleozoico Inferior en Uruguay. **In:** Gutierrez Marco, J.C., Saavedra, J. and Rabano, I. (eds.) Paleozoico Inferior de Iberoamérica. Universidad de Extremadura. España.
- Bossi, J. Campal, N. Hatmann, L.A. and Schipilov, A. (2001) Predevoniano en el Uruguay: terrenos y SHRIMP II. *Actas XI Cong. Latinoam. Geol.* Montevideo. CD-ROM version.
- Bossi, J. Cingolani, C., Llambías, E., Varela, R. and Campal, N. (1993) Características del Magmatismo Post-Orogenico Finibrasiliano en el Uruguay: Formaciones Sierra de Ríos y Sierra de Animas. *Rev. Bras. Geoc.* **23(3):** 282-288.
- Bossi and Ferrando (2001) Carta geológica del Uruguay. Geeditores. Montevideo. CD-ROM version.
- Bossi, J. and Gaucher, C. (2004) The Cuchilla Dionisio Terrane, Uruguay: an allochthonous block accreted in the Cambrian to SW-Gondwana. *Gondawna. Res.* **7(3):** 661-674.
- Bossi, J. Preciozzi, F. and Campal, N. (1993) Predevoniano del Uruguay Parte I: Terreno Piedra Alta. Dirección Nacional de Minería y Geología. Montevideo.
- Boullier, A.M. and Bouchez, J.L. (1978) Le quartz en rubans dans les mylonites. *Bull. Soc. Géol. France* **7:** 235-262.

- Boynton, W.V. (1984) Geochemistry of the rare earth elements: meteorite studies. **In:** Henderson, P. (ed.) Rare earth element geochemistry. Elsevier, New York. pp 63-114.
- Brown, G.C. (1982) Calc-alkaline intrusive rocks: their diversity, evolution, and relation to volcanic arcs. **In:** Thorpe, R.S. (ed.) Orogenic Andesites and Related Rocks. J. Wiley. pp: 437-461.
- Brown, G.C. Thorpe, R.S. and Webb, P.C. (1984) The geochemical characteristics of granitoids in contrasting arcs and comments on magma sources. *Jour. Geol. Soc. London* **141**: 413-426.
- Chemale Jr., F. Mallmann, G. Bitencourt, M.F. and Kawashita, K. (2003) Isotope geology of syntectonic magmatism along the Major Gercino Shear Zone, southern Brazil: implications for the timing of deformation events. *IV South Amer. Symp. Isotope Geol.* Salvador, Brazil.
- Cingolani, C. Spoturno, J. and Bonhomme, M. (1990) Resultados mineralógicos y geocronológicos preliminares sobre las unidades Piedras de Afilas, Lavalleja y Barriga Negra, R. O. del Uruguay. *I Cong. Urug. Geol. Res. Amp.* **1**: 11-17. Montevideo, Uruguay.
- Coronel, N. Oyhantçabal, P. and Spoturno, J. (1982) Características estructurales de la Formación Piedras de Afilas en su Localidad tipo. Canelones. Uruguay. *Actas Vº Cong. Lat. Geol.* **5**: 48 – 60. Buenos Aires, Argentina.
- Cox, K.G. Bell, J.D. and Pankhurst, R.J. (1979) The Interpretation of Igneous Rocks. G. Allen & Unwin, 450 pp.
- Cullers, R.L. and Graf, J.L. (1984) Rare earth elements in igneous rocks of the continental crust: Intermediate and silicic rocks. **In:** Henderson, P. (ed.) Rare earth element geochemistry. Elsevier, New York. pp 237-274.
- Davies, J.H. and von Blanckenburg, F. (1995) Slab breakoff: a model of lithosphere detachment and its test in the magmatism and deformation of collisional orogens. *Earth Plan. Sci. Letters* **129**: 85-102.
- Debon, F. and Le Fort, P. (1988) A cationic classification of common plutonic rocks and their magmatic associations: principles, method, applications. *Bulletin de Minéralogie* **111**: 493-510.
- Dell'Angelo, L.N. Tullis, J. and Yund, R.A. (1987) Transition from dislocation creep to melt-enhanced diffusion creep in fine grained granitic aggregates. *Tectonophysics* **139**: 325-332.
- De La Roche, H. Leterrier, P. Grandclaude, P. and Marchal, M. (1980) A classification of volcanic and plutonic rocks using R₁R₂ diagram and major element analysis – its relationship with current nomenclature. *Chem. Geol.* **29**: 183-210.
- Doe, B.R. (1997) Geochemistry of oceanic igneous rocks-ridges, islands and arcs-with emphasis on manganese, scandium and vanadium. *International Geology Review* **39**: 1053-1112.
- Dürr, S.B. and Dingeldey, D.P. (1996) The Kaoko belt (Namibia): Part of a late Neoproterozoic continental-scale strike-slip system. *Geology* **24**(6): 503-506.
- Egidio-Sylva, M. Vauchez, A. Bascou, J. and Hippertt, J. (2002) High temperature deformation in the Neoproterozoic transpressional Riveira belt, southeast Brazil. *Tectonophysics* **352**: 203-224.
- Fernandes, L.A.D. and Koester, E. (1999) The Neoproterozoic Dorsal de Canguçu strike-slip shear zone: its nature and role in the tectonic evolution of southern Brazil. *Jour. Afr. Earth Sci.* **29**(1): 3-24.
- Fernandes, L.A.D. Tommasi, A. and Porcher, C.C. (1992) Deformation patterns in the southern Brazilian branch of the Dom Feliciano Belt: A reappraisal. *Jour. South Amer. Earth Sci.* **5**:77-96.
- Ferrando, F. and Fernandez, A. (1971) Esquema tectónico - estratigráfico del predevoniano del Uruguay. *XXV Congreso Brasileiro de Geología*, **5**: 2879-2894. Camboriú, Brazil.
- Fisher, R.V. and Schmincke, H.U. (1984) Pyroclastic rocks. Springer, 472 pp.
- Förster, H.J. Tischendorf, G. and Trumbull, R.B. (1997) An evaluation of the Rb vs. (Y+Nb) discrimination diagram to infer tectonic setting of silicic igneous rocks. *Lithos*, **40**: 261-293.
- Fragoso-Cesar, A.R. (1980) O craton do Rio de las Plata e o Cinturão Dom Feliciano no Escudo Uruguaio-Sul Riograndense. *Actas 31 Cong. Bras. Geol.* Camboriú, **5**: 2879-2891.

- Fragoso-Cesar, A.R. (1991) Tectônica de placas no Ciclo Brasileiro: as orogenias dos Cinturões Dom Feliciano e Ribeira no Rio Grande do Sul. Unpublished Ph.D. Thesis. Instituto de Geociências, Univ. São Paulo, 367 p.
- Frantz, J.C. McNaughton, N.J. Marques, J.C. Hartmann, L.A. Botelho, N.F. and Caravaca, G. (2003) Shrimp U-Pb zircon ages of granitoids from southernmost Brazil: constraints on the temporal evolution on the Dorsal do Canguçu transcurrent shear zone and the eastern Dom Feliciano Belt. *IV South Amer. Symp. Isotope Geol.* Salvador, Brazil.
- Garlick and Gromet (2004) Diffusion creep and partial melting in high temperature mylonitic gneiss, Hope Valley shear zone, New England Appalachians, USA. *Jour. Met. Geol.* **24**: 45-62.
- Gastal, M.C.P. (1999) The alkaline and shoshonitic intrusives in the region of the Taquarembó Plateau, southern Brazil: are they genetically related? *Rev. Bras. Geoc.* **29(1)**: 85-98.
- Gaucher, C. (2000) Sedimentology, paleontology, and stratigraphy of Arroyo del Soldado Group (Vendian to Cambrian, Uruguay). *Beringeria* **26**: 1-120.
- Gaucher, C. Chigolino, L. and Pecoits, E. (2004) Southernmost exposures of the Arroyo del Soldado Group (Vendian to Cambrian, Uruguay): Paleogeographic implications for the amalgamation of W.-Gondwana. *Gondwana Res.* **7(3)**: 701-714.
- Goscombe, B. Hand, M. and Gray, D. (2003) Structure of the Kaoko Belt, Namibia: progressive evolution of a classic transpressional orogen. *Jour. Struct. Geol.* **25**: 1049-1081.
- Goscombe, B.D. Passchier, C.E. and Hand, M. (2004) Boudinage classification: end-member boudin types and modified boudin structures. *Jour. Struct. Geol.* **26**: 739-763.
- Gower, R.J.W. and Simpson, C. (1992) Phase boundary mobility in naturally deformed, high grade quartzofeldspathic rocks: evidence for diffusional creep. *Jour. Struct. Geol.* **14**: 301-313.
- Halinann, S.E. Mantovani, S.M.M. (1993) Structural Framework of the Southern Brazilian Shield: the perspective from the Gravity models. *III Intern. Geoph. Congress, Anais, SBGF*, **2**: 1078-1083. Rio de Janeiro, Brazil.
- Halls, H.C. Campal, N. Davis, D.W. and Bossi, J. (2001) Magnetic studies and U/Pb geochronology of the Uruguayan dyke swarm, Rio de la Plata craton, Uruguay: Paleomagnetic and economic implications. *Jour. South Amer. Earth Sci.* **14**: 349-361.
- Handy, M.R. (1994) Flow laws for rocks containing two non-linear viscous phases: a phenomenological approach. *Jour. Struct. Geol.* **16(3)**: 287-301.
- Harris, N. and Marriner, G. (1980) Geochemistry and petrogenesis of a peralkaline granite complex from the Midian Mountains, Saudi Arabia. *Lithos*, **13**: 325-337.
- Hartmann, L.A. Campal, N. Santos, J.O. McNaughton, N. Bossi, J. Schipilov, A. and Lafon, J.M. (2001) Archean crust in the Rio de la Plata Craton, Uruguay – SHRIMP U-Pb zircon reconnaissance geochronology. *Jour. South. Amer. Earth Sci.* **14**: 557-570.
- Hartmann, L.A. Santos, J.O. Bossi, J. Campal, N. Schipilov, A. and McNaughton, N. (2002) Zircon and Titanite U-Pb SHRIMP geochronology of Neoproterozoic felsic magmatism on the eastern border of the Rio de la Plata Craton, Uruguay. *Jour. South Amer. Earth Sci.* **15**: 229-236.
- Hippertt, J. (1999) Are S-C structures, duplexes and conjugate shear zones different manifestations of the same scale-invariant phenomenon?. *Jour. Struct. Geol.* **21**: 975-984.
- Hippertt, J. Rocha, A. Lana, C. Egydio-Silva, M. and Takeshita, T. (2001) Quartz plastic segregation and ribbon development in high-grade striped gneisses. *Jour. Struct. Geol.* **23**: 67-80.
- Hirth, G. Dunlap, W.J. and Teyssier, C.P. (1998) Dislocation creep regimes in naturally deformed quartz aggregates. In: Snoke, A.W. Tullis, J. and Todd, V.R. (eds.) *Fault-Related Rocks, a Photographic Atlas*. Princeton University Press, New Jersey, 617 p., pp 500-501.
- Hutton, D.H.W. and Reavy, R.J. (1992) Strike-slip and granite petrogenesis. *Tectonics*, **11**: 960-967.

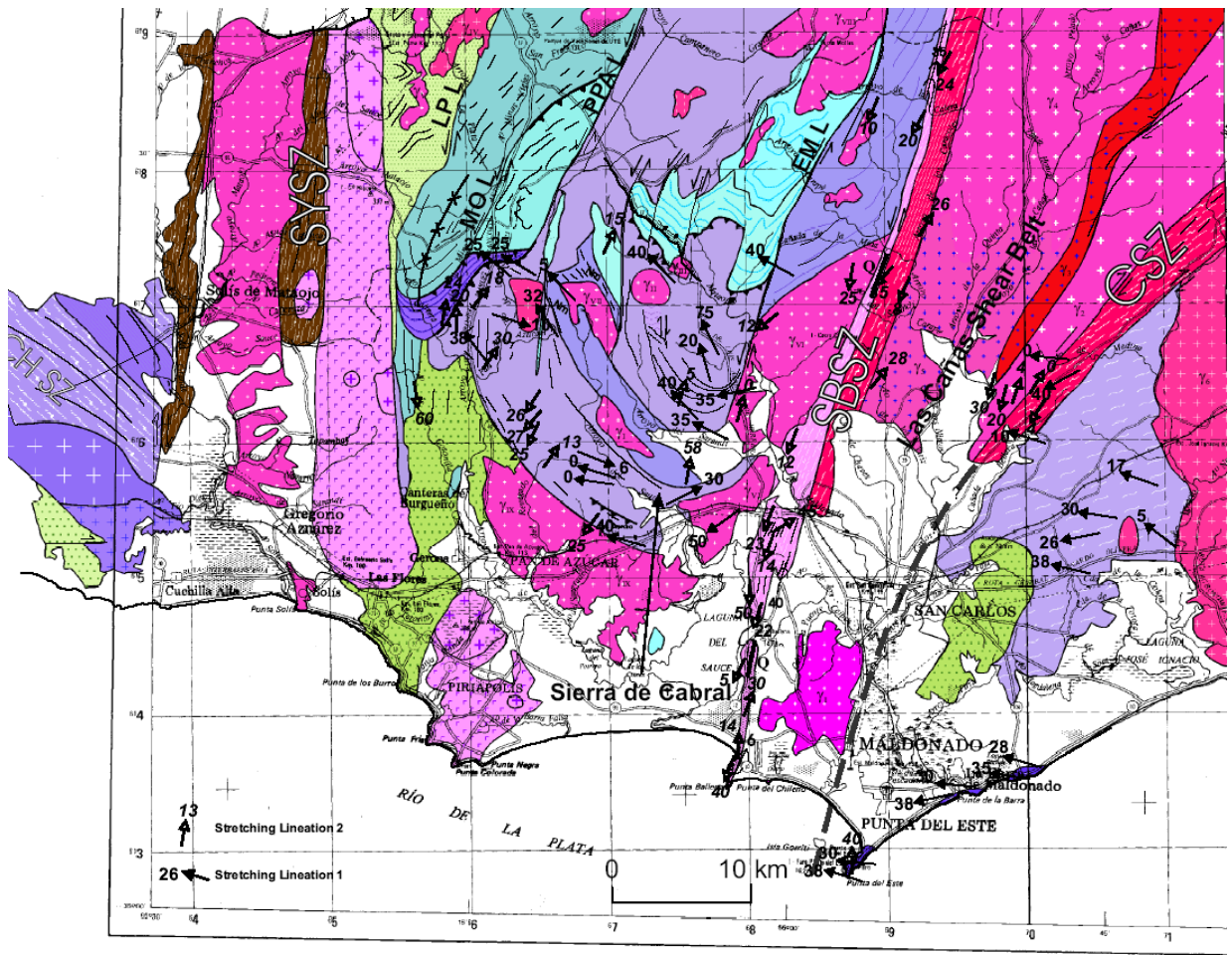
- Imber, J. Holdsworth, R.E. Butler, C.A. and Lloyd, G.E. (1997) Fault-zone weakening processes along the reactivated Outer Hebrides Fault Zone. Scotland. *Jour. Geol. Soc. London* **154(1)**: 105-109.
- Irvine, T.N. and Baragar, W.R.A. (1971) A guide to the chemical classification of the common volcanic rocks. *Can. Jour. Earth. Sci.* **8**: 523-548.
- Jones, R.R. and Tanner, P.W. (1995) Strain partitioning in transpression zones. *Jour. Struct. Geol.* **17(6)**: 793-802.
- Koester, E. Roisenberg, A. Fernandes, L.A.D. Soliani Jr., E. Nardi, L.D.S. and Kraemer, G. (2001) Geologia e geoquímica de granitoides sintectónicos a zona de cisalhamento transcorrente Dorsal do Canguçu. Encruzilhada do Sul. RS. *Rev. Bras. Geoc.* **31(2)**: 141-154.
- Konopásek, J. Kröner, S. Kitt, S.L. Paschier, C.W. and Kröner, A. (2005) Oblique collision and evolution of large-scale transcurrent shear zones in the Kaoko belt, NW Namibia. *Precambrian Res.* **136**: 139-157.
- Kretz, R. (1983) Symbols for rock-forming minerals. *Am. Mineral.* **68**: 277-279.
- Kruhl, J.H. (1996) Prism - and basal - plane parallel subgrain boundaries in quartz: a microstructural geothermobarometer. *Jour. Met. Geol.* **14**: 581-589.
- Leite, J.A.D. Hartmann, L.A. Fernandes, L.A.D. McNaughton, N.J. Soliani Jr., E. Koester, E. Santos, J.O.S. and Vasconcellos, M.A.Z. (2000) Zircon U-Pb SHRIMP dating of gneissic basement of the Dom Feliciano Belt, southern Brazil. *Jour. South Amer. Earth Sci.* **13**: 739-750.
- Lemos, R.S.D. Brown, M. and Strachan, R.A. (1992) Granite ascent and emplacement within a transpressional orogen. *Jour. Geol. Soc. London*, **149**: 487-490.
- Liegeois, J.P. Navez, J. Hertogen, J. and Black, R. (1998) Contrasting origin of post-collisional high-K calc-alkaline and shoshonitic versus alkaline and peralkaline granitoids. The use of sliding normalization. *Lithos* **45**: 1-28.
- MacCready, T. (1996) Misalignment of quartz c-axis fabrics and lineations due to oblique final strain increments in the Ruby Mountains core complex, Nevada. *Jour. Struct. Geol.* **18**: 765-776.
- Mallmann, G. Chemale Jr. F. Armstrong, R. and Kawashita, K. (2003) Sm-Nd and U-Pb Shrimp Zircon Studies of the Nico Pérez Terrane, Reworked Río de la Plata Craton, Uruguay. *IV South Amer. Symp. Isotope Geol.* Salvador, Brazil.
- Masquelin, H. (1990) Análisis estructural de las zonas de cizalla en las migmatitas de Punta del Este. Uruguay. Simposio Sul-Brasileiro de Geología. *Acta Geológica Leopoldensia.* **13(30)**: 139-158. Sao Leopoldo, Brazil.
- Masquelin, H. (2004) El Complejo Cerro Olivo, Sureste de Uruguay: una revisión estratigráfica y tectónica. *IV Cong. Urug. Geol. Actas* CD-ROM version. Montevideo, Uruguay.
- Masquelin, H. C. and Sanchez-Bettucci, L. (1993) Propuesta de evolución tectono- sedimentaria para la fosa tardi- brasiliana en la región de Piriápolis, Uruguay. *Rev. Bras. Geoc.* **23 (3)**: 313-322.
- Masquelin, H. and Pías, J. (1989) Carta geológica de las Hojas San Carlos - Punta del Este, escala 1:100.000. DINAMIGE, Montevideo. Unpublished.
- Masquelin, H. Silva, A.O.M. Porcher, C.C. Fernandes, L.A.D. and Morales, E. (2001) Geología y Geotermobarometría de la Suite Metamórfica Chafalote, Basamento Prebrasiliano, Sureste del Uruguay. *XI Congr. Latinoam. Geol.*, Montevideo, Actas, CD-ROM version.
- Martelat, J.E. Schulmann, K. Lardeaux, J.M. Nicollet, C. and Cardon, H. (1999) Granulite microfabrics and deformation mechanism in southern Madagascar. *Jour. Struct. Geol.* **21**: 671-687.
- Mielke, P. and Winkler, H.G.F. (1979) Eine bessere Berechnung der Mesonorm für granitische Gesteine. *Neu Jb Mineral. Mh.* 471-480.
- Midot, D. (1984) Etude géologique et diagnostique métallogénique pour l'exploration du secteur Minas (Uruguay); Unpublished Thesis, 3eme. Cycle, Univ. P. et M. Curie. Paris. France.

- Moore, E.M. and Twiss, R.J. (1995) *Tectonics*. Freeman, 415 pp.
- Morrison, G.W. (1980) Characteristics and tectonic setting of the shoshonite rock association. *Lithos*, **13**: 97-108.
- Nilsen, H. and Sylvester, A.G. (1995) Strike-slip basins. **In**: Busby, C.J. and Ingersoll, R.V. (eds.) *Tectonics of sedimentary basins*.
- Oyhantçabal, P.; Derregibus, M. and De Souza, S. (1993a) Geología do extremo sul da Formação Sierra de Animas (Uruguay) *V Simposio Sul-Brasileiro de Geologia*. Boletín de Resumos. **I**: 4-5. Curitiba, Brazil.
- Oyhantçabal, P. Derregibus, M. Muzio, R. De Souza, S. and Peel, E. (1993b) Complejo Granítico Solis de Mataojo: Evidencias de magmatismo sinclinal relacionado a subducción. *Rev. Bras. Geoc.* **23(3)**: 242-247.
- Oyhantçabal, P. Derregibus, M. Muzio, R. and Nardi, L.V.S. (1998) The Soca intrusion: a rapakivi granite of Uruguay. *Jour. South Amer. Earth Sci.* **11(2)**: 169-178.
- Oyhantçabal, P. Heimann, A. and Miranda, S. (2001a) An evaluation of strain in the syntectonic Solis de Mataojo Granitic Complex, Uruguay. *Jour. Struct. Geol.* **23**: 807-817.
- Oyhantçabal, P. Muzio, R. and De Souza, S. (1993c) Geología y aspectos estructurales del borde orogénico en el extremo sur del Cinturón Dom Feliciano *Rev. Bras. Geoc.* **23(3)**: 296-300.
- Oyhantçabal, P. Spoturno, J. Aubet, N. Cazaux, S. and Huelmo, S. (2003) Proterozoico del suroeste del Uruguay: nueva propuesta estratigráfica para la Formación Montevideo y el magmatismo asociado. *Rev. Soc. Urug. Geol. Pub. Esp.* **1**: 38-48.
- Oyhantçabal, P. Spoturno, J. Goso, E. Heimann, A. Bergalli, L. (2001b) Asociaciones litológicas en las Supercrustales del Grupo Lavalaja y Magmatismo asociado, en la Hoja "Fuente Del Puma" (Sur De Minas, Uruguay) *Actas XI Cong. Lat. de Geología*, Montevideo, Uruguay. CD-ROM version.
- Paschier, C.W. Trouw, R.A.J. (1996) *Microtectonics*. Springer. 289 pp.
- Paschier, C.W. Trouw, R.A.J. Ribero, A. and Paciullo, F.V.P. (2002) Tectonic evolution of southern Kaoko belt, Namibia. *Jour. Afr. Earth. Sci.* **35**: 61-75.
- Pázos, J. and Sánchez, L. (1999) Rasgos mareales en la sucesión neoproterozoica de la Pedrera, Grupo Rocha, Uruguay. *XIV Cong. Geol. Arg.* **I**: 71. Salta, Argentina.
- Pearce, J.A. (1996) Sources and settings of granitic rocks. *Episodes*, **19(4)**: 120-125.
- Pearce, J.A. Harris, N.W. and Tindle, A.G. (1984) Trace element discrimination diagrams for the tectonic interpretation of granitic rocks. *Jour. Petrol.* **25**: 956-983.
- Pearce, J.A. and Norry, M.J. (1979) Petrogenetic implications of Ti, Zr, Y, and Nb variations in volcanic rocks. *Contrib. Mineral. Petrol.* **69**: 33-47.
- Peccerillo, R. and Taylor, S.R. (1976) Geochemistry of Eocene calc-alkaline volcanic rocks from the Kastamonu area, Northern Turkey. *Contrib Mineral Petrol.* **58**: 63-81.
- Pecoits, E. (2003) Sedimentología y consideraciones estratigráficas de la Formación Las Ventanas en su área tipo, departamento de Maldonado, Uruguay. *Rev. Soc. Urug. Geol. Pub. Esp.* **Nº 1**: 124-140.
- Pecoits, E. Aubet, N. Oyhantçabal, P. and Sánchez Bettucci, L. (2005) Estratigrafía de Sucesiones Sedimentarias y volcanosedimentarias Neoproterozoicas del Uruguay. *Rev. Soc. Urug. Geol.* In press.
- Philip, R. and Machado, R. (2001) Suites graníticas do batolito Pelotas no Rio Grande do Sul: petrografia, tectónica e aspectos petrogenéticos. *Rev. Bras. Geoc.* **31(3)**: 257-266.
- Platt, J.P. and Vissers, R.L.M. (1980) Extensional structures in anisotropic rocks. *Jour. Struct. Geol.* **2**: 397-410.

- Porada, H. (1979) The Damara-Ribeira Orogen of Pan-African-Brasiliano Cycle in Namibia (Southwest Africa) and Brazil interpreted in terms of continental collision. *Tectonophysics*, **57**: 237-268.
- Porada, H. (1989) Pan-African rifting and orogenesis in southern equatorial Africa and eastern Brazil. *Precambrian Res.* **44**: 103-136.
- Preciozzi, F. (1989) Líneas estructurales de la secuencia volcano-sedimentaria del Grupo Lavallega (ciclo brasiliano): región Minas – Pan de Azúcar, Uruguay. *Contribuciones a la Geología del Uruguay*. Dirección Nacional de Minería y Geología. **1**: 1-16. Montevideo. Uruguay.
- Preciozzi, F. Masquelín, H. and Sánchez-Bettucci, L. (1993) Geología de la porción sur del Cinturón Cuchilla Dionisio. Guía de Excursión, *I Simposio del Neo Proterozoico - Cámbrico de la Cuenca del Plata*. 3-39. La Paloma, Uruguay.
- Preciozzi, F. Masquelín, H. and Basei, M.A. (1999) The Namaqua/Grenville Terrane of eastern Uruguay. *II South Amer. Symp. Isotope Geol.* Carlos Paz, Argentina.
- Preciozzi, F. Peel, E. Muzio, R. Ledesma, J.J. and Guerequiz, R. (2001) Dom Feliciano Belt and Punta del este terrane: Geochronological features. *III South Amer. Symp. Isotope Geol.* Pucón, Chile.
- Preciozzi, F. Spoturno, J. and Heinzen, W. (1979) Carta geo-estructural del Uruguay. Escala 1/2.000.000. 62 pp. Inst. Geol. Ing. E. Terra Arocena. Montevideo, Uruguay.
- Preciozzi, F. Spoturno, J. Heinzen, W. and Rossi, P. (1985) Memoria explicativa de la Carta Geológica del Uruguay a escala 1/500.000. Ed. DINAMIGE. Montevideo, Uruguay.
- Ramsay, J.G. (1980) Shear zone geometry: a review. *Jour. Struct. Geol.*, **2**:83-99.
- Rossini, C. Aubet, N. (2000) La región Zanja del Tigre-Carapé (Maldonado-Uruguay) y sus rocas metacalcáreas. Estudio geológico e implicancias estratigráficas y económicas. *Rev. Soc. Urug. Geol.* **7**: 36-47.
- Rossini, C. and Legrand, J.M. (2003) Eventos Tecto-metamórficos del Grupo Carapé: un modelo para su evolución Neoproterozoica. *Rev. Soc. Urug. Geol.* Pub. Esp. **1**: 49-67. CD-ROM version.
- Sánchez-Bettucci, L. (1998) Evolución tectónica del Cinturón Dom Feliciano en la región Minas-Piriápolis, Uruguay. Universidad de Buenos Aires, Buenos Aires, Unpublished PhD Thesis, 344 p.
- Sánchez-Bettucci, L. Cosarinsky, M. and Ramos, V.A. (2003) Tectonic setting of the late Proterozoic Lavallega Group (Dom Feliciano Belt), Uruguay. *Gondwana Res.* **4**: 395-407.
- Sánchez-Bettucci, L. and Linares, E. (1996) Primeras edades en Basaltos del Complejo Sierra de las Animas. *XIII Congreso Geológico Argentino*. **1**: 399-404. Buenos Aires. Argentina.
- Sánchez-Bettucci, L. Oyhantçabal, P. Page, S. and Ramos, V.A. (2003) Petrography and Geochemistry of the Carapé Complex, (Southeastern Uruguay). *Gondwana Res.* **6**: 89-105.
- Sánchez-Bettucci, L. Preciozzi, F. Basei, M.A.S. Oyhantçabal, P. Peel, E. and Loureiro, J. (2003) Campanero Unit: A Probable Paleoproterozoic Basement and its Correlation to other Units of Southeastern Uruguay. *IV South Amer. Symp. Isotope Geol.* Salvador, Brazil.
- Sánchez-Bettucci, L. and Ramos, V.A. (1999) Aspectos geológicos de las rocas metavolcánicas y metasedimentarias del Grupo Lavallega, sudeste de Uruguay. *Rev. Bras. Geoc.* **29(4)**:557-570.
- Sánchez-Bettucci, L. and Rapalini, A. (2002) Paleomagnetism of the Sierra de Las Animas Complex, southern Uruguay: its implications in the assembly of western Gondwana, *Precambrian Res.* **118**: 243-265.
- Schäfer, W. (2002) Neutron diffraction applied to geological texture and stress analysis. *Eur. Jour. Mineral.* **14**: 263-289.
- Schmid, S.M. and Casey, M. (1986) Complete fabric analysis of some commonly observed quartz c-axis patterns. In: Hobbs, B.E. and Heard, H.C. (eds.) Mineral and rock deformation: laboratory studies. The Paterson volume. *Geophysical Monograph* **36**: 263-286. Am. Geoph. Union.
- Shand, H.S. (1943) Eruptive Rocks. John Wiley and Sons.

- Silva da, L.C. McNaughton, N.J., Armstrong, R. Hartmann, L.A. and Fletcher, I.R. (2005) The Neoproterozoic Mantiqueira Province and its African connections: a zircon-based U-Pb geochronology subdivision for the Brasiliano-Pan-African systems of orogens. *Precambrian. Res.* **136**: 203-240.
- Simpson, C. (1980) Oblique girdle orientation patterns of quartz c-axis from a shear zone in the basement core of the Maggia nappe Ticcino, Switzerland. *Jour. Struct. Geol.* **2**: 243-247.
- Snoke, A.W. Tullis, J. and Todd, V.R. (1998) *Fault-Related Rocks, a Photographic Atlas*, Princeton University Press, New Jersey, 617 p.
- Spoturno, J. Oyhantçabal, P. Goso, C. Aubet, N. Cazaux, S. Huelmo, S. and Morales, E. (2005) Mapa geológico y de recursos minerales del departamento de Canelones a escala 1:100 000. CD-ROM version. Facultad de Ciencias-DINAMIGE.
- Stipp, M. Stünitz, H. Heilbronner, R. and Schmid, S.M. (2002) The eastern Tonale fault zone: a 'natural laboratory' for crystal plastic deformation of quartz over a temperature range from 250 to 700°C. *Jour. Struc. Geol.* **24**: 1861-1884.
- Streckeisen, A. and Le Maitre, R.W. (1979) A chemical approximation to the modal QAPF classification of the igneous rocks. *Neu. Jb. Mineral. Abh.* **136**: 169-206.
- Sylvester, P.L. (1989) Post-collisional alkaline granites. *Jour. Geol.* **97**: 261-280.
- Tischendorf, G. and Förster, H. J. (1992) Central European granitoids and their tectonic setting: Implications from a new discrimination diagram. Teil I. *Zentralbl. Geol. Palæont.* **1994**: 791-801.
- Tommasi, A. Vauchez, A. Fernandes, L.A.D. Porcher, C.C. (1994) Magma-assisted strain localization in an orogen-parallel transcurrent shear zone of southern Brazil. *Tectonics* **13**: 421-437.
- Trompette, R. (1994) Geology of western Gondwanaland 2000-500 Ma. The Pan-African/Braziliano amalgamation of South America and adjacent Africa. Balkema, 350 pp.
- Tullis, J. Stünitz, H. Teyssier, C. and Heilbronner, R. (2000) Deformation microstructures in quartzofeldspathic rocks. **In**: Jessell, M.W. and Urai, J.L. (eds.) *Stress, Strain and Structure. A volume in honour of W. D. Means. Volume 2, Journal of the Virtual Explorer.*
- Ullemeyer, K. and Weber, K. (1999) Lattice preferred orientation as an indicator of a complex deformation history of rocks. *Textures and Microstructures* **33**: 45-60.
- Umpierre, M. and Halpern, M. (1971) Edades Sr - Rb del Sur de la República Oriental del Uruguay. *Revista Asociación Geológica Argentina.* **26**: 133-155.
- Vollbrecht, A. Siegesmund, S. and Flaig, C. (1997) High-temperature deformation of a granitoid from the Zone of Erbendorf-Vohenstrauß (ZEV) *Inter. Jour. Earth Sci.* **86**: 141-154.
- Wimmenauer, W. and Bryhni, I. (2002) Towards a unified nomenclature of metamorphic rocks: 6. Migmatites and related rocks. A proposal on behalf of the IUGS Subcommission on the Systematics of Metamorphic Rocks. <http://www.iugs.org>. Web version, 31.07.2002.
- Weinberg, R. (2004) Granite transport and Emplacement: a review. *Ishihara Symp. Granites and Assoc. Metallogenesis.* 125-127.
- Winchester J.A. and Floyd P.A. (1977) Geochemical discrimination of different magma series and their differentiation products using immobile elements. *Chem. Geol.* **20**: 325-343

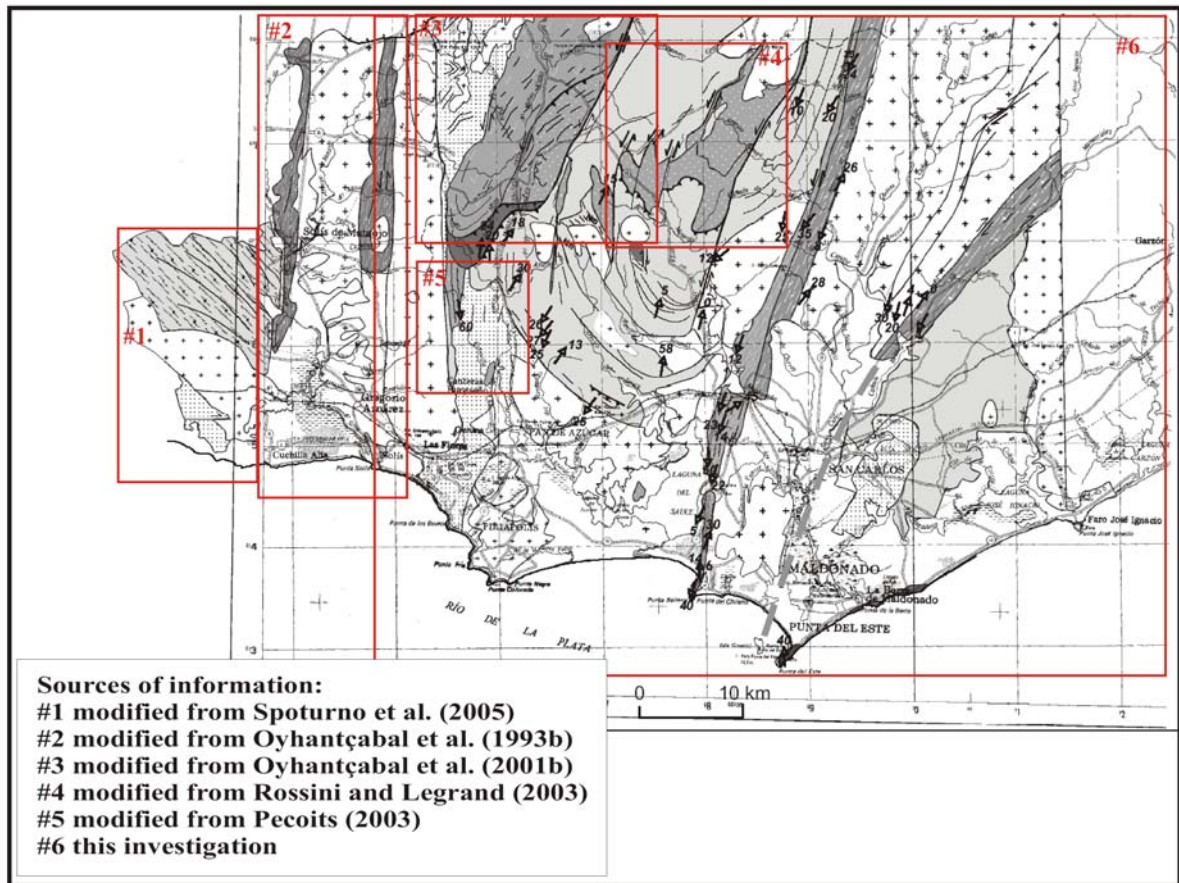
APPENDIX 1



Domain	I West of SYSZ	II SYSZ	III SYSZ - SBSZ	IV SBSZ - CSZ	V East of CSZ	
Strain partitioning	Low Strain	High Strain	Low Strain	High Strain	Low Strain	
Terrane	Piedra Alta		Nico Perez		Punta del Este	
Neoproterozoic - Cambrian	<p><i>Piedras de Afilar F.</i> (sandstones, pelites, limestones)</p> <p>Solis de Matajojo Granite γ_c</p>	<p>Cerro Caperauzo Gr. γ_c</p> <p>Solis de Matajojo Granite γ_c</p> <p>Mylonites (normal shearing)</p>	<p><i>Sierra de las Animas Cx.</i> (alk. volc., subvolc. / intrusives)</p> <p><i>Arroyo del Soldado Gr.</i> (shales, sandstones, limestones)</p> <p><i>Maldonado Gr.</i> <i>Las Ventanas F.</i> (conglomerates, sandstones, pelites, basic & acid volcanics)</p> <p><i>Playa Hermosa F.</i> (diamictites, sandstones, pelites)</p> <p>Campe Cx (calc-alk. granites γ)</p>	<p>Mylonitic porphyries</p> <p>Quartz mylonites</p> <p>Phylonites</p> <p>Granitic mylonites</p> <p>Granites</p> <p>γ A' de la Quinta</p> <p>γ Agua</p> <p>γ Florencia</p> <p>γ Valdivia</p> <p>γ Maldonado</p>	<p>γ José Ignacio Granite</p> <p><i>San Carlos F.</i> (conglomerates, sandstones, pelites, acid volcanics)</p>	<p>D₁ ~540 Ma</p> <p>D₂</p>
Neoproterozoic - Mesoproterozoic?		<p>Mylonites (dextral shearing)</p>	<p><i>Lavalleja Gr.</i> (basic volc., schists, limestones)</p> <p><i>Zanja del Tigre Gr.</i> (marbles, metapelites, BIF's) PS</p>			<p>D₁ ~800 Ma</p>
Paleoproterozoic	<p>Granites</p> <p>γ Soca</p> <p>γ A' Coronilla</p> <p><i>Cuch. Cabo de Hornos SZ</i></p> <p>Granitic mylonites</p> <p>Mylonites (Gr., Sill., Graph.)</p>		<p><i>Campanero Unit</i></p> <p>Orthogneisses, stripped orthogneisses</p> <p>Scapolite gneisses</p> <p>Amphibolites, migmatites and BIF's</p> <p>Micaschists</p>		<p><i>Cerro Olivo Complex</i> (para gneisses)</p>	

* Carapé Complex Granites: γ : Sauce, γ_b : Bombero, γ_m : Dos Hermanos, γ_n : Minas, γ_o : Cortez Blanco, γ_p : Guayabo, γ_{re} : Matzo, γ_{ca} : La Calera, γ_{re} : Renegado.

Map 1. Geological map of the study area



Map 2. Source of information

APPENDIX 2

Abbreviations

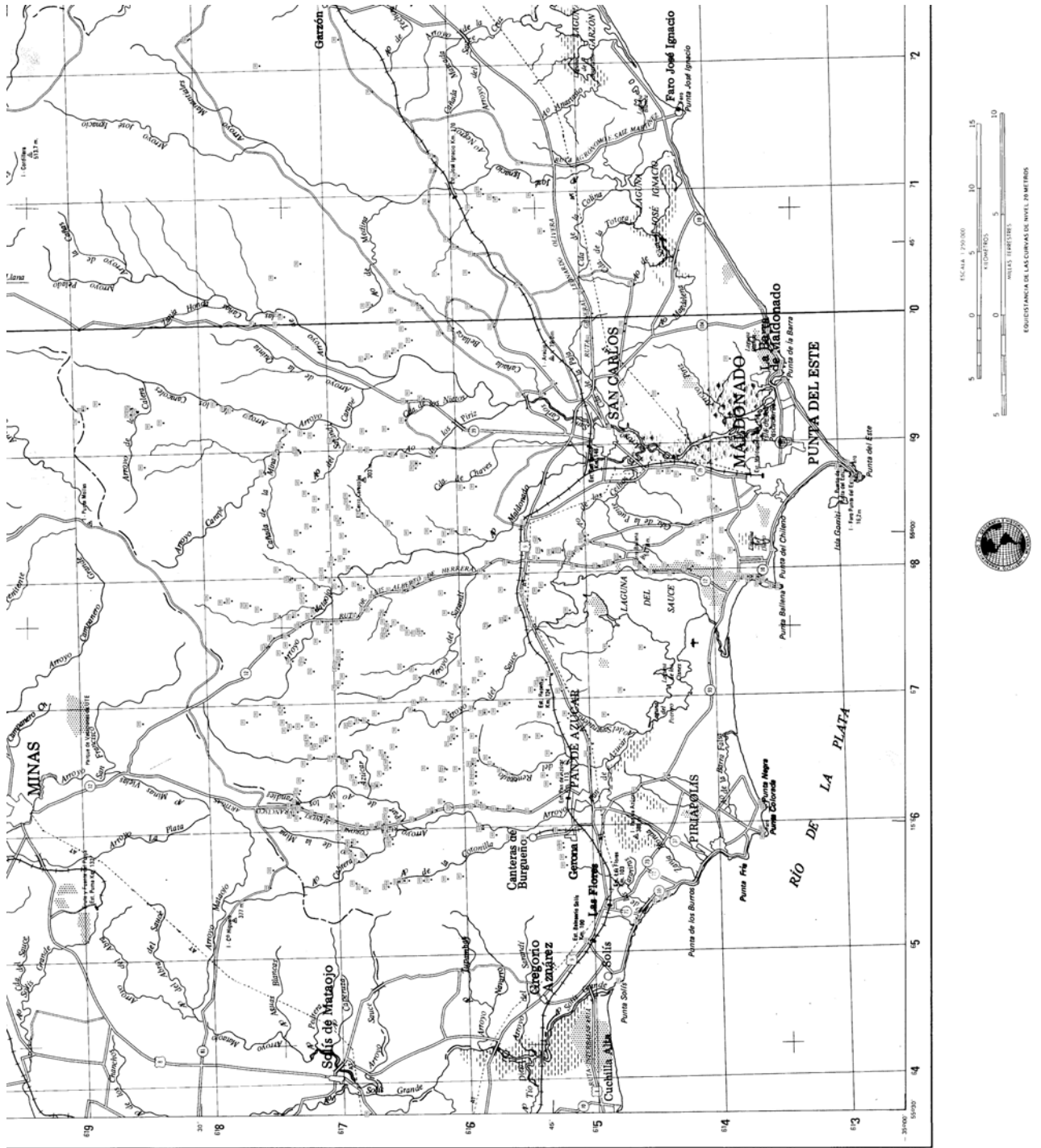
A/CNK	$\text{Al}_2\text{O}_3/(\text{CaO}+\text{Na}_2\text{O}+\text{K}_2\text{O})$ molar ratio
A/NK	$\text{Al}_2\text{O}_3/(\text{Na}_2\text{O}+\text{K}_2\text{O})$ molar ratio
HFS	High Field Strength elements
HREE	Heavy Rare Earth elements
LREE	Light Rare Earth elements
LIL	Large Ion Lithophile elements
MORB	Mid-Ocean Ridge basalts
ORG	Ocean Ridge Granite
REE	Rare Earths
syn-COLG	syn collision Granite
TAS	Silica vs. Total alkalis diagram
VAG	Volcanic Arc Granite
WPG	Within-plate Granite

Mineral abbreviations (after Kretz, 1983)

Amp	Amphibole
Ap	Apatite
Bt	Biotite
Chl	Chlorite
Ep	Epidote
Hbl	Hornblende
Kfs	K-feldspar
Mic	Microcline
Ms	Muscovite
Or	Orthoclase
Qtz	Quartz
Pl	Plagioclase
Ser	Sericite
Ttn	Titanite
Zrn	Zircon

APPENDIX 3

Location of field observation points



Coordinates of geochronology samples

	Latitude	Longitude
UY 10-04	34° 55.07' S	054° 51.423' W
SB 042	34° 55.017' S	054° 51.179' W
UY 3-04	34° 33.387' S	055° 17.208' W
UY 4-04	34° 33.062' S	055° 17.018' W
UY 5-04	34° 33.062' S	055° 17.018' W
SB 527	34° 38.803' S	055° 06.866' W
SB 553	34° 34.091' S	055° 06.566' W
SB 632	34° 35.4' S	055° 26.5' W

APPENDIX 4

Major, trace and rare earth elements analysis

Analytical methods

Determinations were performed on representative samples screened for alteration in hand specimens and thin sections.

Samples were broken using iron hammer and further reduced by means of an iron jaw crusher and the analytical powder was obtained with an agate mill. Determinations were made using XRF for major elements and MS for trace and rare earth elements using the facilities of the Geowissenschaftliches Zentrum der Universität Göttingen.

Data from samples 2058, 6127, 6190, 6191, 6192, 6194, 6195 and 6198 of Campero Unit (Table A.4.1) were performed at Act Lab using the package Code 4 LithoResearch including ICP for major elements and ICP/MS for trace and rare earth elements.

	2058	6127	6190	6191	6192	6194	6195	6198	SB 148	SB 163	SB 201	SB 363	SB 388	SB 390	SB 399	SB 454B	SB 503	SB 506	SB 510
SiO₂ %	69.6	73.0	74.2	73.6	73.2	67.7	74.1	68.1	67	70.2	55.7	69.9	71.3	73.9	76.4	68.8	74	88.6	67
TiO₂ %	0.25	0.16	0.06	0.05	0.21	0.9	0.37	0.93	0.35	0.2	0.18	0.35	0.16	0.09	0.16	0.35	0.11	0.06	0.45
Al₂O₃ %	15.5	14.91	15.52	15.31	14.75	13.72	13.21	13.75	16.3	14.9	21.3	14.7	15.6	14.4	11.6	15.5	14.5	6.3	15.4
Fe₂O₃ %	2.33	1.19	0.6	0.91	1.73	4.91	2.55	5.28	2.92	2.01	6.04	2.64	1.14	0.95	1.75	3.06	0.96	0.52	3.8
MnO %	0.03	0.01		0.01	0.02	0.09	0.04	0.08	0.05	0.04	0.19	0.04	0.03	0.01	0.01	0.04	0.01	0	0.06
MgO %	0.36	0.26	0.08	0.07	0.49	0.9	0.38	0.96	0.8	0.43	0.21	1.34	0.46	0.19	0.08	1.09	0.25	0.14	1.62
CaO %	1.6	1.22	0.78	1.1	1.61	2.9	1.25	2.83	2.32	1.6	0.42	1.92	1.41	1.11	0.27	3.26	0.96	0.14	2.05
Na₂O %	4.69	4.62	5.9	5.06	4.86	3.12	2.81	3.11	5.04	3.9	8.14	3.13	5.35	4.59	3.01	4.95	4.54	1.36	3.76
K₂O %	4.5	4.2	3.3	3.71	2.92	4.29	5.51	4.36	3.52	5.36	5.69	4.01	3.12	3.55	5.48	1.3	3.61	1.49	4.07
P₂O₅ %	0.14	0.09	0.03	0.02	0.1	0.32	0.09	0.36	0.19	0.11	0.05	0.23	0.09	0.08	0.04	0.14	0.07	0.04	0.18
LOI %	0.43	0.19	0.24	0.29	0.28	0.4	0.17	0.52											
Cr ppm	89	162	134	106	82	130	195	141	530	87	187	49	144	229	160	272	134	130	449
Co ppm	2	3	1	1	3	7	3	5					2				2		10
V ppm	17	14	5	5	21	46	17	54	36	24	10	35	17	10	10	37	17	13	53
Pb ppm	47	70	90	40	91	80	57	16					43				60.1		33.3
Bi ppm	0.14	0.16	0.13	0.13	0.22	0.24	0.11	0.13											
Rb ppm	60	62	42	69	48	103	134	90	59	124	141	71	60	55	86	33	84	49	106
Cs ppm	0.3	0.4	0.3	0.8	0.8	0.9	0.5	0.8					1.73				1.32		1.13
Ba ppm	3100	2470	1920	732	2190	3190	2130	3130	3240	1317	172	3143	1711	1785	110	453	1538	449	927
Sr ppm	1340	1340	1220	550	2570	695	536	705	1730	676	111	1952	1460	1027	77	520	1080	147	473
Tl ppm	0.4	0.51	0.44	0.43	0.44	0.79	0.75	0.43					0.32				0.41		0.52
CO₂ %									0.59	0.45	1.14	0.84	0.61	0.44	0.37	1	0.65	0.72	1.24
Mg	23.4	30.2	20.9	13.2	36.0	26.7	22.8	26.5	35.2	29.8	6.45	50.2	44.4	28.4	8.31	41.4	34.0	34.8	45.8
FeOt %	2.1	1.07	0.54	0.82	1.56	4.42	2.29	4.75	2.63	1.81	5.43	2.38	1.03	0.85	1.57	2.75	0.86	0.47	3.42
A/NK	1.2	1.23	1.17	1.24	1.32	1.4	1.25	1.4	1.35	1.22	1.09	1.55	1.28	1.26	1.07	1.62	1.27	1.64	1.45
A/CNK	1.0	1.04	1.06	1.07	1.05	0.91	1.03	0.92	1.00	0.99	1.05	1.13	1.06	1.07	1.02	1.00	1.11	1.53	1.08
K₂O/Na₂O	0.96	0.91	0.56	0.73	0.6	1.38	1.96	1.4	0.7	1.37	0.7	1.28	0.58	0.77	1.82	0.26	0.8	1.1	1.08
H₂O %									0.15	0.01	0.18	0.05	0.06	0.02		0.06			0.22
Total %	99.43	99.85	100.7	100.1	100.1	99.25	100.5	100.3	99.23	99.21	99.24	99.15	99.33	99.33	99.17	99.55	99.66	99.37	99.85

Table A.4.1 Chemical composition of orthogneisses from Campanero Unit

	2058	6127	6190	6191	6192	6194	6195	6198	SB 148	SB 163	SB 201	SB 363	SB 388	SB 390	SB 399	SB 454B	SB 503	SB 506	SB 510
Ga	26	22	23	22	19	21	21	20	19	18	20	20	21	19	24	20	20	12	18
Ta	1.4	0.4	0.4	0.6	0.4	1.9	1.3	1.6					0.68				0.59		0.69
Nb	18.3	5.6	5.8	5	4.7	32.4	22.7	27	14	16	48	10	10	10	39	10	10	10	10
Hf	6.2	4.1	2	3.4	3.8	15.1	13.9	13.7					3.2				2.93		3.99
Zr	235	141	51	80	149	655	443	616	261	228	78	177	113	91	498	124	97	57	237
Y	15.5	5.9	2.6	4.9	5.9	79.7	33.9	69.5	13	33	10	14		10	16		11	10	13
Th	18.2	9.14		1.8	9.32	20.5	26.6						5.08						29.22
U	1.42	2.07	1.15	1.53	1.69	2.32	2.08	1.86											1.48
La	115	35.5	4.06	3.8		241	232										15.99		64.22
Ce	261	62.9	6.6		56	428	344	391					33.18				27.31		119.7
Pr	22.3	6.7	0.94	0.77	6.41	46	30	41.7					3.8				3.45		12.65
Nd	82.5	24.8	3.8	2.92	24	169	91.5	150					13.55				12.47		43.1
Sm	13.1	4.1	1	0.69	4.11	25.1	10.7	22.1					2.59				2.42		7.22
Eu	2.85	1	0.28	0.19	1.22	5.52	1.97	4.83									0.71		1.42
Gd	7.74	2.79	0.9	0.68	2.89	20.3	8.19	18.2					2.02				1.96		5.57
Tb	0.83	0.29	0.13		0.3	2.63	1						0.24						0.63
Dy	3.34	1.12	0.55	0.74	1.13	13.9	5.48	12.6					1.1				1.2		2.96
Ho	0.49	0.16	0.09	0.16	0.17	2.6	1.05	2.36					0.19				0.23		0.52
Er	1.24	0.4	0.25	0.5	0.49	7.65	3.27	6.98					0.49				0.66		1.28
Tm	0.15	0.05	0.03	0.08	0.05	1.11	0.53	0.99					0.06				0.09		0.15
Yb	0.91	0.32	0.21	0.53	0.39	6.88	3.54	6.26					0.43				0.62		0.94
Lu	0.14	0.05	0.03	0.08	0.06	1.01	0.62	0.93					0.06				0.1		0.14
Sc									13	10	10	10	10	10	10	15	10	10	10
Zn									66	34	113	71	44	12	58	53	35	10	75
Li													7.93				7.37		17.94
Ni													55				42		135
Cu													2				2		14
Sn													1.21				1.31		2.01
Sb													0.05				0.03		0.05

Table A.4.1 Chemical composition of orthogneisses from Campanero Unit (continuation). All trace elements in ppm.

Table A.4.2 Chemical composition of rocks from Solís de Matajojo Granitic Complex

	SM 1815	SM 22-1	SM 23-2	SM 31-2	SM 47-2	SM 52-1	SM 53-2	SM 97-1	SM 100-1	SM 164-1
SiO ₂ %	43.6	66.5	59.2	65.6	62.8	68.9	58	64.4	63.7	69.4
TiO ₂ %	1.2	0.48	0.93	0.72	0.78	0.35	1.19	0.63	0.83	0.24
Al ₂ O ₃ %	16.3	16.6	14.9	14	14.7	15.9	13.9	14.6	14	15.3
Fe ₂ O ₃ %	11.67	2.76	6.09	4.87	5.31	2.18	7.75	4.48	5.48	2.48
MnO %	0.18	0.03	0.09	0.09	0.09	0.04	0.13	0.08	0.09	0.04
MgO %	6.99	1.14	4.95	2.25	3.57	0.92	4.89	2.95	3.75	0.42
CaO %	9	2.25	5.55		4.27	1.84	5.34	2.99	3.69	1.51
Na ₂ O %	2.73	4.63	3.77	3.47	3.6	4.25	3.23	3.69	3.55	3.69
K ₂ O %	2.49	3.58	1.71	3.41	2.62	3.82	2.49	3.45	2.43	4.91
P ₂ O ₅ %	0.64	0.17	0.58	0.39	0.4	0.16	0.49	0.33	0.33	0.14
CO ₂ %	1.69	0.04	0.18	0.31	0.33	0.25	0.47	0.48	0.22	0.07
H ₂ O %	3.11	1.01	1.7	1.39	0.73	1.01	1.99	1.29	1.04	1.1
Total %	99.6	99.19	99.65	99.63	99.2	99.62	99.87	99.37	99.11	99.3
Ba ppm	348	2390	1219	1225	923	2212	1114	1452	901	878
Rb ppm	67	36	26	74	71	40	52	58	56	139
Sr ppm	771	2057	1367	689	965	1922	704	935	891	198
Y ppm	24	10	19	13	17	10	35	14	16	25
Zn ppm	151	77	71	82	74	54	86	75	82	56
Zr ppm	202	172	297	290	367	141	485	254	290	320
Li ppm		21.52	16.93		24.06					
Sc ppm		3.92	15.79		13.74					
V ppm		34	110		95					
Mn ppm		273	718		748					
Co ppm		5	21		16					
Ni ppm		7	87		51					
Cu ppm		4	62		17					
Nb ppm		3.6	11.1		12.57					
Sn ppm		0.92	1.22		1.68					
Sb ppm		0.03	0.05		0.06					
Cs ppm		0.46	0.56		1.75					
FeOt	10.5	2.48	5.48	4.38	4.78	1.96	6.97	4.03	4.93	2.23
Mg	54.28	45.02	61.7	47.8	57.13	45.55	55.57	56.62	57.56	25.13
Mg										
A/NK	2.27	1.44	1.85	1.49	1.68	1.43	1.74	1.49	1.65	1.34
A/CNK	0.69	1.07	0.82	0.93	0.89	1.1	0.78	0.96	0.92	1.08
K ₂ O/Na ₂ O	0.91	0.77	0.45	0.98	0.73	0.9	0.77	0.93	0.68	1.33

Table A.4.2 (cont.) Chemical composition of rocks from Solís de Mataojo Granitic Complex. All trace elements in ppm.

	SM 1815	SM 22-1	SM 23-2	SM 31-2	SM 47-2	SM 52-1	SM 53-2	SM 97-1	SM 100-1	SM 164-1
La		30.67	49.41		39.77					
Ce		56.35	96.73		74.29					
Pr		6.26	11.21		8.28					
Nd		21.83	41.67		30.54					
Sm		3.1	7.18		5.63					
Eu		0.95	2.24		1.77					
Gd		2.01	5.76		4.92					
Tb		0.2	0.7		0.63					
Dy		0.85	3.6		3.51					
Ho		0.16	0.68		0.69					
Er		0.39	1.79		1.92					
Tm		0.05	0.23		0.27					
Yb		0.32	1.5		1.75					
Lu		0.05	0.22		0.28					
Hf		3.95	3.29		5.49					
Ta		0.26	0.42		0.62					
Tl		0.18	0.15		0.36					
Pb		25.7	13.4		13.7					
Th		3.68	3.06		5.8					
U		0.53	0.87		1.54					

Table A.4.3 Chemical compositions of rocks from Maldonado granite.

	SB 033	SB 048	SB 049	SB 050	SB 051	SB 053
SiO₂ %	76.4	71.6	74.5	74.2	74.1	73.1
TiO₂ %	0.15	0.42	0.25	0.26	0.27	0.25
Al₂O₃ %	11.7	13.3	12.5	12.7	12.7	13.2
Fe₂O₃ %	1.53	3.13	1.9	1.89	2.01	2.02
MnO %	0.03	0.06	0.04	0.04	0.04	0.03
MgO %	0.18	0.53	0.37	0.38	0.4	0.37
CaO %	0.6	1.52	0.96	1.01	1.02	1.05
Na₂O %	2.88	2.97	2.78	2.8	2.79	2.98
K₂O %	4.98	4.94	5.24	5.27	5.33	5.69
P₂O₅ %	0.05	0.14	0.1	0.1	0.1	0.08
CO₂ %	0.55	0.66	0.48	0.51	0.46	0.52
H₂O %	0.02	0.03	0.01	0.05	0.02	0.01
Total %	99.07	99.30	99.13	99.21	99.24	99.3
Ba ppm	39	334	253	252	317	315
Rb ppm	342	288	299	318	309	315
Sr ppm	11	89	54	55	59	60
Y ppm	53	49	36	39	39	31
Zn ppm	34	59	38	39	36	36
Zr ppm	146	237	159	186	196	220
Li ppm	70.75	82.91		75.44		
Sc ppm	4.34	6.66		4.62		
V ppm	7.1	26.3		19		
Mn ppm	227	444		349		
Co ppm	2	4		6		
Ni ppm	128	67		347		
Cu ppm	5	10		10		
Nb ppm	16.46	19.16		17.37		
Sn ppm	8.46	7.04		10.15		
Sb ppm	0.08	0.11		0.17		
Cs ppm	12.67	13.58		21.38		
FeOt %	1.38	2.82	1.71	1.7	1.81	1.82
Mg	18.91	25.13	27.85	28.5	28.29	26.64
A/NK	1.16	1.3	1.22	1.23	1.23	1.19
A/CNK	1.04	1.02	1.04	1.05	1.04	1.02
K₂O/Na₂O	1.73	1.66	1.88	1.88	1.91	1.91

Table A.4.3 (cont.) Chemical compositions of rocks from Maldonado granite. All trace elements in ppm.

	SB 033	SB 048	SB 049	SB 050	SB 051	SB 053
La	57.19	62.93		48.95		
Ce	126.42	140.63		106.81		
Pr	14.62	15.85		12.35		
Nd	51.85	58.17		44.82		
Sm	10.53	11.43		9.01		
Eu	0.27	1.06		0.59		
Gd	9.25	10.21		7.97		
Tb	1.47	1.54		1.18		
Dy	8.98	9.17		6.78		
Ho	1.81	1.81		1.29		
Er	5.34	5.26		3.64		
Tm	0.79	0.75		0.52		
Yb	5.17	4.93		3.36		
Lu	0.76	0.72		0.49		
Hf	4.92	5.49		5.02		
Ta	1.99	1.94		1.84		
Tl	1.74	1.13		1.61		
Pb	30.1	21.1		28.6		
Th	31.37	24.27		26.8		
U	5.64	4.26		6.59		

Table A.4.4 Chemical compositions of rocks from Pan de Azúcar pluton.

	SA 29-2	SA 82	SA 83	SA 84	SA 85-1	SA 90-1	SA 90-2	SA 116	SA 118
SiO₂ %	60.4	59.8	60.3	60.3	58.5	66.3	66.7	71.3	73.4
TiO₂ %	0.68	0.59	0.55	0.66	0.82	0.29	0.27	0.29	0.22
Al₂O₃ %	16.3	15.1	16.5	17.5	16.3	14.9	14.5	12.7	10.5
Fe₂O₃ %	6.7	8.85	6.35	5.51	7.8	5.17	5.17	4.77	5.41
MnO %	0.31	0.42	0.31	0.23	0.29	0.24	0.25	0.19	0.2
MgO %	0.53	0.35	0.4	0.62	0.84	0.13	0.12	0.11	0.13
CaO %	2.21	2.51	1.92	2.36	3.29	0.77	0.64	0.49	0.87
Na₂O %	5.14	5.09	5.74	5.78	5.46	6.11	5.4	4.29	3.47
K₂O %	6.16	5.55		5.07	4.53	5.11	4.91	4.5	3.87
P₂O₅ %	0.22	0.14	0.13	0.19	0.33	0.04	0.04	0.04	0.04
CO₂ %	0.47	0.49	0.25	0.25	0.4	0.22	1.49	0.5	0.49
H₂O %	1.14	1.33	1.04	1.14	1.15	0.77	0.69	1.15	0.91
Total %	100.26	100.22	99.15	99.61	99.71	100.05	100.18	100.33	99.51
Ba ppm	375	72	1813	2089	1710	56		140	81
Rb ppm	38	40	59	54	61	88	106	202	266
Sr ppm	45	22	177	500	428	12	14	38	21
Y ppm	31	43	30	42	90	82	85	164	445
Zn ppm	101	158	120	117	178	169	177	257	458
Zr ppm	202	373	209	899	1575	1126	1032	1455	3658
Li ppm	6.3					35.55			
Sc ppm	13.41					1.79		1.69	
V ppm	6.3					5.7		7.8	
Mn ppm	2510					1913		1356	
Co ppm	3					2		2	
Ni ppm	5					6		6	
Cu ppm	40					55		22	
Nb ppm	27.88					101.59		177.2	
Sn ppm	4.75					9.29		12.95	
Sb ppm	0.27					0.39		0.41	
Cs ppm						0.45		0.26	

Table A.4.4 (cont.) Chemical compositions of rocks from Pan de Azúcar pluton. All trace elements in ppm.

	SA 29-2	SA 82	SA 83	SA 84	SA 85-1	SA 90-1	SA 90-2	SA 116	SA 118
Ce	142.27					585.18		342.27	
Pr	16.81					60.15		33.97	
Nd	62.82					192.68		110.29	
Sm	10.41					26.34		20.61	
Eu	2.75					0.65		0.55	
Gd	8.39					20.09		18.83	
Tb	1.08					2.57		3.42	
Dy	5.69					13.88		22.85	
Ho	1.11					2.9			
Er	3.06					8.81		17.29	
Tm	0.41					1.28		2.75	
Yb	2.67					8.65		19.69	
Lu	0.43					1.42		2.93	
Hf	4.02					21.01		33.72	
Ta	1.47					5.1		9.8	
Tl	0.19					0.42		0.92	
Pb	12.4					27.2		40.1	
Th	3.69					15.98		58.11	
U	0.64					3.11		7.33	

Table A.4.5. Chemical compositions of mylonitic porphyries.

	SB091	SB111	SB030	SB171
SiO₂ %	75.8	75.3	71.2	73.3
TiO₂ %	0.2	0.14	0.2	0.09
Al₂O₃ %	10.5	11.1	15.4	14.8
Fe₂O₃ %	3.93	2.97	1.43	1.25
MnO %	0.01	0.04	0.01	0.03
MgO %	0.17	0.11	0.46	0.31
CaO %	0.34	0.3	1.32	1.15
Na₂O %	2.9	2.82	5.37	4.24
K₂O %	4.88	6.13	3.07	3.05
P₂O₅ %	0.05	0.03	0.15	0.1
CO₂ %	0.39	0.4	0.55	0.87
H₂O %	0.01	0.16	0.04	0.01
Total %	99.18	99.50	99.20	99.20
Ba ppm	138	12	2628	946
Cr ppm	426	531	44	39
Ga ppm	31	34	23	19
Nb ppm	115	99	10	15
Rb ppm	187	382	46	109
Sc ppm	10	10	11	10
Sr ppm	10	12	1711	270
V ppm	12	10	21	10
Y ppm	170	168	10	10
Zn ppm	224	250	53	51
Zr ppm	1807	963	147	82
Cr₂O₃	0.06	0.08	0.01	0.01
FeOt	3.54	2.67	1.29	1.12
A/NK	1.04	0.98	1.27	1.44
A/CNK	0.98	0.94	1.06	1.2
K₂O/Na₂O	1.68	2.17	0.57	0.72
mg	7.9	6.84	38.94	32.96

Table A.4.6. Chemical composition of basic rocks from Las Flores basalts (Sierra de las Animas Complex).

	SB467	SB478	SB454A	U91-21*	U91-22*
SiO₂ %	56.2	55.7	50.5	50.9	50
TiO₂ %	1.4	1.31	1.4	0.19	1.44
Al₂O₃ %	14.9	15.4	18.9	15.8	15.2
Fe₂O₃ %	8.64	8.08	8.34	10.8	11.8
MnO %	0.117	0.148	0.132	0.15	0.15
MgO %	3.31	3.66	4.1	4.86	4.66
CaO %	5.29	5.17	8.71	5.6	8.2
Na₂O %	4.22	2.86	3.36	3.2	2
K₂O %	2.65	4.16	1.68	2.91	3.2
P₂O₅ %	0.87	0.76	0.59	0.09	0.87
CO₂ %	1.63	1.75	1.51		
H₂O %	0.08	0.43	0.13	5.86	2.88
Total %	99.31	99.43	99.35	100.36	100.4
Ba ppm	1661	1839	1086		
Cr ppm	583	886	288		
Ga ppm	16	19	17		
Nb ppm	22	27	17		
Rb ppm	45	69	25		
Sc ppm	21	22	23		
Sr ppm	847	710	977		
V ppm	102	121	125		
Y ppm	35	33	27		
Zn ppm	97	87	65		
Zr ppm	454	454	229		
FeOt %	7.77	7.27	7.50	9.77	10.62
A/NK	1.52	1.67	2.57	1.88	2.25
A/CNK	0.77	0.83	0.82	0.85	0.7
K₂O/Na₂O	0.63	1.45	0.5	0.91	1.6
mg	43.16	47.31	49.35	46.21	43.91

* Data from Bossi *et al.* (1993)

Lebenslauf

Persönliche Daten

- Name: Pedro Bernardo Oyhantçabal Cironi
- Geboren am: 24.05.1956
- In: Montevideo, Uruguay
- Staatsangehörigkeit: uruguayisch/italienisch
- Familienstand: verheiratet. Zwei Kinder

Ausbildungsdaten

- 1973 Allgemeine Hochschulreife, erworben am Bauza-Gymnasium
- 1974 – 1982 Landwirtschaftliche Fakultät, Montevideo, Uruguay
- 1982 Diplom: Ingenieur der Landwirtschaft
- 8-monatiger Studienaufenthalt in Hannover um ein Mineralogie und Petrographie Kurs an der Bundesanstalt für Geowissenschaften und Rohstoffe zu besuchen
- 1997-2004 Magister der Umweltwissenschaften, Faculty of Sciences, Montevideo, Uruguay
- 2004 Erlangung des Grades: Magister der Umweltwissenschaften am Faculty of Sciences of Montevideo, Uruguay

Berufliche Beschäftigungen

- 1977-1982 Hilfsgeologe an der DINAMIGE (Geologischer Dienst aus Uruguay)
- 1982-1991 Geologe der DINAMIGE (Geologischer Dienst aus Uruguay)
- Seit 1986 beschäftige ich bei der Department of Geology (Geologie Abteilung) der Universität von Uruguay als Associate Profesor von Geologie